Estimation of current-season carbon fluxes in the rhizosphere of a tundra wetland soil

Dissertation

zur Erlangung des Doktorgrades
an der Fakultät für Mathematik, Informatik und Naturwissenschaften
Fachbereich Geowissenschaften
der Universität Hamburg

vorgelegt von
Norman Rüggen
aus
Hamburg

Hamburg 2017

Tag der Disputation: 03.07.2017

Folgende Gutachter empfehlen die Annahme der Dissertation:

Prof. Dr. Eva-Maria Pfeiffer

Dr. Christian Knoblauch

Vorsitz der Prüfungskommission: Prof. Dr. Eva-Maria Pfeiffer

"[…]. There is something irreversible about acquiring knowledge; and the simulation of the search for it differs in a most profound way from the reality. […]"

Robert Oppenheimer (Bulletin of the Atomic Scientists, February 1948, Vol. 4, No. 2, p. 86)

Content

Zusammenfassung

Veränderte Umwelt- und Klimabedingungen zwingen viele Ökosysteme und die menschliche Gesellschaft zur Anpassung. Der globale Kohlenstoffkreislauf ist hierbei von besonderer Bedeutung, da eine Zunahme des atmosphärischen Kohlenstoffdioxid - und Methangehaltes maßgeblich für steigende Temperaturen in der Atmosphäre verantwortlich gemacht wird. Insbesondere für die an extreme Kälte angepassten arktischen Ökosysteme werden gravierende klimabedingte Veränderungen prognostiziert, unter anderem erhöhte Treibhausgasemissionen. Die Prognostizierung von Treibhausgasmissionen aus Tundrafeuchtgebieten stellt ein wichtiges Ziel der arktischen Klimawandelfolgenforschung dar, da ein Auftauen des Permafrostbodens zu erhöhten Emissionen führen könnte. Die Untersuchung der Kohlenstoffflüsse im Bereich des Auftauhorizontes ist hierbei wichtig, da von dort Kohlenstoff in Form von Methan und Kohlenstoffdioxid in die Atmosphäre emittiert wird. Zur Quantifizierung der Kohlenstoffflüsse im Boden wird einem Pflanzen-Bodensystem der polygonalen Tundra zunächst CO_2 mit erhöhtem $^{13}C/^{12}C$-Isotopenverhältnis zugegeben, welches photosynthetisch aufgenommen wird. Dadurch entsteht im System ein messbarer zeitabhängiger ^{13}C-Marker-Impuls, welcher atmosphärisch-stämmigen Kohlenstoff im Bodensystem beobachtbar macht. Durch Entwicklung und Implementierung eines Kompartment-Models zur Beschreibung des ^{13}C-Impulses im Bodensystems und Kalibration des Models mit den beobachten erhöhten ^{13}C-Werten, lassen sich die Kohlenstoffflüsse im Boden erfassen und quantifizieren. Diese Studie zeigt, dass etwa 26 % des Kohlenstoffes, welcher während des Experimentzeitraumes aufgenommen wurde, in das *Scorpidium*-Moos innerhalb der obersten 20 cm eingebaut wurde. In den *Carex*-Wurzeln fand der Marker den Weg bis in eine Tiefe von 36 cm, dies entspricht einer Tiefe nahe der Permafrosttafel. Die Modellierung zeigt, dass 68 % des im System erzeugten Methans durch CO_2-Reduzierung entsteht und dass die modellierten CO_2 - und CH_4 - Emissionen (0.274 und 0.258 mg C $L^{-}h^{-1}$) vergleichbar mit Messergebnissen anderer Studien sind.

Summary

Changing environmental and climate conditions require adaptation strategies from both ecosystems and the human society. The global carbon cycle is important in this context, because increasing atmospheric carbon dioxide and methane concentrations are responsible for rising atmospheric temperatures. Particularly in Arctic ecosystems, which are adapted to extreme cold, significant climate-related changes are predicted, like increased greenhouse gas emissions. Predicting greenhouse gas emissions from tundra wetland areas is an important goal for the Arctic climate change impact research, because thawing permafrost soils might show substantially increased greenhouse gas emissions. The investigation of carbon fluxes in the active layer is important, because greenhouse gas emissions (methane and carbon dioxide) originate there. For quantifying the carbon fluxes in the soil, a polygonal plant soil system was exposed to ^{13}C-enriched CO_2, which was taken up during photosynthesis. Thus, a detectable time-dependent ^{13}C-tracer impulse in the sub-surface carbon cycle was produced, which allows measuring atmospheric-derived carbon in the soil system. For the description and quantification of carbon fluxes in the belowground, a compartment model was developed and implemented. The model was calibrated against the observed increased ^{13}C-concentrations. This study shows that about 26 % of the carbon, which is incorporated into the system during the experimental period, was allocated into the *Scorpidium*-moss in the first 20 cm. In *Carex*-roots, the tracer was found in a depth of 36 cm, which is close to the permafrost table. The model shows that 68 % of methane is produced by CO_2 - reduction. The modelled CO_2 and CH_4 emissions (0.274 and 0.258 mg $CL^{-1}h^{-1}$, respectively) are similar to results of other publications.

Acknowledgements

I would like to express thanks to my supervisor Eva-Maria Pfeiffer, who influenced on the success of this thesis with comments and advice and supported my unconventional working style. And I say thank you to Tim Rixen and Christian Knoblauch, who, as advisory panel chair and co-supervisor, respectively, impacted on my work. I believe, without their support, this project, in its current shape, would have never been realized. Thanks are due to Benjamin Runkle, who supported me with helpful comments regarding, among other subjects, my unconventional style of working. Other people, who significantly influenced on the success of this project, are Birgit Schwinge, Birgit Grabellus, Susi, Christian Wille, Volker Kleinschmidt, Wilfried Gläseker, Tanja Döbler, and Lars Kutzbach. Particularly, I want to thank David Holl, who influenced my way of thinking, which was an enormous help. Other people, who helped with either technical advice or moral support, were my PhD colleagues, Olga Vybornova, Kerstin Hansen, Tim Eckhardt, Mercedes Molina Gámez, and Josefine Walz. This project has been supported by the student assistants Sebastian Bieber and Christopher Breuer. Very helpful input I received by Victor Brovkin and Victor Dolin. The entire staff of the Intsitute of Soil Science deserve thanks as well. Thank you all! Many thanks also to Ingo Harms and the SICSS Grad school team for supporting my research. I want to thank Günter Stoof and Waldemar Schneider for help, support, and interesting conversations during my field campaign. And I want to thank the staff of the Samoylov research station for a help and support. The several stages of this project had their challenges, mental and technical ones, and I received both splendid ideas and necessary distraction from my brothers Mathies und Lennart Rüggen. Warm thanks also to my friend Arpan Chatterjee, who supported me whenever necessary. And "Thank you!" to my uncle Detlef. Last but not least I want to thank my parents, Birgit and Christian Rüggen, who not only taught me to think independently, but also to do things my way.

My warmest and deepest thanks earned my beloved wife, Yulia Polkova, who, with loving care and support, is the main reason for me succeeding in this project.

List of Tables

List of Figures

List of abbreviations and terms

Term/Abbreviation	-	Explanation
^{13}C	-	The stable carbon isotope with the atomic mass of 13
ADC	-	atmospheric-derived carbon, atmospheric-derived C
C	-	Carbon
CH_4	-	Methane
CM	-	Compartment model
CMIP5	-	Coupled Modelling Intercomparison Project Phase 5
CO_2	-	carbon dioxide
DIC	-	Dissolved inorganic carbon
DOC	-	Dissolved organic carbon
GA	-	Genetic Algorithm. A summarizing term for numerical optimization procedures, which apply gene-like operations to develop the optimal solution
Global minimum	-	The lowest value of a function (or a function region of interest). From here the function ascends into all directions.
intra-system fluxes	-	intra-system fluxes are fluxes that occur inside a defined system (e.g. soil), i.e. they do not cross the defined borders of the system
IRMS	-	Isotope-ratio mass spectroscopy
Label	-	tracer
LM	-	lognormal model
Local minimum	-	A point or an area of a function, from where the function into all directions increases – i.e. the lowest function value of this area. However, in at least one other region of the function exists a similar value, which is even lower (see "Global minimum")
MRT	-	Mean residence time (Mass/flux)
s.t.	-	subject to (list of constraints and conditions)
SCP	-	Sub-surface carbon pools
Search space	-	A mathematical set, discrete or continuous, in which variables of an optimization function can be sampled (see "feasible search space" and "unfeasible search space").

SoSy		Soil-system
TCTS	-	Tracer concentration time series
TCTS_obs	-	observed tracer concentration time series
TCTS_sim	-	simulated (model-produced) tracer concentration time series
Tracer		Also label. Any substance that is mixed into a larger chemical pool to observe physical or chemical properties. In this work usually used to describe artificially increased ^{13}C concentrations
transfer coefficient	-	coefficient that determines the amount of material being transferred from one compartment/pool to another; in stationary systems it appears as a constant
VPDB	-	Vienna Pee Dee Belemnite; refers to an artificial reference standard for ^{13}C. The $\delta\ ^{13}C$ signature of the VPDB standard is per definition 0
WETCHIMP	-	Wetland and Wetland CH_4 Inter-comparison of Models project

1 Introduction and objectives

At the dawn of the "Anthropocene", while the Earth's biogeochemical cycles are irreversible changed by human activities, the magnitude of these changes and the prediction of future biogeochemical cycles has become crucial for human society (IPCC, 2013; Steffen et al., 2011). Changes of the carbon cycle and the future concentration of atmospheric CO_2 and CH_4 concentrations are in the focus, because they are connected to rising global average temperature will become a social and economic challenge of unprecedented dimensions (Steffen et al., 2011).

Computing possibilities and technical innovations allow investigating global and regional matter fluxes on an ever sophisticated level. The oceans are spiked with ARGO floats that supply oceanographers and meteorologists with a previously unknown amount of data (Gould et al., 2004). Satellites orbit the planet and record soil humidity, surface roughness, atmospheric chemistry and numerous other data (e. g. Mecklenburg et al., 2012), increasing the understanding of the global carbon cycle.

However, while our understanding of the role of oceans and the atmosphere in the global carbon cycle is developing, the understanding of the carbon cycle in permafrost-affected soils and wetland soil is insufficient, despite their potential of releasing additional amounts of CO_2 and CH_4 in the atmosphere (Schuur et al., 2013). While technology is at hand to measure the carbon transfer across the soil-atmosphere-boundary (e.g. chambers, eddy covariance mentioned by Wille et al. (2008)), it is technologically challenging to quantify carbon transfer inside soils and most of the measurement campaigns in permafrost soil landscapes aim at catching the carbon that crosses the soil-atmosphere interface. Nonetheless, information about the belowground carbon cycle is essential.

For studying the carbon cycle inside the soil environment, natural and man-changed isotopic signatures of soil carbon are regularly used with great success to highlight the role of sub-surface carbon pools in the soil carbon cycle (Ainsworth and Long, 2005; Dorrepaal et al., 2009; Knoblauch et al., 2013). Such experiments rely either on enormous technical efforts, laboratory-based incubation experiments, or pronounced isotope differences in different pools.

Carbon isotope tracer experiments in combination with various model approaches have been in use in chemical and medical science for quite a long time (Munk, Keiding, and Bass, 2003; Beven and Young, 1988; Norwich, 1977). Tracers, in combination with compartmental approaches, have the potential to foster the qualitative investigation into which part of the investigated soil system atmospheric-derived carbon is allocated.

In this project, the carbon ^{13}C isotope is used to trace atmospheric-derived C (ADC) in the current-season carbon cycle of a permafrost-affected tundra soil. The tracer is introduced into the system via the photosynthetic uptake, in order to study the behavior of recently, freshly incorporated ADC in the plant-soil system. The tracer is measured in three sub-surface carbon pools: dissolved inorganic carbon, dissolved methane, and dissolved organic carbon.

The tracer concentration time series, i.e. the time-dependent decline (or rise) of tracer concentration in all three carbon pools contains information, which can be used to calibrate a compartmental model against them. The best-fitted parameterization of the compartmental model is chosen as the best representation of the soil carbon cycle.

The parameter estimation task can be solved in two steps:

Firstly, a conceptual model of the current-season soil carbon cycle is developed. The model is translated into an algorithm, in which the tracer concentration of the system's carbon pools is a function of model parameters which represent the fluxes and mean residence times of a compartmental model.

Secondly, now, having obtained a possibility to reproduce the soil system, parameters have to be found, which give a model output satisfyingly close to the observed real data set.

Finding the best-fitting model parameters is done by a Genetic-Algorithm numerical optimization procedure.

1.1 Objectives and working questions

Generally, this study aims to show the distribution of recently incorporated ADC in the belowground of permafrost-affected wetland soils and their contribution to DIC, CH_4, and DOC in the rhizosphere. A stable carbon isotope pulse-labeling experiment is conducted, which allows observing tracer

concentration time series in three selected sub-surface carbon pools (DIC, CH_4, DOC). A newly developed compartmental model of the sub-surface carbon cycle is calibrated against the observed tracer concentrations, where the parameters of the best-fitted model realization represent the quantified sub-surface carbon fluxes of the soil system.

To address this research goal, the following four research questions are formulated as the projects framework:

Q1) How does recently incorporated atmospheric-derived carbon redistribute in carbon pools of a high-latitude tundra plant-soil system?

Q2) Does the ^{13}C tracer display a tracer concentration time series in sub-surface carbon pools that allows modelling the sub-surface carbon cycle in a permafrost-affected tundra soil?

Q3) What is the mean residence time of freshly incorporated carbon a tundra wetland soil?

Q4) What is the ratio of both produced methane and produced carbon dioxide to up taken atmospheric carbon in the emission from the current-season carbon cycle (root exudates and respired carbon)? Are the fluxes among sub-surface carbon pools quantifiable by a compartmental model?

2 Background and theory

This section gives an overview of the state-of-the art in the field of carbon cycling investigation in wetlands with respect to changing climatic conditions and introduces the background knowledge based upon which the methods of this study are developed. The current study is situated in the field of carbon cycle investigation in permafrost-affected wetlands, with special focus on investigating and understanding current-season carbon cycle processes. The scientific fields into which this study is grouped is outlined in Figure 1.

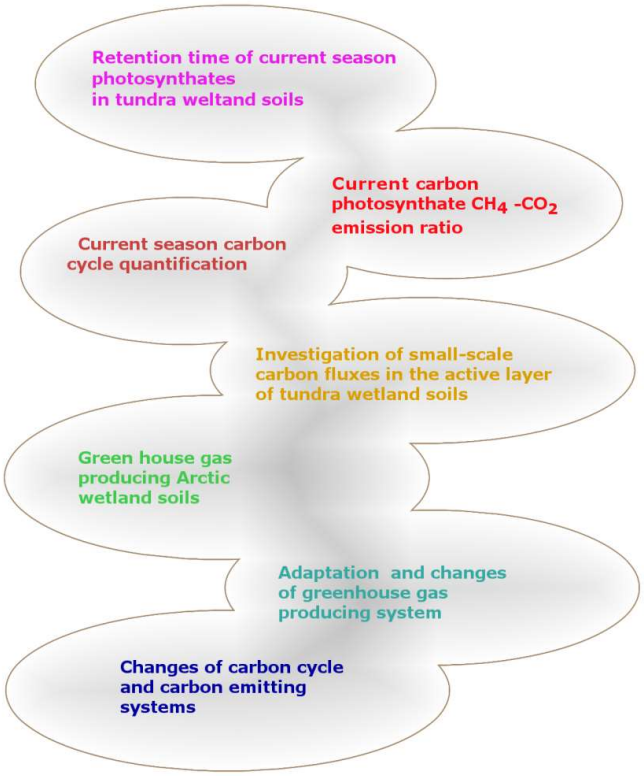

Figure 1. The figure outlines conceptually the research fields into which the current study is nested. The reader is offered an overview of different research fields in Arctic and carbon cycle research.

2.1 Arctic soils and atmospheric greenhouse gas concentrations

The globally observed changes in climatic conditions are linked to an ongoing increase of atmospheric concentrations of carbon dioxide, methane, and a number of other greenhouse-gases in the Earth's atmosphere (e.g. in IPCC, 2013). The concentrations of CO_2 and CH_4 are exceeded due to anthropogenic induced changes of the global carbon cycle. CO_2 and CH_4 are the most important greenhouse gases with respect to climate change (Ciais et al., 2013). Therefore, collecting information and knowledge about greenhouse gas fluxes between atmosphere and the various terrestrial and oceanic systems is an important task for scientific research efforts. This research is

crucial for predicting the concentration changes of both gases in future climate scenarios (Schuur et al., 2013; IPCC, 2013a). The global carbon cycle pools can be coarsely divided into oceanic, terrestrial and atmospheric carbon pools. Among the terrestrial carbon pools, soils store 1500-2400 PgC and represent the largest stock (Ciais et al., 2013).

Permafrost-affected soils store huge amounts of carbon in organic compounds, namely about 217 ± 12 PgC in the upper 30 cm of permafrost-soils (Hugelius et al., 2014), which is slightly more than one quarter of atmospheric-stored carbon (829 ±10 PgC in Ciais et al., 2013). The total amount of carbon stored in perennial frozen ground is estimated with 1700 PgC; carbon, which has been accumulated in the course of millennia (Ciais et al., 2013). Due to their low temperature regimes, such soils exclude a huge fraction of carbon from the active global carbon cycle. If warming of permafrost-affected soil organic lead to higher respiration rates, these soils might turn into net carbon emitters and might significantly increase the atmospheric CO_2 and CH_4 concentrations (IPCC, 2013).

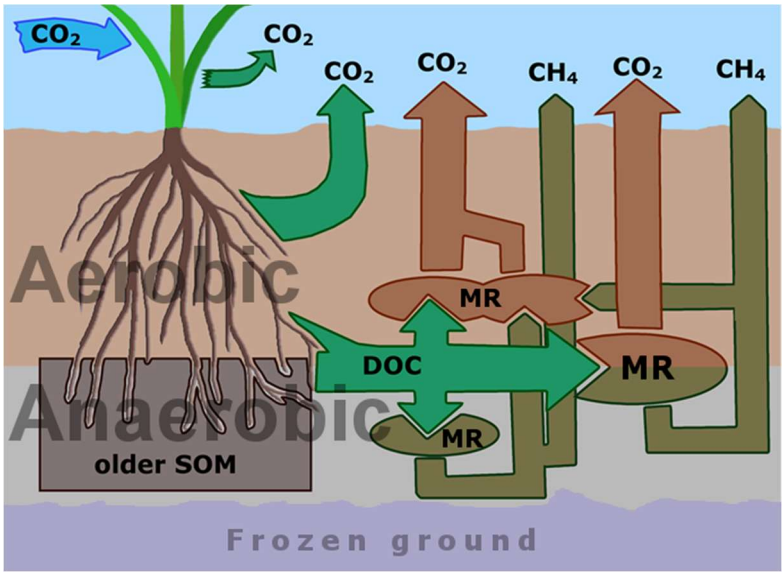

Figure 2. Schematic permafrost-affected wetland soil carbon cycle. In this conceptual model, atmospheric-derived CO_2 migrates through the different soil system compartments and might be released as either CO_2, or CH_4, or DOC. Green: plant products, brown: aerobic microbial products, olive: anaerobic microbial products. MR: microbial respiration. SOM: soil organic matter (inspired and based on information from: Schlesinger (1997); IPCC (2013b)).

In fact, for the Arctic regions the impact of global warming is predicted to be significant in terms of temperature increase and precipitation increase during the next decades. The CMIP5 models predict a temperature increase of up to 2°C of the global average until the year 2100, but a temperature increase of about 1°C to 2°C in summer and 4°C to 15°C in winter for the Arctic regions (IPCC,

2013b). Precipitation is predicted to increase by more than 50 % in Arctic areas. These are still predictions, but during the last decades, at almost all sites where permafrost temperature was measured, an increase of permafrost temperature and a growth of active layer thickness have been observed throughout the Northern Hemisphere (Christiansen et al., 2010; Romanovsky et al., 2010. In: Vaughan et al., 2013), which is related to rising temperatures and changing snow cover characteristics in the Arctic regions.

Thawing permafrost, or better, increasing active layer depths in permafrost soils, might cause higher carbon emissions due to additional respiration of long-term stored carbon from the system (Dorrepaal et al., 2009; Hugelius et al., 2014; Tagesson et al., 2012; Knoblauch et al., 2013). Depending on the hydrological and climatic conditions, it is possible that carbon dioxide and methane emission will be higher compared to their present emissions (Wille et al., 2008; Tagesson et al., 2012; Christensen et al., 2004), which could significantly change the atmospheric CO_2 and CH_4 concentrations. The CO_2 and CH_4 emissions are controlled by biochemical reactions in the upper few centimeters, in the root-affected part of the soil (rhizosphere) of the permafrost-affected wetland (Whiticar, Faber, and Schoell, 1986; Jones, Nguyen, and Finlay, 2009).

2.2 Current-season carbon cycle in the permafrost- soil system

The carbon cycle in a permafrost-affected wetland soil starts with the incorporation of atmospheric-CO_2 by photosynthesis (agents: vascular plants, mosses). The atmospheric-derived C is either immediately released back into the atmosphere (plant respiration) or transformed into organic compounds with different degrees of stability (simple sugars and acids, proteins, lipids, lignin and other stable macromolecules (Jones, Nguyen, and Finlay, 2009). Wetland soil systems emit carbon mainly in the form of carbon dioxide and methane. Whether carbon from the soil environment is released into the atmosphere as CO_2 or CH_4 depends on the oxygen availability in the soil, but also on plant species, microbial communities, temperature and precipitation regime (Whiticar, 1999; Knoblauch et al., 2015; Nakagawa et al., 2002; Schuur et al., 2013). Thus, wetland soils can be described as systems that take up carbon dioxide and release it – after some time – either as CO_2, CH_4, or organic molecules (the latter can – under conserving conditions – remain in the soil for years

to millennia). Any single carbon-bearing molecule, released by the soil, can originate from different carbon pools inside the soil system (e.g. from plant roots, litter, microbial biomass, plant root exudates, dead plant cells, other plant remainder or long-term stored soil organic matter). It can be released from different parts of the soil (aerobic, anaerobic, different depths). Grouping released carbon molecules by their originating sources is termed source partitioning (interpretation based on Schlesinger, 1997). Figure 2 gives an overview about the major carbon fluxes and carbon pools in the permafrost-affected wetland soil system. Several studies indicate that under warmer conditions or higher precipitation regimes the current permafrost-soil carbon cycle will change and that older, long-term stored carbon is potentially released into the atmosphere. This would turn permafrost-soils from net carbon sinks into net carbon sources (Dorrepaal et al., 2009; Schuur et al., 2009; Hicks Pries, Schuur, and Crummer, 2012; Blodau and Siems, 2012). Methane and carbon dioxide emissions might increase under a higher soil temperature regime. Such conclusions are deduced by in-situ warming studies (Dorrepaal et al., 2009), in long-term studies in thawing, permafrost (Schuur et al., 2009), by building an isotope-mixing model including $\delta^{13}C$ and $\delta^{14}C$ signatures of respired permafrost organic matter (Hicks Pries, Schuur, and Crummer, 2012), and with in-vitro experiments (Knoblauch et al., 2013).

Such findings intuitively demand a detailed investigation of carbon transfer processes in the rhizosphere of permafrost-affected soils.

2.3 What to investigate?

So far, carbon emission predictions of the remote permafrost-affected landscapes remain problematic, which is largely due to the lack of data. Models, which are used to predict the emission behavior of such natural systems, use limited sets of established data sources (Melton et al., 2013; Kaiser et al., 2017). More data sets, especially from intra-system carbon transfer fluxes, would allow comparing and calibrating such models with observations, increase the model confidence, and possibly increase the trustworthiness of future carbon cycle predictions. Consequently, the need for additional data sets was stressed in the conclusion of the WETCHIMP project report (Melton et al. 2013; Wania et al., 2013).

Information about how much CO_2 and CH_4 is emitted per each carbon atom incorporated into the system is crucial for predicting the potential additional radiative forcing imposed by a respiration of long-term stored organic matter in permafrost-affected soils (Schuur et al., 2013). That is, because methane has a radiative forcing which is significantly higher compared to that of CO_2 (i.e. the same concentration increase would lead to a stronger greenhouse effect for methane than for CO_2. The radiative efficiency in W m^{-2} ppb^{-1} is $1.37 \cdot 10^{-5}$ and $3.63 \cdot 10^{-4}$ for CO_2 and CH_4, respectively (Myhre et al., 2011)).

2.4 How to investigate the current-season carbon cycle in the rhizosphere?

Carbon emissions, both CO_2 and CH_4, has been investigated around the Arctic, measured by chamber measurements or eddy covariance (EC) technique (Kutzbach et al., 2007; Knoblauch et al., 2015; Wille et al., 2008). However, although usually in the same order of magnitude, methane fluxes from wetlands might differ, depending on the method applied (chamber or EC (Marushchak et al., 2016)). These fluxes are controlled by environmental parameters such as photosynthetic active radiation, soil and air temperature, wind speed, oxygen concentration in the soil, vegetation and other parameters. Based on these environmental parameters, modelling the overall methane and carbon dioxide emissions from permafrost-affected soils has been done successfully (Wille et al., 2008; T. Sachs et al., 2008; Kutzbach, Wille, and Pfeiffer, 2007). Micrometeorological measurements, EC data and data analysis are applied to formulate carbon emission models for tundra soils (Sachs et al., 2008; Kaiser et al., 2017).

However, such studies give little information about the mean residence time (MRT) of current-season carbon in the soil and do not allow quantifying fluxes inside the soil system, because these studies investigate only the total carbon emissions from the soil system in a region or at a site, without differentiating between the respiration of long-term stored carbon and current-season produced carbon compounds. Hence, processes, which actually control the carbon emission from permafrost-soil systems, are conceptually explained, but remain challenging to measure and to quantify in situ (Jones, Nguyen, and Finlay, 2009). Investigating these processes will promote the understanding of carbon emissions from soils (Kuzyakov, 2011) and should be investigated to increase the confidence

in currently existing models (Earth system models, ESM) of terrestrial ecosystems (Hugelius et al., 2014). Finding a method, which allows displaying the behavior of sub-surface carbon pools as the processes take place, in-situ, in addition to ongoing long-term eddy covariance or chamber measurement campaigns, is of interest in order to investigate the effect of various climatic conditions on sub-surface carbon fluxes and source partitioning.

2.5 State-of-the-art in source partitioning

As mentioned, measuring only fluxes that cross the soil-atmosphere interface usually does not allow source partitioning, i.e. does not allow determining, which of the numerous sub-surface carbon pools (e.g. DIC, CH_4, DOC, soil organic matter etc.) contribute how much to both emitted CO_2 and CH_4.

However, some methods in use address source partitioning in soils, few of which have been applied in permafrost-affected wetlands. Generally, they can be grouped into invasive methods and non-invasive (tracer) methods. An outstanding evaluation and overview about different existing methods gives the reviews by (Subke, Inglima, and Francesca Cotrufo, 2006; Kuzyakov, 2006). Since the method applied in this study – that much is now disguised – is an isotope labeling experiment, the physical-invasive methods are only mentioned here and the interested reader is referred to the reviews by Subke, Inglima, and Francesca Cotrufo (2006) and Kuzyakov (2006).

Invasive methods include trenching and girdling (cutting the connection between plant and their roots in tree stands and investigate the system changes), clipping and gapping (cut all plants of an defined area, which stops any new plant-produced carbon input into the system), physical separation of plant or system parts (soil sample incubation experiments) and others (Subke, Inglima, and Francesca Cotrufo, 2006; Kuzyakov, 2006). Non-invasive methods include modelling and isotope-labeling (Kuzyakov, 2006; Subke, Inglima, and Francesca Cotrufo, 2006). Hicks Pries, Schuur, and Crummer (2012) and Natali et al. (2010) used $\delta^{13}C$ and $\delta^{14}C$ ratios in the soil-emitted CO_2 by comparing them to the $\delta^{13}C$ ratio in different soil depths and calculating the fraction of each layer's isotope signature in the released carbon. King and Reeburgh (2002) and Dorodnikov et al. (2011) exposed ^{14}C in a pulse-labeling experiment to mesocoms from Arctic wetlands and boreal grasslands, respectively. Thus, with parallel total flux measurements, they were able to calculate the fraction of current-season

produced photosynthates to the total emitted CH_4. Both studies used mesocosm-setups, i.e. they did not investigate the soil system in-situ. Wu et al. (2010) did an in-situ ^{13}C pulse-labeling experiment were the Summer uptake of ^{13}C-labeled carbon in a grass-pasture ecosystem is interpreted as the average annual incorporation of freshly photosynthesized carbon into the system. Warembourg and Paul (1977) and Allessio and Tieszen (1975) used the distribution of ^{14}C-tracer in plant systems to determine the prominent incorporation location of newly photosynthesized carbon. Other labeling-experimenters added isotopically-labeled acetate to plant systems in order to examine methane production processes (Lin et al., 2015; Ström et al., 2003). Another experimental approach to look into soils by application of carbon isotopes are FACE-experiments. In such experiments, artificially increased ^{13}C-CO_2 is exposed to research areas. With time, the artificial ^{13}C-carbon signature changes the carbon signature in all carbon pools of the system, hence allowing investigation of various carbon cycle related processes and beyond (e.g.: Ainsworth and Long, 2005; Tokida et al., 2011).

Kuzyakov, Kretzschmar, and Stahr (1999) applied a model to simulate $^{14}CO_2$ emissions from a pulse-labeling experiment on *Lolium perenne* grass with 9 parameters, two of them fitting variables - to fit against data – and the tracer emission curve published also displays the typical shape of a tracer outwash curve. The results of King and Reeburgh (2002), Johnson et al. (2002), and Dorodnikov et al. (2011) show that the soil system is impacted by the tracer until deep inside the pedon, because DOC and dissolved carbon-bearing gases are affected by tracer immediately after the plant system is labeled. The data presented by King and Reeburgh (2002) show a distinctive tracer outwash curve for dissolved inorganic carbon, dissolved methane, and dissolved organic carbon in a tundra soil.

2.6 Tracer experiments and the soil system

Where it is not physically feasible (i.e. no technologies available to do the job) to measure the fluxes of a system or a system's pool, the only way to obtain information about fluxes is to measure the mean residence time by application of tracers (Turner and Barnes, 1998; Hearon, 1968; Anderson et al., 1977 (In: Anderson, 1983). The tracer is supposed to be chemically indistinguishable from the tracee (the "normal" molecules in a pool), but detectable (Norwich, 1977). Generally, tracer concentration curves represent detectable phenomena of system impulse response behavior.

Isotopes are ideal tracers, because they are detectable, but can be assumed to be subject to the same physico-chemical processes as is the tracee (Norwich, 1977). They are widely used in biological, chemical, hydrological and medical investigations to gain information about compartments and connection of a system (plant-parts, animal and human organs, water bodies), which cannot be measured directly by putting measurement devices between systems compartments (i.e. the classical flux measurement cannot be undertaken easily in microscopic small blood vessels, plant vessels etc.) (Norwich, 1977; Anderson, 1983; Munk, Keiding, and Bass, 2003; Bassingthwaighte and Beard, 1995; Hearon, 1968; Luo and Nobel, 1992; Turner and Barnes, 1998). In such cases, the investigated system can be defined as a compartmental system and the tracer concentration in the various compartments as a function of all the system's transfer coefficients between pools and to the system's environment and the mean residence time of the system pools. Hence, the tracer concentration curve in each system's department depends on parameters such as input into a compartment, mean residence time in a compartment, and output from a compartment (Anderson, 1983; Norwich, 1977). As pointed out by Norwich (1977), under the assumption that the system is in a steady-state, compartmentally modelled tracer concentration time series of the system can be calibrated against the observed data in a way that they reproduce the observed tracer concentrations. This way, the system parameters such as transfer coefficients (system fluxes) and mean residence times can be defined by the tracer functions. The tracer decline in a mono-compartmental system can be described by

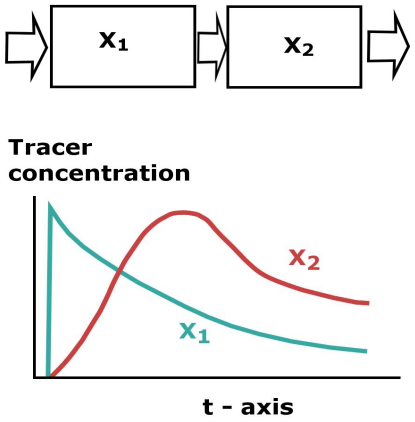

Figure 3. Tracer concentration in two carbon pools in series. The pools X_1 and X_2 represent matter pools, for example carbon pools. The evolution of tracer concentration time series of a simple two-compartmental model is shown in green (tracer concentration in pool X_1) and red (tracer concentration in pool X_2). (based on Norwich,1977).

$$1) \qquad \frac{\delta C}{\delta t} = -kC,$$

where δC is the change of tracer concentration, δt is the time difference, $-k$ is a constant and C is the tracer concentration at time t. This first-order differential equation describes the loss of tracer per time step t (e.g. in Knoblauch et al., 2013). This equation would be, as an example, suitable to model the concentration change of a detergent in a pot, in which the in and outflushing water is in equilibrium.

In more complex systems, with several pools and links, since the observed pools receive inputs from various other pools, the tracer dynamics (and hence the system response functions) observed in the pools of a plant-soil-atmosphere system is a function of all mean residence times and fluxes. Sometimes, certain pools can be connected cyclically, i.e. a molecule which enters pool A coming from pool B can be either lost (e.g. to pool C) or end up again in pool A. Therefore, in such rather complex system as the soil-plant system is, the functions are usually complex.

A model, which aims to produce simulated tracer concentrations of the system, has to be parametrized in such a way that the model output (the model tracer concentration) is comparable to observed tracer concentrations. Such a process is called *inverse modelling*, because the undetermined equations of the system can be approximated by finding parameters that produce modelled mean residence times, which sufficiently resembles the observed mean residence times (Tarantola, 2005).

Subsequently, this approach can be used to deduce the connections among the compartments with a method described by Norwich (1977) as the "Solution of the inverse problem". The inverse problem, according to Norwich, requires a mathematical procedure which deduces the transfer rates from the observed tracer functions.

A compartmental model of the sub-surface carbon cycle in permafrost-affected soils

All carbon fixed in organic compounds in the sub-surface soil comprise the total organic C-pool of that soil.

The organic carbon pool (C_{org}-pool) of a soil consists of all carbon, which is fixed in organic molecules and compounds in the soil.

This total C-pool can be divided into a number of sub-surface carbon pools. For this study, the sub-surface soil C-pool is divided into the following carbon pools: root C, soil substrate C, dissolved

inorganic carbon, dissolved CH_4 and dissolved organic carbon (DOC). This division takes into account the role of each C-pool in the soil environment and its degradability. Two examples are given here. 1) Roots consist of fine and coarse specimen, both with different physical-chemical significance for the carbon allocation by the plant metabolism. Both root types can be expected to show different mean residence times with respect to carbon (According to Gill and Jackson, 2000), the lifespan of roots depends on the root diameter and on the mean annual temperature). Roots directly allocate carbon into the DOC, DIC pool and indirectly (via the DOC and the DIC pool) into the CH_4 pool (Jones, Nguyen, and Finlay, 2009). If the mean residence time of carbon in a certain carbon pool is taken as an input parameter for a carbon allocation model of the sub-surface environment, the carbon fluxes (allocations) between the pools are the output parameters of such a model. The parameter combination, which produces the best correlation between modelled mean residence times and observed mean residence times, is then the solution of a multidimensional optimization problem.

2.7 System parameter finding with constraint-satisfying GA numerical optimization

The solution of the inverse problem in this project is done with the application of a numerical optimization algorithm (Norwich, 1970). Numerical optimization algorithms are a large family of computational-based numerical algorithms aiming to find optimal solutions of multidimensional problems with an infinite or quasi-infinite search space (Holland, 1992). During the optimization procedure the model parameters (which in our example represent fluxes and mean residence times) are the search space. The search space is a mathematical space, from which possible parameter-values can be selected. This space can be further divided into feasible and unfeasible search space. The feasible search space is that part of the search space, in which variable combinations are sampled that do not violate the system's constraints. Constraints are conditions superimposed on the search space by the structure of the mathematical model and other requirements which cannot be violated. This simply means that certain parameter combinations are "not allowed", because they would lead to a violation of the steady-state condition or would be unfeasible (Yang, 2014).

In a next step, a target function is formulated. In a target function, the model results and the observational data are compared and the difference of both functions is evaluated. Generally spoken, if the target function is smallest (ideally zero), the modelled data are as close as possible to the observed data. The parameters (variables) that produced these values are hence a solution of the inverse problem, i.e. the flux and mean residence values that are searched for. Since the search space is literally infinite, it is unlikely to find the optimal or at least a close-to-optimal solution in any amount of time with a simple trial-and-error method. Even in a discrete search space with a few parameters, the number of possible parameter combinations reaches swindling heights (called the "curse of dimensionality" by Bellman (2003)), because with every new parameter (which adds a new dimension to the search space), the possible combinations multiply exponentially (compare Table 1).

Table 1. Number of possible variable combinations in different search spaces (inspired by Bellmann, 2003).

Number of dimensions	Subunits	Possible variable combinations
2	100	10.000
5	100	10.000.000.000
10	100	10.000.000.000.000.000.000

There exists a long-list of numerical optimization algorithms that have the potential to successfully avoid to be trapped at a local minimum. The most widely used optimization algorithms are Hill climbing, Simulated Annealing (SA), Genetic Algorithm (GA), Particle Swarm Optimization (see Yang, 2014) for further information on the most wide-spread numerical optimization algorithm). The Genetic Algorithm (GA) was chosen to solve the numerical optimization problem (finding the mean residence time and the carbon pool fluxes by fitting a model to the observed tracer concentration changes in the soil system (Yang, 2014; Nocedal and Wright, 2006).

The Genetic Algorithm (GA)

The Genetic Algorithm is based on the work of John H. Holland and his colleagues (Yang, 2014; Holland, 1992; Whitley, 1994) and it is used for optimization problems in many disciplines. Holland (1992) pointed out that the working questions, which fostered the development of the genetic algorithm, came from various disciplines, among them biological evolution, learning theory, artificial

intelligence and economy (Holland, 1992). For this method, depending on the field of research, the parameters or variables of a function, which shall be optimized, are transformed into an algorithm that bears resemblance to the biological process of breeding or species adaptation (evolutionary theory). Holland (1992) describes evolution of species as an optimization process, which final (best-fitted) result is achieved after iterative cross-combination of genes and mutations. Whereas in nature the fitting function is the competitiveness of the species, the general principle can be applied to mathematical problems as well.

In this study, the mathematical problem's search space (the mathematical set from where a functions parameters are sampled) appears as a population with different species (a single set of parameters sampled from the search space, i.e. one possible parametrization of the function). After randomly defining a starting population, the evolutionary process starts. New generations are produced by crossover, recombination, mutation, and selection, with the aim to obtain ever fitter parameter sets. Fit in this sense means close to the optimal solution of the problem (Whitley, 1994; Yang, 2014; Holland, 1992). Depending on the discipline, the "evolution process" takes on various forms, as can be seen in Table 2.

Table 2. Genetic Algorithm schemes in different disciplines (modified from Holland, 1992).

Discipline	*Structures*	*Operators*
Genetics	chromosomes	mutation, recombination, etc.
Economic	mixes of goods	Bayes'rule, successive approximation, etc.
Physiological psychology	cell assemblies	
Game theory	strategies	rules for iterative approximation of optimal strategy
Artificial intelligence	programs	"learning rules"

Starting with this very general information about genetic algorithms, the special algorithm used for this study is developed. According to Whitley (1994) and Holland (1992), the formulation of the algorithm is developed along the following steps:

- a genetic representation of all possible parameter sets that are to be optimized (referred to as "strings" or "candidate solutions" of a "candidate solution population" (the term "candidate solution" was adapted from the inspiring Wikipedia-resource 'Genetic Algorithm', 2016)).
- a fitness function that allows assigning a "fitness value" to each parameter set and hence allowing to decide which parameter set is likely to survive.

A set of strings is created as starting population, which is exposed to operators such as "mutation", "crossover", and "selection".

The initial problem, i.e. finding the optimal ("best") set of parameters for a given function is then solved iteratively:

1. Creation of a start population
2. Defining the fitness of each candidate solution by the fitness function
3. Applying the genetic operators (mutation, cross-over) to the strings of the start population (this creates new strings, a next generation)
4. From the new population, the least-fittest specimen are eliminated (selection)

Refer to Whitley (1994), Yang (2014) and Holland (1992) for further information. The explanation in this section is based on their publications and ideas.

The fitness function $F(X_2, X_2, \ldots X_n)$ of a numerical optimization problem has to be minimized. As for this study, the operators and structure are given in Table 3.

Table 3. Conceptual Genetic Algorithm scheme for the current study project (inspired by Holland, 1992).

Discipline	*Structures*	*Operators*
Sub-surface soil carbon model	fluxes between pool, mean residence time of carbon pools	"mutation" and "crossover" (i.e. parameters are recombined and modified to resemble genetic processes).

2.8 Summary

In this study, a compartmental model is used, which simulates time-dependent tracer concentrations in the system's C-pools (dissolved CH_4, dissolved CO_2, and dissolved DOC). This model is calibrated

against observed time-dependent tracer concentration in the respective C-pools. Properly designed, the model can be used to find the fluxes between sub-surface carbon pools with inverse approach (finding the parameters of a system by fitting a tracer concentration model to observed tracer concentrations was called "inverse modelling" by Norwich (1997)).

In a simple compartmental model of a tundra wetland soil, the carbon pool mean residence time and fluxes among carbon pools are the input parameters of the model. The output parameters are tracer concentration curves. In such model, the carbon flux in the system is represented by simple, ordinary differential equations.

The task is now to find input parameters (i.e. intra-system fluxes and mean residence times of carbon pools) which produce time-dependent tracer concentration curves with the same dC/dt-characteristics as the observed data.

3 Methods and experimental site

3.1 Site and geographical site information

The polygonal tundra is an important source of soil-atmosphere carbon fluxes and therefore chosen for this case study. Samoylov (N 72°22', E 126°30') is an island in the Lena delta, which is, with 32.000 km^2, the largest river delta of the Arctic ocean and is formed of modern, Holocene sediments that are deposited between Pleistocene deposits (Kutzbach, Wagner, and Pfeiffer, 2004; Zubrzycki et al., 2013; Are and Reimnitz, 2000). The island itself is divided into two main geomorphological units (an annually flooded floodplain in the western part and an irregularly flooded in the eastern part). The polygonal tundra is found in the eastern island area. According to Schneider, Grosse, and Wagner (2009), the wet sedge- and moss dominated tundra is the most widely spread land cover class in the Lena Delta with an area of 8277 km^2 (about 26 % of the total delta surface), in which the polygonal centers emit the highest amounts of methane (Schneider, Grosse, and Wagner, 2009). The site of this study is located in the wet polygonal tundra in the eastern part of the island about 50 meters south of the site that has been described by Preuss et al. (2013). Zubrzycki et al. (2013) reported an active layer of less than 60 centimeters and the soils has been classified as "*Typic Aquorthel* (Soil Taxonomy) or as *Histic Cryosols* (WRB, 2006)" by Preuss et al. (2013). The plants in the polygonal center have been identified as *Carex aquatilis* and *Scorpidium scorpidoides*.

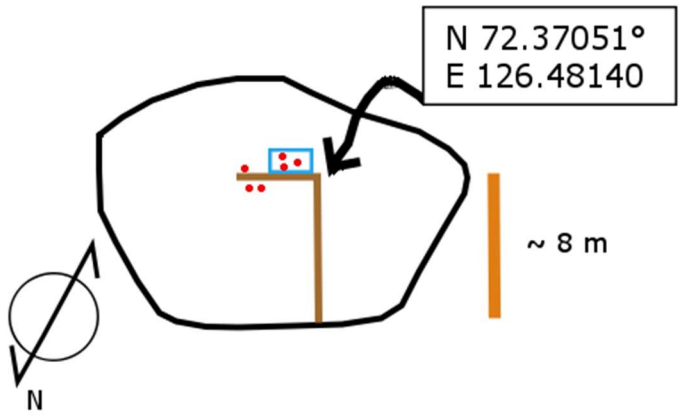

Figure 4. A schematic map of the selected low-centered tundra polygon. Red dots: six replica sites for sampling of sub-surfa ce CH_4, CO_2, and DOC. Blue rectangle: The labeling area. Brown line: boardwalk. Black line: polygonal rim, white: tundra vegetation.

3.2 Pulse-labeling

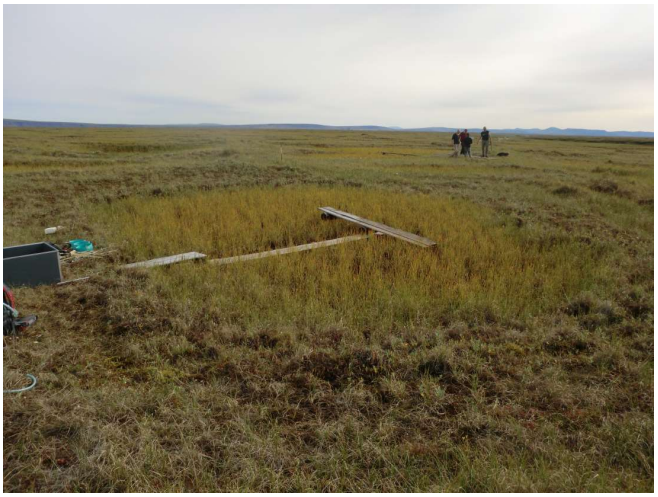

Figure 5. The experimental site in the low-center polygon. The wooden boardwalk was already installed. The site chosen for labeling and sampling represents only the polygonal centre, i.e. a wet sedge-moss tundra.

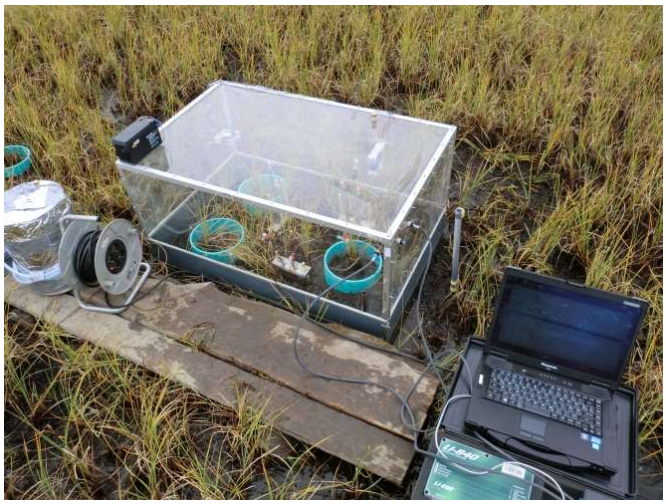

Figure 6. Label chamber erected at field site. The robust design enables its application in remote and off-road areas. The CO_2-concentration in the chamber was constantly measured by a LI-840 IR gas analyzer.

Different methods for carbon isotope labeling have been used (King and Reeburgh, 2002; Johnson et al., 2002; Ostle et al., 2000; Street et al., 2013; Subke et al., 2012). For this study, I focused on transportability and robustness of the experiment design. For the chamber collar, grey PVC boards have been used. The ground area of the chamber (0.63 m x 1.00 m) that should be covered by the chamber was determined as a good compromise between the maximum of area and transportability. The chamber had a height of 0.35 m and the estimated chamber volume (including some centimeters between collar rim and soil surface) added up to 285 liters.

The chamber was constructed in such a way that it can be quickly disassembled and transported in parts, which can be recombined at the research location. The chamber material was acrylic glass. For strengthening the construction, chamber walls, as well as the PVC walls of the collar, were joined together by an alumina frame and stainless steel screws. The whole construction was made air-tight by a silicon

seal. To avoid lateral distribution of the labeled material into the polygon, the soil of the label site was hydraulically separated from the surrounding soil by the collar. The collar reached 40 cm deep into the soil, which was 10 centimeters above the permafrost-table at the time of the construction. The chamber was joined to the collar via an H-shaped alumina angle that was glued on the top rim of the collar. Polyurethane sponges were inserted into the hollow shaped H-rim and filled with water from the site to seal the chamber from the ambient air. The chamber CO_2 concentration was directly measured with an infrared CO_2-H_2O gas analyser (Li-840, Li-COR Biosciences, USA). Both data streams are stored by a data logger (CR 850, Campbell Scientific, USA). A seal-hose adapter an 3.0 mm inner diameter ISO-versinic-Viton hose (Ochs Laborbedarf, Germany) was wired from one end of the chamber via a filter (Li-Cor Biosciences, USA), a CO_2 absorbent (SodaLime) containing glass bottle and a polypropylene box (Lock&Lock HPL 836, ISI, Germany) that contained frozen cooling packs, to a membrane pump (N03512AN18, KNF Neuberger, Germany) and back into the chamber (the setup is schematically depicted in Figure 7). The cool packs, as well as the CO_2 sorbent could be switch off from the chamber air by 3-way-stop cocks (Discofix, B.Braun, Germany). The gas space of the chamber could be accessed during labeling by a septum that was mounted on top of the chamber. Inside the chamber, two 12-volt PC fans mixed the air to prevent the acrylic glass walls to get foggy (see Figure 7). The working principle of the labeling device was as follows:

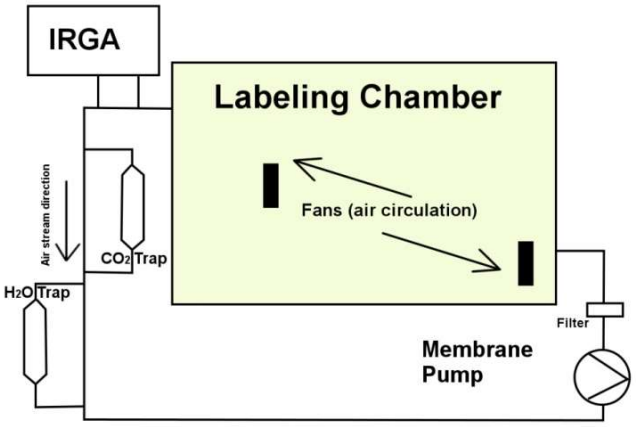

Figure 7. Work principle of the labeling experiment setup. The IRGA (infra-red gas analyzer, Li-840) detects the CO_2 concentration during the labeling phase. The CO_2- trap and the H_2O-trap are manually connectible and allow decreasing both CO_2 and H_2O concentrations in the system.

Phase 1: The chamber was set on top of the collar and covered by a thick darkening plastic foil and the air pump was activated. The chamber air was guided through the CO_2 absorber and the cooling pack, to trap the CO_2 and prevent the chamber from warming. Additionally, the plastic foil was covered by a highly reflective alumina thermo blanket which reflected sun radiation. The plants, standing then in complete darkness, stopped photosynthesis. The CO_2 level was lowered as much as possible (from about 400 ppm to slightly above 60 ppm).

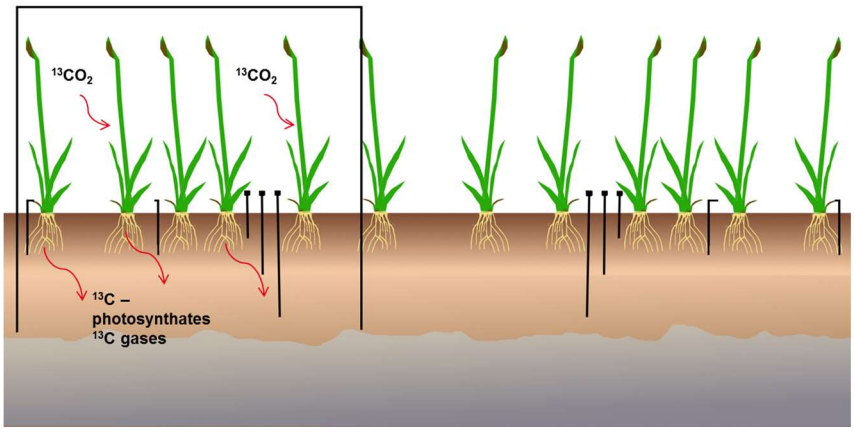

Figure 8. Experimental set-up. The labeling phase. The labeled area is hydraulically and atmospherically confined from the environment.

Phase 2: The CO_2 level was increased by inserting 100 ml of 99 % $^{13}CO_2$ and the darkening cover was removed. The carbon dioxide content inside the chamber was further increased by several times insertion of $^{13}CO_2$. Since no direct decrease of carbon dioxide could be observed, due to possibly lacking photosynthetic activity, it was decided to repeat the experiment the next day under the same conditions. The temperature inside and outside of the chamber was measured sporadically to make sure that the chamber temperature was not increasing above ambient atmospheric conditions.

The water vapor concentration was also checked and it increased slowly during the course of Phase 1 and 2. Phase 3: After five hours, the chamber was removed and the remaining ^{13}C-CO_2 was quickly removed by air turbulences.

The first label was set on August 16, 2013 (16:52-20:02, 3.16 hours) and the second label the next day on August 17, 2013 (12:26-17:30, 5.07 hours). It was labeled two times, in order to thoroughly and homogeneously label the belowground C-pools.

3.3 Sampling

The sampling took place one day before the labeling and subsequently daily after the labeling had been finished. Pore water was sampled daily from August, 18 to August, 29.

DIC and CH_4

The sampling occurred according to the following scheme: Water samples from 3 depths (6, 16 and 36 cm below ground surface) were taken with 50 ml syringes (Omnifix 50 ml, B.Braun, Germany). The syringe was locked to a fitting (female Luer Lock-to-barb) that connected the syringe via an Isoversinic hose to a stainless steel pipe (3.4 mm outer diameter, 2.0 mm inner diameter), which was inserted into the assigned depth. The pipe was closed on the bottom and had four small openings that allow water inflow. The syringe was rinsed two times with 20 ml pore water from the according depth, before the sample was taken and via a needle immediately inserted into a 60 ml lab vial. This vial were filled with the amount NaCl (p.a) that is necessary in order to oversaturate 60 ml of water (21.6 g), then made air tight with a grey chlorobutyl-stopper, and subsequently evacuated three times and then flushed with pure nitrogen. Finally, the bottle had a pure nitrogen atmosphere inside and was ready for sample water. The sample bottle was filled to about 75 to 80 % of its volume, in order to leave enough headspace volume for outgassing of pore water gases (CH_4 and CO_2, where CO_2 is the proxy for the DIC concentration in the soil pore water sample). The samples were stored at 5-7°C and kept under such conditions until they were analysed. Although gas leakage due to diffusion through the stopper (grey chlorobutyl stoppers, "20 mm Butyl-Hohlstopfen grau", IVA Analysentechnik e.K., Germany)

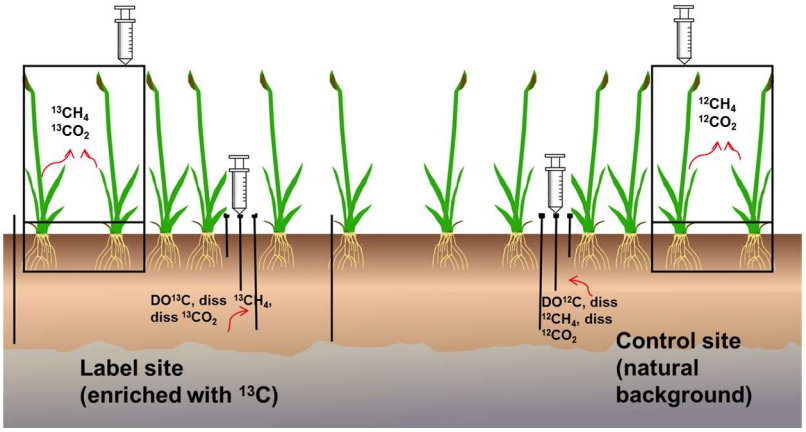

Figure 9. Experimental set-up. The sampling phase, after the pulse-labeling ceded.

was neglectible low, nonetheless the samples have been stored and transported bottom up to avoid direct contact between head space and the septum.

DOC

DOC was sampled the same way as DIC and CH_4. After sampling, the pore water has been inserted into a 15 ml lab vessel with a black bromo-butyl stopper (Glasgerätebau Ochs, Laborfachhandel e.K., Germany). The sample tubes have been filled with 1.5 ml of 0.05 m HCl solution to acidify the inserted sample and prevent it from microbial degradation. Together with the planned amount of about total 12 ml sample of about 6 pH (5.6-6.2 pH is expected in the polygon center according to Preuss (2013).

Soil and plant samples

Soil and plant samples were taken prior to and after the labeling experiment conduction. The samples were frozen and shipped to the Institute of Soil Science in Hamburg. A block of soil (from the surface to the depth of 40 cm, see Figure 10) was cut and further separated into sub-samples representing the material of the soil in the depths 0-10 cm, 10 – 20 cm, 20 – 30 cm, and 30 – 40 cm. All replicas were taken from the same block.

3.4 Physical and chemical soil properties

The frozen soil samples were used for determination of several basic soil parameters. If not noted otherwise, the methods explained in this section are based on the standard procedures in the Institute of Soil Science, Hamburg University, or based on Tan (2005).

Bulk density – soil particle density - Soil water content/porosity

The soil water content (porosity) was calculated with soil bulk density and soil particle density. Due to the small sample amount, both parameters are determined with a modified version of the method presented in (Tan, 2005). Then the pore space (porosity) can be calculated via the ratio of particle size density and soil bulk density.

$$2) \qquad pore\ space\ volume\ \% = \frac{100 \cdot bulk\ density \frac{g}{cm^3}}{particle\ size\ density \frac{g}{cm^3}}$$

Additional information is given in section A VI .

pH and HCO_3^-

The dried soil samples were diluted in water to create a suspension in which the pH value and the electrical conductivity were measured. Since the unlabeled soil samples were used up already for other measurements, the ^{13}C-labeled soil samples were used. Since the same sample material was to used for further analysis, the pH value was measured only in deionized H_2O.

Additionally, frozen soil samples (from the same site, this time unlabeled) were sliced out of a sample block (10 by 10 by 20 cm) of frozen surface soil). The mixed soil samples represent the soil depths 0-10, 10-20, 20-30 and 30-42 cm, while the freshly unfrozen soil samples represents the depths 5-6, 11-12 and 15-16 cm.

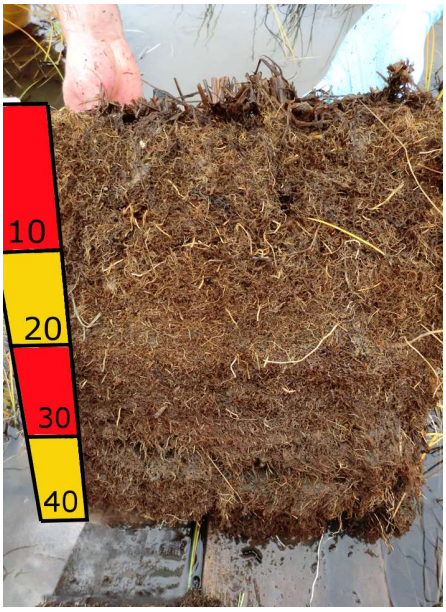

Figure 10. A sample block cut from the investigated soil. The picture represents the soil of about 40 cm of active layer. The permafrost table was in a depth of about 50 cm at the time of the experiment's end. The yardstick unit is in cm. The original photograph is digitally modified to insert the yardstick.

The pH directly controls the concentration of HCO_3^- and CO_2 in the pore water. It depends on the proton concentration how much of the dissolved inorganic carbon is transformed to HCO_3^-. The fraction of HCO_3^- is derived from Butler (1982) applying the equation

$$3) \quad log[HCO_3^-] = logK_{a1} + log[CO_2] + pH,$$

where $log[HCO_3^-]$ is the decadal logarithm of the hydrogen carbonate concentration, $logK_{a1}$ is the equilibrium constant, and $log[CO_2]$ is the concentration of carbon dioxide in the pore water. In this study, the data available is DIC concentration, i.e. HCO_3^- + CO_2, the equation can be used to find the fraction of HCO_3^- in DIC. Because of the relatively low expected pH values, the concentration of CO_3^{-2} was a priori neglected for this study.

For the pH values measured in the soil environment, the percentage of HCO_3^- is then used to estimate the amount of bicarbonate in the soil system.

Carbon content

Carbon content of plant leaves, plant roots and soil organic matter (SOM) was detected with an elemental analyser (vario Max cube, Elementar, Germany). Prior to measuring, the sample material was dried (at 70° C [1]) and ground.

Plant masses and plant $\delta^{13}C$, root masses and root $\delta^{13}C$

In order to estimate the uptake of tracer ^{13}C into the plant biomass, the plant mass per area unit and the ^{13}C content after the labeling experiment, together with plant C amount, root C amount and ^{13}C content were determined. The plant and root mass and C content was determined by weighing a sample of dried material before and after four hours incineration at 550° C in a muffle furnace. The weight difference between the dried sample (here dried at 70° C[1]) and the ash weight, is assumed to represent 2 times the carbon that is stored in the sample. Additionally, C/N was determined as mentioned in the C section above. The ^{13}C content was determined with the IRMS as mentioned in section 3.6 different instrument settings to allow detecting stable carbon isotope content in solid (dried and ground) substances.

3.5 Concentration of DIC, DOC, CH_4 in subsurface carbon pools

CH_4 and DIC

Prior to analysis, the samples were placed under laboratory conditions (about 20°C) for two days to allow a new equilibria between headspace CO_2 ($CO_{2\text{-}gas}$) and CH_4 ($CH_{4\text{-}gas}$) and dissolved CO_2 ($CO_{2\text{-}diss}$) and CH_4 ($CH_{4\text{-}diss}$). The CO_2 in both headspace and solution is assumed to represent the DIC fraction of the soil pore water. Due to the high solubility of CO_2 even in saturated NaCl solution, Henry´s law ($k_{cp} = cCO_{2diss}/pCO_2$) with k_{pc} being a constant for CO_2 in saturated NaCl solution, can be applied to obtain the total amount of DIC in the sample. More information about the Henry's constant and the correction factors applied for the CO_2 data processing is given in appendix A VII.

[1] In the sample preparation procedure of the Institute of soil science, plant and organic-rich soil samples that are subject to dry-weight based analytics (e.g. C/N content, $\delta^{13}C$ analyses) are not dried at 105 °C but at 70°C. At 70°C, practically all water that is contained in the organic matter is already evaporated. At higher temperatures there is a risk that already instable organic compounds such as certain lipids, organic-acids are cracked and released as gaseous carbon compounds. These compounds might contain significant amounts of label and their removal prior to analysis is to be avoided.

Due to the negligible solubility of CH_4 in saturated NaCl solution, the amount of CH_4 in the headspace already represents the total methane in the sample volume and hence does not require further data processing. The concentration of CO_2 and CH_4 in the headspace was measured with a gas chromatography (Gas chromotograph GC System 7890A, Agilent Technologies, USA). The headspace pressure was measured with a hand-held manometer (LEO 1, Keller, Switzerland) and the temperature was the ambient laboratory temperature (about 298 K).

The DIC concentration was calculated with Henry´s law, after a correction factor, which compensates for the pH –dependent formation of HCO_3^- in the solution, was applied (for additional information about obtaining the correction factors for CO_2 and data presentation, refer to section Appendices).

DOC

The DOC concentration was measured with a wet heated persulfate oxidation method (Aurora Model 1030, O-I-Analytical, USA). The sample preparation was the same as described for the $\delta^{13}C$ measurement of DOC and is explained in more detail there. The sample material, originally sampled for DOC analysis, was unfortunately lost. Therefore, the DOC concentration was measured from the sample material for the DIC and CH_4 analysis. As mentioned in that section, here the DOC-bearing solution is a saturated (6.12 mol) NaCl solution. An aliquote of the solution was extracted and the extinction behavior across the spectral wavelength range from 200 to 750 nm (UV-VIS range) was detected for each sample by means of a photospectrometer (Genesys 10uv, ThermoScientific, USA). Some liquid from 30 samples was filtered with a Whatman® GF/F filter (0.7 µm nominal filter offset, GE Healthcare Life Sciences, USA) with a syringe. The filtered aliquote was acidified with HCl and the organic carbon concentration was detected on a combustion catalytic oxidation TOC analyser (TOC-L, Shimadzu, Japan). The carbon concentrations of these selected 30 samples were related to the wavelength solution absorbance at the 254 nm wavelength, in order to obtain a calibration function that allows calculating the DOC concentration based on the absorbance at wavelength 254 nm from all other samples. Thus, by correlating the extinction intensity at 254 nm with the DOC-concentration obtained by the TOC-L analyser (which is regarded as being the "gold

standard"), the DOC-concentration of all samples was calculated. This method is inspired by work of Avagyan, Runkle, and Kutzbach (2014). The data is found in Appendices.

3.6 $\delta^{13}C$ value of the sub-surface carbon pools

$\delta^{13}C$ values (as basic data for calculation of ^{13}C concentration in the carbon pools), were determined with isotope-ratio mass spectroscopy.

$\delta^{13}C$ of CH_4 and DIC

The $\delta^{13}C$ values of both gases were detected with the same GC-IRMS (Gaschromatography-Isotope-Ratio-Mass-Spectrometry instrument, Delta Plus, Thermoquest Finnigan, USA). The gaseous sample was taken out of the vial headspace with a microliter syringe. Since the total C amount injected would be detected as signal, the injected amount had to be adapted to the calibrated signal strength of the ion detection cups. The syringe is flushed once with 50 µl of sample gas, then inserted into the sample gas and 5 to 6 times flushed with head space gas (to produce a well-mixed headspace gas in the vial) and then taken out. It followed the injection into the GC-device. In the GC, the CH_4 and CO_2 are separated on a Porapak Q column and the CH_4 is at 940 °C oxidized to carbon dioxide, since the MS-device detects only CO_2 molecules. Both CO_2 and CH_4 can be detected in the same detection process, however, due to the different concentrations (because a certain minimum amount of carbon has to be injected) they are usually measured separately. Each sample was measured two times. If both values differ more than ± 0.5 $\delta^{13}C$ from each other, the measurement is repeated a third time and mean values of the measurements were calculated. For quality control the standards LSVEC (Lithium Carbonate, $\delta^{13}C$ = -46.6) and IAEA B7 (Limestone, $\delta^{13}C$ = -3.0) were measured at least twice at each measurement day. The standards were measured to the beginning and at the end of each measurement campaign. When the measured $\delta^{13}C$ values of the standards were close to their expected values (device calibration, as given above), the spectrometry device was operational and the $\delta^{13}C$ given by the device is quality-checked.

$\delta^{13}C$ of DOC

DOC was measured with a GC-IRMS instrument (Delta Plus V, Thermoquest Finnigan, USA). Prior to injection into the GC-IRMS device (by an autosampler), the DOC material is oxidized in a TOC analyzer (Aurora Model 1030, O·I·Analytical, USA). The CO_2 produced in this process is then transmitted to the GC-IRMS device.

Prior to analysis, the sample was filtered with a syringe through a Whatman® GF/F filter (0.7 µm nominal filter offset, GE Healthcare Life Sciences, USA). For quality control the standards USGS 40 (L-glutamic acid, $\delta^{13}C$ = -26.39, VPDB) and IAEA C6 (Sucrose, $\delta^{13}C$ = -10.8, VPDB) were taken. These standards have been measured in the automatized procedure before and after each series of samples, each time with three replicas.

$\delta^{13}C$ as tracer

The observed tracer concentration in the investigated carbon pools DIC, CH_4, and DOC is the foundation of the model-based plant-soil system analysis. Since the carbon pools of interest have a natural $^{13}C/^{12}C$ isotope composition, the isotope signal induced by the labeling experiment has to be separated from the natural background signal prior to further analysis. The natural background ^{13}C content of all carbon pools is about 1% ^{13}C of the total carbon. The applied highly ^{13}C-enriched CO_2 is used to trace atmospheric-derived carbon (ADC) allocation into the belowground. To quantify the label incorporation, the sample $\delta^{13}C$ value has to be compared to a natural background $\delta^{13}C$, which can be obtained by analyzing unlabeled carbon pools samples. Wu et al. (2010) used the ^{13}C-excess % to quantify the tracer incorporation into a carbon pool with the equation

$$4) \qquad {}^{13}C_{labelled}\,\% - {}^{13}C_{natur\ \ background}\% = {}^{13}C - excess\,\%$$

a term that represents additional incorporated ^{13}C into the pool and hence quantifies the label incorporation. With this unit, the total label recovered in all pools can be estimated and set to 100 % of recovered label. This enables the calculation of percentages of label incorporation into each single pool (% label of total ^{13}C recovered). And with this term it is possible to estimate the percentage of ADC which is allocated to the different sub-surface carbon pools and hence allows establishing the distribution of photosynthetically incorporated carbon into the belowground carbon pools.

Another variant to express the tracer concentration is to calculate the amount of "labeled" ^{13}C, i.e. ^{13}C which is higher as the background ^{13}C concentration, in relation to the total C in a pool. This is shown by

$$5) \qquad mg\ {}^{13}C_{excess}\ L^{-1} = {}^{13}C_{excess}\ \% * 100 * Carbon_{content},$$

where $Carbon_{content}$ is the carbon concentration per liter (equation from Wu, 2010).

Upscaling

For comparison with related studies, carbon content and tracer concentration data is scaled up to an area unit. In such cases, bulk density of soil and pore space values are used to estimate the amount of carbon or of carbon-tracer per square meter. Then, for error propagation estimation, the error propagation equation is used (e.g. Sachs and Hedderich, 2009).

3.7 Modelling tracer concentration time series

Lognormal model (LM)

Tracer outwash curves may appear in many shapes, because they are functions which at least depend on the size of the traced pool (the amount of "tracee"), the turnover rate of this pool and the tracer concentration in the influx. To define, whether an observed time series of tracer concentration in the sub-surface carbon pools qualifies as a tracer outwash curve is difficult, because often – especially in studies with low sample numbers – the tracer outwash curve is not fully observed (observational period is too short, or starts too late, or both) and only a fragment of the total tracer concentration time series is observed. In soil systems, where some pools have turnover rates of months to years, it is almost impossible to measure the entire tracer outwash function (until it is indifferent from the natural background value of the tracer). For more information about this topic refer to publications from Norwich (1977) and Anderson (1983).

(Norwich, 1977) mentions the use of lognormal and gamma function to model the tracer outwash curve, stressing that this comes without a physical basis. However, existing tracer outwash curves from several studies and different shapes of lognormal function intuitively seem to be related. Qian and Bassingthwaighte (2000) gave a mathematical foundation to the use of lognormal functions as

models for tracer concentration time series in vascular networks, i.e. systems in which the tracer is incorporated into many different compartments with different sizes and different mean residence times. It seems logical to assume that the soil system with its numerous sub-carbon pools with different sizes and different mean residence times (e.g. roots, fine roots, old roots, microorganisms, plant stems and leaves, soil organic matter and dissolved carbon) is in principle comparable to a vascular network. Lognormal models for TCTS modelling in a constructed wetland is successfully done by – for example - Cui et al. (2012).

Therefore, in this study, to analyze whether or not the observed tracer time series in dissolved sub-surface carbon pools are tracer outwash curves, a simple model will find the best-fitting lognormal function for each tracer time series.

The standard lognormal distribution is given (e.g. in Sachs and Hedderich, 2009) as

$$6)\ f(x) = \frac{1}{\sigma x\sqrt{2\pi}}\, e^{\frac{(ln\, x-\mu)^2}{2\sigma^2}}$$

where σ is the standard deviation of the lognormal distribution, x the input variable, μ the expectation value. The formula was modified in the sense that a scaling factor is added and the μ-variable is always set to zero. To achieve faster results, a scale-term is added, which allow scaling the function in the region of the observed tracer time series. A simple GA algorithm is used to find the best-fit parameters which produce a lognormal distribution that fits well to the observed tracer concentration series. These model approach only models the tracer concentration in the system pools and gives no further information about the system parameters. However, it allows estimating the general tracer concentration in the system and its extrapolation beyond the observation period.

Having successfully established an adequately parametrized log-normal function, which allows describing the outwash curves of carbon in the different sub-surface carbon pools, these function can be applied to extrapolate the carbon retention in the respective carbon pool. Thus, by establishing a set of log-normal tracer outwash function for all sub-surface carbon pools, the average retention time of each carbon pool can be estimated.

Compartmental model (CM)

The lognormal model (LM) reproduces only the TCTS observed in a system. With this information, the mean residence time of the traced substance can be estimated. To obtain information about the connection among system compartments, compartmental models are needed, because the simple tracer concentration curve itself allows only the estimation of the mean residence time of ADC in the system. Compartmental models are used to estimate turnover rates and fluxes in an investigated system (e.g.: Luo et al., 2003). The research plan outlined for the current study requires the formulation of a conceptual and then a mathematical model of the sub-surface tundra soil system.

Conceptual compartmental model formulation

Firstly, a conceptual compartmental model of the investigated system is developed. Then, based on the information of the analytical procedure and the constraints imposed by the conceptual model, a mathematical model is developed, which purpose is to quantify fluxes between carbon pools in the belowground soil environment.

Table 4. List of major carbon pools in the investigated system.

atmospheric CH_4
atmospheric DIC
plant stem and leaves (in our system only *Carex* aquatilis)
moss (only Scorpidium scorpidoides)
fine *Carex* roots
coarse *Carex* roots
dead *Carex* roots
dead moss
dissolved inorganic carbon
dissolved methane
dissolved organic carbon
other soil organic matter*.

* This category encompasses old soil organic matter, recalcitrant carbon compounds (such as lignin) and other organic compounds that are not included in the model and the investigation.

Usually, the model of choice is a simplified, mathematical copy of the system, which represents the system in such a way that it allows estimating how the observed system's states will evolve during

the modelling period (Jørgensen and Fath, 2011). The potential pathways of C fluxes between the different pools are given in Table 5.

Table 5. Matter transfer connections of carbon pools in the investigated system (inspired by Schlesinger (1997) and Whiticar (1999)).

atmospheric CO_2 – plants/mosses
plant-stem-plant roots
moss (suprasurface)-moss (sub-surface)
roots – pore water DIC (auto respired CO_2)
roots – pore water dissolved organic carbon (DOC, photosynthates (exsudates))
pore water DOC- pore water CH_4
pore water DIC – pore water CH_4 (hydrogenotrophic methanogenesis)
pore water DOC – pore water DIC (acetoclastic methanogenesis)
pore water CH_4 – pore water DIC (methanotrophic reactions)
roots – pore water DOC (dying roots)
other soil organic matter – pore water DOC, pore water DIC and pore water CH_4
pore water DIC – atmospheric CO_2 pool
pore water CH_4 – atmospheric CH_4 pool

Firstly, all systems states have to be defined (e.g. in a soil-plant system these states can be roots, leaves, soil organic matter etc.). The major carbon pools in the system under investigation are listed in Table 4. The pools are interconnected by different pathways, along with which carbon is allocated into the system. In comparison to many medical-biological tracer studies (e.g. Anderson, 1982) it is difficult to formulate spatially distinctive pool connections for a soil-plant-atmosphere, because of the microscale of the different pools and because of the diffuse connections of the pools among each other. All our pools are spatially close together, practically continuously connected across plant root-water interfaces, moss-water interfaces. This brings a high degree of complexity. A list of pool-pool interconnections is given in Table 5 and Figure 11. The system of the tundra wetland soil is assumed to be sufficiently described by the compartments (carbon pools) given in Table 6.

Table 6. The final compartments and fluxes that are applied to model the sub-surface carbon system.

Pools	Transfer coefficients (outbound flux)

X_1 (dissolved CO_2 , or DIC)	a_{17}, a_{12}
X_2 (dissolved CH_4)	a_{27}, a_{21}
X_3 (DOC)	a_{31}, a_{32}
X_4 (fast-turnover soil carbon pool)	a_{41}, a_{42}, a_{43}
X_5 (mediate-turnover soil carbon pool)	a_{51}, a_{52}, a_{53}
X_6 (slow-turnover soil carbon pool)	a_{61}, a_{62}, a_{63}
X_7 (atmospheric carbon pool)	plant and sub-surface pools

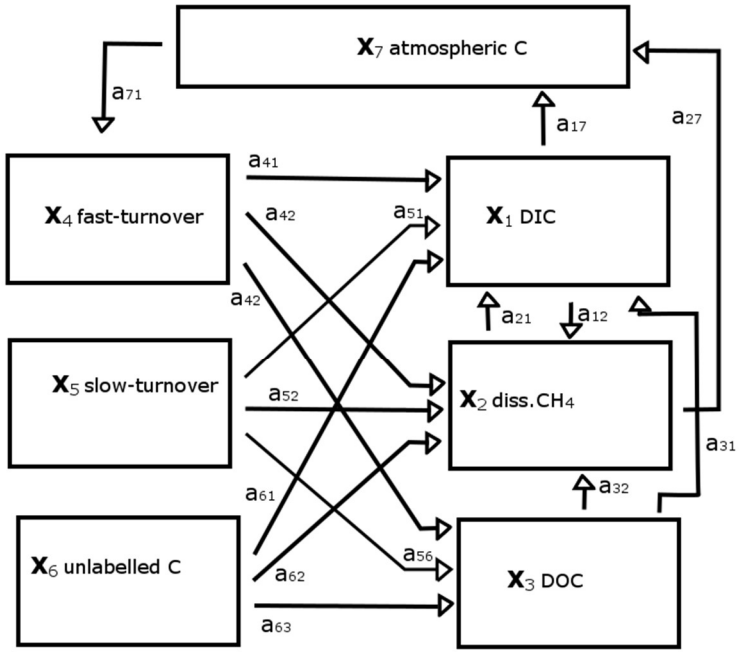

Figure 11. Conceptual model of the sub-surface interconnections of carbon pools as assumed for this investigation project. The soil carbon pools X_1 (DIC), X_2 (CH_4), and X_3 (DOC) were measured for tracer concentration. The pools X_4, X_5, and X_6 represent a fast-turnover carbon pool (X_4; simple sugars and acids with short turnover rates), a mediate-turnover pool (X_5; more recalcitrant compounds such as lignin or cellulose), and unlabeled carbon (X_6; encompasses all carbon which is not affected by the label and still enters the sub-surface carbon cycle). The fluxes between the pools are a_{ij}, where i and j stand for the pools from and to which the flux is directed (for further explanation see text and Table 7).

Additional assumptions are made to apply a compartmental model (according to Norwich, 1977; Anderson, 1982):

- Only the introduced label leads to changes of the δ^{13} signature
- no major carbon pool is missed
- the system is in steady state
- the pools are well-mixed

Mathematical model formulation

The model formulation is based upon the assumption that the compartments of the system (plant tissue, roots, dissolved carbon pools etc.) are steady-state pools (hence the system is a stationary system; this assumption is tested with the Cox-and-Stuart test). In steady-state pools (compartments) of a system (e.g. sub-surface dissolved inorganic carbon concentration) do not vary in size. This implies that the amount of material brought into one compartment (from a neighboring compartment or from outside) is equal to the amount of material that leaves the compartment (to a neighboring compartment or out of the system). Theoretically, no changes of concentration are observable in a stationary system and hence no time-dependent concentration change in system carbon pools is detectable.

However, the dynamics can still be simulated by following a tracer particle on its way through the system. The mathematical model is developed to deliver a sufficient accurate depiction of the natural carbon cycle pathways and fluxes. The mathematical formulation for the tracer concentrations in the sub-surface carbon pools (conceptually depicted in Figure 11) are defined by the following equations:

7) $$\frac{dC_{tracer\_DIC}}{dt} = a_{21}C_{tracer\_CH4}(t) + a_{31}C_{tracer\_DOC}(t) + a_{41}C_{tracer\_X4}(t) + a_{51}C_{tracer\_X5}(t) + a_{61}C_{tracer\_X6}(t) - (a_{12} + a_{17})\, C_{tracer\_CO2}$$

8) $$\frac{dC_{tracer\_CH4}}{dt} = a_{12}C_{tracer\_CO2}(t) + a_{32}C_{tracer\_DOC}(t) + a_{42}C_{tracer\_X4}(t) + a_{52}C_{tracer\_X5}(t) + a_{62}C_{tracer\_X6}(t) - (a_{21} + a_{27})\, C_{tracer\_CH4}$$

9) $$\frac{dC_{tracer_{DOC}}}{dt} = a_{43}C_{trace\ _{X4}}(t) + a_{53}C_{trac\ \ _{X5}}(t) + a_{63}C_{trac\ \ _{X6}}(t) - (a_{31} + a_{32})\, C_{tracer\_DOC}$$

.

Here, it is assumed that the pools X_4, X_5, and X_6 represent pre-pools, i.e. pools that potentially transfer carbon to the pools X_1, X_2, or X_3. These pools might be sugars, proteins, lipids – theoretically all plant-produced compounds which have been synthesized by the plant during the labeling phase and which are now subject to microbial or plant respiration. The complexity of these different pools makes it literally impossible to separate them and analyze their $\delta\ ^{13}C$ signature. Therefore, they are seen as potential suppliers of tracer, which insert material into the three sub-surface carbon pools DIC, CH_4, and DOC. Since they are huge in comparison to those dissolved carbon pools, the time-dependent tracer concentration in these pools will have a major effect on the time-dependent tracer concentration displayed in the dissolved carbon pools. The development of these equations was inspired by Norwich (1977) and Anderson (1983).

The equations above mean that, for example in compartment X1 (the carbon dioxide pool), at an infinitesimal small time step (Δt), a_{12} times the amount of X1 is transferred to X2 (the methane pool) and a_{17} times the amount of X1 is transferred to X7 (the atmospheric carbon pool). With transferring the model formulation into an algorithm the tracer concentration dynamics in each carbon pool of interest can be simulated. Of course, the parameters must be defined accordingly. The model was developed for this study, inspired by publications from various authors (for the compartmental model theory: Norwich, 1977; Anderson, 1983; Munk, Keiding, and Bass, 2003; Bassingthwaighte and Beard, 1995; for background knowledge of the soil system in wetlands: Whiticar, 1999; Jones, Nguyen, and Finlay 2009; Wania et al., 2013; Marushchak et al., 2016)).

The assumption is made that this mathematical formulated model can be parametrized in a way that the model- produced TCTS best fit the observed TCTS.

A genetic algorithm (GA) is used for solving the inverse problem of finding the best (optimal) tracer concentration reproduction of observed tracer concentration values in the natural soil system, i.e. the TCTS_sim which is the best approximation of the TCTS_obs. The genetic algorithm serves as a tool for extracting the information of interest (the fluxes in the sub-surface carbon system) by finding the model reproduction of the system that bears the closest resemblance to the in-situ detected tracer concentration changes. The GA- program used for finding the best-fitting CM model parameters is explained in section 3.9.

3.8 Mean Residence Time

The mean residence time (MRT) is defined as the reservoir-mass to reservoir net-flux ratio; a synonym is turnover time. Another widely used term, turnover rate, is expressed as 1/MRT (Schlesinger, 1997; Zilversmit, Entenman, and Fishler, 1943). Danckwerts (1953) and Fogler (2016) published equations which allow the calculation of the mean residence time (MRT) based on a TCTS. The procedure is explained here following the nomenclature given by Fogler (2016). The same terms and equation formulation as used by Fogler (2016) are used in the following section and for the calculation of the mean residence time of the tracer for this study.

The time-dependent function of the tracer concentration, so far mostly termed TCTS, is a function

$$10) \qquad C(t) = TCTS,$$

where *C(t)* is the concentration function and *TCTS* is the tracer concentration time series. Equation 10 can be transformed to the residence time distribution function E(t) as shown in equation 11).

$$11) \qquad E(t) = \frac{C(t)}{\int_0^\infty C(t)dt}.$$

According to Fogler (2016) from this equation the mean residence time of a substance in a chemical reactor – as which the soil system in this study is interpreted – can be obtained by equation 12:

$$12) \qquad t_m = \int_0^\infty tE(t)dt,$$

where t_m is the mean residence time.

With this set of simple equations, the mean residence time of any tracer in a pool can be calculated, even when the particles in the system – or "chemical reactor" [2], as written by Fogler (2016) – have different mean residence times.

Because the natural background $^{13}C/^{12}C$-value is obtained by a Monte-Carlo approach from a set of natural background $^{13}C/^{12}C$-values. Therefore, randomly 15 natural background $^{13}C/^{12}C$-values are selected, from which one is selected to be the denominator. All selected values are divided by this denominator and reduced by 1. From all these values the standard deviation is calculated. This

[2] Fogler (2016) terms all reactors non-ideal, in which the particles, or molecules spent different times in the system or reactor. Some of molecules might leave the system almost immediately after introduction; others might spend significantly longer in the system until they are excreted.

process is repeated 1000 times, i.e. 1000 different standard deviations for the zero-line (the natural background $^{13}C/^{12}C$ ratio is set to zero) are produced. From these thousand values, the simple mean is taken as the standard deviation from zero for the zero-line value (which represents the natural background). The mean residence time is calculated according to the equations 10, 11, and 12. From the E(t)- function a linear function is subtracted which has the following form:

$$13) \qquad y = t(t_{cut} - t_0)\frac{1}{t_{cut}},$$

where t_{cut} is the time when the modelled tracer washout function crosses the zero-line standard deviation. The tracer is assumed to be completely washed out at the time step t_{cut}, where the modelled tracer concentration is smaller than the zero-line standard deviation. The MRT is calculated based on three replicas. The error of MRT was calculated by producing thousand Gaussian-distributed random values based on the mean and the standard deviation of the three replicas. For each of this thousand TCTS the MRT was calculated (simple Monte-Carlo method). The mean and the median, and standard deviation and the 15 % and 85 % quantile, respectively, of these thousand ensembles is calculated and given as error data.

3.9 Genetic algorithm (GA) program

In this section, the development of the compartmental soil system model (CARBUCKS) and the genetic algorithm for solving the inverse modelling by numerical optimization is described.

A list of model parameters is defined in Table 7. The constraints are formulated because of the requirement that each pool and the total system of aquatic carbon pools represents a steady-state system.

Table 7. List of parameters (model input constants and variables), which have to be optimized to find the optimal model parametrization, and constraints, which reduce the vastness of the feasible search space.

No	*Parameter name (fixed)*	*Description*
1	poolsize_DIC	the fixed size of the DIC pool
2	poolsize_CH_4	the fixed size of the CH_4 pool
3	poolsize_DOC	the fixed size of the DOC pool
4	time_step_0.25	fixed model time step of 0.25 hours (900 seconds)
No.	*Parameter name (variable)*	*Description/constraint*

1	x_1	mean residence time of the DIC pool (X_1)
2	x_2	mean residence time of the CH_4 pool (X_2)
3	x_3	mean residence time of the DOC pool (X_3)
4	a_{21}	amount of C transported from X_2 to X_1
5	a_{31}	amount of C transported from X_3 to X_1
6	a_{41}	amount of C transported from X_4 to X_1
7	a_{51}	amount of C transported from X_5 to X_1
8	a_{61}	amount of C transported from X_6 to X_1
9	a_{12}	amount of C transported from X_1 to X_2
10	a_{32}	amount of C transported from X_3 to X_2
11	a_{42}	amount of C transported from X_4 to X_2
12	a_{52}	amount of C transported from X_5 to X_2
13	a_{62}	amount of C transported from X_6 to X_2
14	a_{43}	amount of C transported from X_4 to X_3
15	a_{53}	amount of C transported from X_5 to X_3
16	a_{63}	amount of C transported from X_6 to X_3
17	ini_tracX$_4$	initial tracer concentration in pool X_4
18	decl_tracX$_4$	mean residence time in pool X_4
19	ini_tracX$_5$	initial tracer concentration in pool X_5
20	decl_tracX$_5$	mean residence time in pool X_5
	Constraints	*Description*
1	$X_1+X_2 \geq X_3$	X_3 cannot be larger than a_{31} and a_{32}, because these are the only fluxes that go out of the pool. Since a_{31} cannot be larger than X_1 and a_{32} not larger than X_2, the constraint is explained
2	$a_{17} = X_1 - a_{12}$	the pool X_1 has two fluxes that take carbon out of the pool and a_{12} is chosen for randomly
3	$a_{27} = X_2 - a_{21}$	the pool X_2 has two fluxes that take carbon out of the pool and a_{21} is chosen for randomly
4	$a_{32}+a_{31} = X_3$	since a_{31} and a_{32} are the only fluxes that leave X_3, they cannot be larger or smaller than X_3 (the turnover rate of X_3)
5	$a_{21} + a_{31} + a_{41} + a_{51} + a_{61} = a_{17} + a_{12}$	The steady-state condition for each pool (i.e. the amount of matter that leaves and enters the pool at any time step)
6	$a_{12} + a_{32} + a_{42} + a_{52} + a_{62} = a_{27}$	The steady-state condition for each pool (i.e. the amount of matter that

	$+ a_{21}$	leaves and enters the pool at any time step)
7	$a_{41} + a_{42} + a_{43} + a_{51} + a_{52} + a_{53} + a_{61} + a_{62} + a_{63} = a_{17} + a_{27}$	The steady-state condition for the total system. The system cannot receive more matter than what it releases in the outer-system environment

In Table 8 all elements of the computer program which is used for genetic algorithm optimization are presented.

Table 8. Elements of the optimization program.

Data source or algorithm	*Description*
Observed tracer concentration	the data to compare and fit the modelled tracer concentrations to (i.e. tracer concentrations from dissolved DIC, CH_4, and DOC
CARBUCKS (system model)	numerical model. Input: flux values in mgL^{-1} -timestep, mean residence time of carbon pools in percentage · $timestep^{-1}$, output: tracer concentration time graphs
optimization function	a function that evaluates the goodness of fit between the produced tracer concentrations (by CARBUCKS) and the observed tracer concentrations
genetic algorithm	a program that tries to find ever-better parametrizations for CARBUCKS by applying a simple genetic algorithm

In general, an optimization program seeks to find minima or maxima values of a (objective) function f(x).

$$14) \quad \min_{x \in R^d} f(x) \ , \ so\ that\ the\ constraints\ are\ fulfilled$$

where *f(x)* is an objective function and $x \in R^d$ is a set of variables x from the total possible search space R^d (Nocedal and Wright, 2006). In the current study, the optimization program seeks to find the optimal set of parameters for the CARBUCKS model, i.e. the parametrization of CARBUCKS that best reproduces observed tracer concentration in DIC, CH_4, and DOC. The list of parameters (set x) is given in Table 7. The multi-dimensionality of the problem strongly suggests a numerical optimization approach to find the best values for the parametrization of the model CARBUCKS.

The numerical optimization process was separated into sub-processes, because the enormous calculation time needed (called "The curse of dimensionality" by Bellman (2003)) to do the optimization with all parameters was unsuited for investigating the optimization procedure performance with the technology at hand (desktop PC). In the sub-parameter GA optimization process, the mean residence times X_1, X_2, and X_3, as well as the tracer concentration and decline in X_4 and X_5, are constants and the optimization procedure seeks to find the optimal parameter fitting

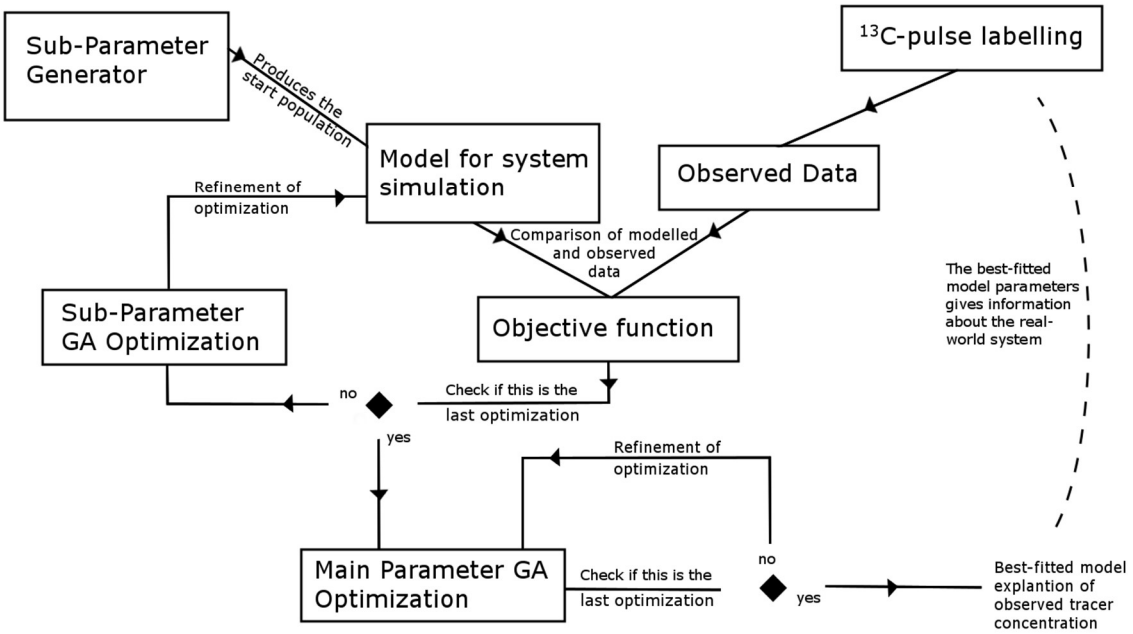

Figure 12. The search process for finding the best-fitting model parameter is displayed. The main programs and data sources are shown as rectangular boxes. The lines represent the information flux. For further explanation see text. The main parameters are the mean residence times (x_1, x_2, x_3) of the pools, the sub-parameters are the flux parameters (a_{12},..., a_{ij}).

with these fixed constants. This strategy enables to investigate, whether or not the optimization procedure can find a set of optimal values under these given conditions. This is also shown in Figure 12. After it is generally clear, whether or not the optimization procedure finds a set of optimized parameters for the given constants, the optimization procedure can be run more general, seeking to find sets of optimal parameters for all unknown variables (in the total feasible search space). In order to optimize a system, an objective function has to be formulated. An objective function is a function

that maps the function's co-domain (all possible output values of a function) onto a single value. The goal of the optimization process is to find the smallest value of the objective function. In this case study, the objective function is a set of numbers given to a certain function realization, which gives information about how close the model produced function is to the observed, observed data. In this study, because the optimization procedure optimizes the fit to three different functions (DIC, CH_4, DOC), it is a multi-objective optimization problem. A multi-objective optimization problem requires an objective function which is optimized in several dimensions. The model output has to be optimized against the three observed TCTS (TCTS_obs) in DIC, CH_4, and DOC. To achieve this, two simple objective functions were developed as shown in the next sub-section, a simple residual-least-square-sum method (RLSS) and a newly-developed penalty method, which was necessary to avoid the system being stuck in a local minimum.

For each observed tracer concentration point C_{tracer} (t) in time the related CARBUCKS-produced tracer concentration point C_{model} (t) is chosen and the difference d_{t_m} (t) calculated with ($d_{t\_m} = (C_{tracer} - C_{model})^2)^{0.5}$. A value $a_{penalty}$ is calculated by $a_{penalty} = d_{t\_m}/C_{tracer}$. A list of penalty thresholds is defined such that the penalty value $p_{penalty} = \exp(a_{penalty})$. Thus, the higher the difference between observed and modelled tracer concentration point at time t, the higher is the value $p_{penalty}$ assigned to time t. The sum of all $p_{penalty}$ of DIC-, CH_4-, and DOC – tracer points is the objective function $f_{obj}(x)$ and x is the set of the parameters to be optimized. With this approach the impact of the huge difference between the tracer concentrations in DIC, CH_4, and DOC is levelled out, because the objective function consists of the relative distance of a newly produced model-data point from its observed counterpart. Because a fairly good-fit can be unrelated to the actual shape of the TCTS_obs, another term in the objective function (with a weight of 40 %) is implemented, which compares the dC/dt-function of TCTS_obs with the dC/dt-function of modelled TCTS (TCTS_sim) and decides whether they are similar or not (a simple pattern-recognition method). Additionally, the algorithms structure allowed the investigator to interfere, i.e. if the algorithm tended to be stuck in a local minimum, producing TCTS_sim which were not close to TCTS_obs, the user could "help" the algorithm to get out and sniff through other parts of the search space. The interference of the user is possible because the different operators of the GA algorithm, mutation and crossover, which control the algorithm, have

certain probabilities to occur. In the beginning phase, when the system is totally unknown, each member of the start population (in this study: fluxes and mean residence times), can be recombined with any other member. Each member could be subject to mutation. After the system found a number of better-fitting realizations, the probability is increased that only better-fitting specimen recombine or mutate, to produce new specimen. At an even later stage, worst-fitting members are excluded from any further population development. Because this process requires a lot of time, the user can dynamically interact with the running algorithm and play around with the probability that certain population members are selected for "breeding". This helps to reduce the total amount of time required to find adequate optimal solutions for the system.

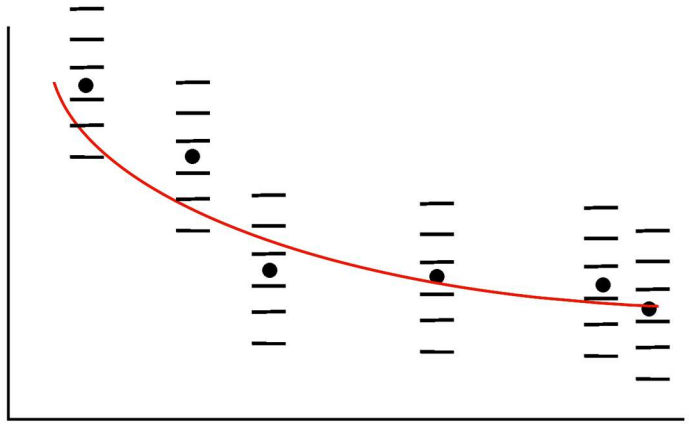

Figure 13. A penalty-objective function is schematically depicted. In certain distances from the y-value of the observed data point (black dots) a threshold is defined (e.g. ± 0.1 · y +y, ± 0.5 · y +y etc., black lines). The model output value (red line) crosses the y-line of the data point and falls into the defined interval between thresholds. In dependence of the definition, a penalty value is given for each model y-value. The further away the threshold interval it falls, the higher the penalty value. The smallest penalty value is given if the model y-value falls in the central interval, which also contains the observed data point.

3.10 Statistics and calculations

The model approach (see below) requires a stationary system. To test, whether the carbon pools in the system (DIC, CH_4, and DOC) have invariant sizes or not, the observed time series is investigated with the Cox-and-Stuart trend test. This trend test result gives information, where any observed trend in the concentration data of the sub-surface carbon pools is significant or not.

The statistical calculations and most of the descriptive data graphs in this study are mostly done with the R language R Core Team (2012) or with Microsoft Excel from Microsoft Corporation (2010). If other programs are used, it is explicitly mentioned in the text. Image manipulation was done with the GIMP program GIMP developer team (1997). The model algorithm and the simulations are also done with R.

T-Test for difference between $\delta^{13}C$ signature in control and label

An important task in this study is the decision whether or not there is a $\delta^{13}C$ signature difference between label and control samples. This decision is made with the help of a t –test (One sided or One sample t-test) in R. The confidence level is set to 95 % (According to Sachs and Hedderich (2009) and the R Core Team (2012)). The t-test is the recommended test to test for an actual difference between two sample population means, when the sample size is small (de Winter 2013). Moreover, the one-sided t-test is the right choice if only higher values can occur in the comparison ($\delta^{13}C$ values can only increase with added label) and has a higher power (Sachs and Hedderich, 2009).

Cox-and-Stuart trend test

To determine whether or not a trend is observable in a time series data of carbon pool concentration in dissolved carbon pools, the Cox-Stuart trend analysis is used according to Sachs and Hedderich (2009) and the 'snpar'-Package R (R Core Team, 2012). The Cox-and-Stuart test allows testing a time series for an observable trend.

Goodness of fitting

In this study, two different models, the LM and the CM, are fitted against the observed tracer concentration time series. As a measurement for the goodness of fit, the adjusted R^2-value is applied (as, for example, by Ronkanen and Kløve (2007) and by Beven and Young 1988)).

Error estimation with Monte-Carlo simulation and Gaussian distribution

In cases where a result value is to be calculated based on a number of parameter-values, all coming

along with standard deviation, a simple Monte-Carlo approach is usually used for error estimation. Randomly, based on the mean and the standard deviation of the parameters used for the calculation, ensembles with n=500 or n=1000 are produced. From this number of values, the mean and the standard deviation is taken and given as data. For example, this approach has been used to calculate the MRT values from the compartmental model-produced transfer coefficients and the carbon pool size. The carbon pool size comes along with a simple standard deviation, the transfer coefficients are only given with their quantiles 0.15 and 0.85. So for each value of the transfer coefficients (n = 20), 500 Gaussian distributed pool sizes have been randomly created using the R function 'rnorm'. Each value is combined with the transfer coefficient, so 10000 values are created. From this value set, the mean and the simple standard deviation are given as MRT data. This method is inspired by the publication of Anderson (1976).

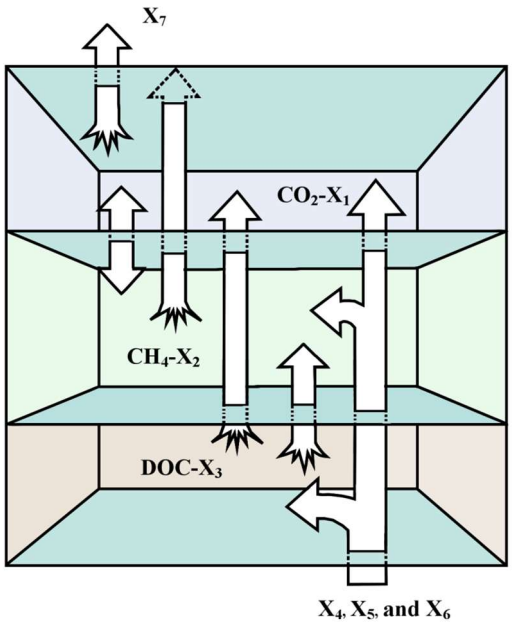

Figure 14. Conceptual graph explaining the transformation of L^{-1} to m^{-2} for comparison with different investigations of the carbon cycle in tundra soils. The cube represents the liter volume (with 10 cm side lengths). The white arrows represent the carbon flux into one of the three sub-surface carbon pools (DIC, CH_4, DOC). Note that CO_2 is identical with DIC.

Transformation of fluxes with the unit $mgL^{-1}h^{-1}$ to mg Cm^{-2} d^{-1}

In this study the flux is usually expressed as mg C $L^{-1}h^{-1}$. This can be transformed to mg C $m^{-2}d^{-1}$ with the factor 2400 (100 times 24). If the liter-unit is expressed as 10 cm^3, then it has a total surface of 60 cm^2 (6 times 10 cm^2). Conceptually, it is assumed that the soil system consists of many "liters". New carbon atoms enter the volume (liter) from the fast-, slow-, and very slow-turnover pools X_4, X_5, and X_6. It "appears" in a liter of soil pore water being excreted by a plant root or a moss thallus. Inside the "liter"-volume, each C molecule can appear in one of the carbon pools DOC, DIC, or CH_4. Each

atom could migrate among the compartments or leave the "liter" of pore water in upward direction. This can be interpreted as crossing the upper surface of a 10 cm^3 cube (a liter), hence the fluxes into the cube, inside the cube and from the cube can be interpreted as mg C 0.01 m^{-2} h^{-1}. For example, to scale this unit up to the commonly used flux unit mg C m^{-2} d^{-1}, the observed value has to be multiplied by 2400.

4 Results

4.1 Soil properties

The data presented in Table 9 shows the high porosity of the soil material and also the relatively high C content in the soil. The top layer (0-10 cm) C content (0.15 g C g^{-1} soil) is more than twice as high as the carbon content of the deeper layers and has also a higher pore space (i.e. porosity). The soil substrate in the upper layer consists of living *Scorpidium*-moss, into which the *Carex*-roots grow. Soil layers below 10 cm show a higher particle size density and bulk density (0.3-0.56 g cm^{-3}), indicating a higher deposition of mineral (fluviatile and aeolian) sediments. The porosity is highest (91 %) in the first layer and decreases further downward. The water level was on the surface during the investigation period of 2 weeks.

Table 9. Bulk density, particle size, porosity and C content in the 0-42 cm depth of the polygonal center soil

Depth (m)	Dry weight (g)		Bulk density (g cm^{-3})		Particle size density (g cm^{-3})		Pore Space L/L		C per soil weight (%)	
	Mean	SD	Mean	SD	Mean	SD	Mean	SD	Mean	SD
0-0.1	15.42	3.00	0.20	0.04	2.09	0.01	0.91	0.04	18.38	4.25
0.1-0.2	23.37	2.11	0.30	0.03	2.52	0.03	0.88	0.03	8.16	2.10
0.2-0.3	26.17	6.49	0.33	0.08	2.19	0.52	0.86	0.12	6.17	1.82
0.3-0.42	43.78	4.71	0.56	0.06	0.18	0.18	0.78	0.09	6.03	0.93

The pore water is slightly acid and has a relatively high electrical conductivity (208.3 ± 28 µS cm^{-3} in 0-10 cm depth, 258.7 ± 53 µS cm^{-3} in the depth 30-40 cm, see Table 10 and Table 45). The pH controls the fraction of HCO_3^- (see equation 3), which concentration is calculated by the bulk DIC concentration and the pH value. At the depths of 6, 16 and 36 cm the fraction of HCO_3^- is about 5 % of the total DIC concentration, so the HCO_3^- constitutes only a small fraction of the DIC. Only in the lowest parts of the active layer, in the depth of 30 cm and deeper, the fraction of HCO_3^- reaches about 10 %.

Table 10. Ph and HCO_3^{-1} in four depths.

Depth (cm)	0-10	10-20	20-30	30-40
pH	4.6	4.66	5.18	5.59
HCO_3 in DIC %	1.19	1.36	4.44	10.51

4.2 C pools and content

The soil-plant system is separated into supra-surface carbon pools (in this system only *Carex* shoots) and sub-surface carbon pools (*Carex* roots, *Scorpidium* -mosses, soil organic matter, dissolved carbon pools). The mosses serve as substrate for the *Carex*-roots, which are found in all depths growing around moss thalli. It is obvious from Figure 15 that the vascular plant vegetation (*Carex*) is a small carbon pool, compared to the total amount of carbon stored in the soil horizons. Figure 16 gives a more detailed carbon distribution pattern; in this figure, the carbon content is given as percentage of the total carbon and is further divided into sub-carbon pools, which are shown in Figure 17. Most of the C is stored in the mosses in the upper two layers (24.11 and 20.53 %, respectively). The second largest fraction is the small-particle size organic rich material, which is not analyzed any further, and which is about 4 and 5 % in layer 1 and layer 2, respectively.

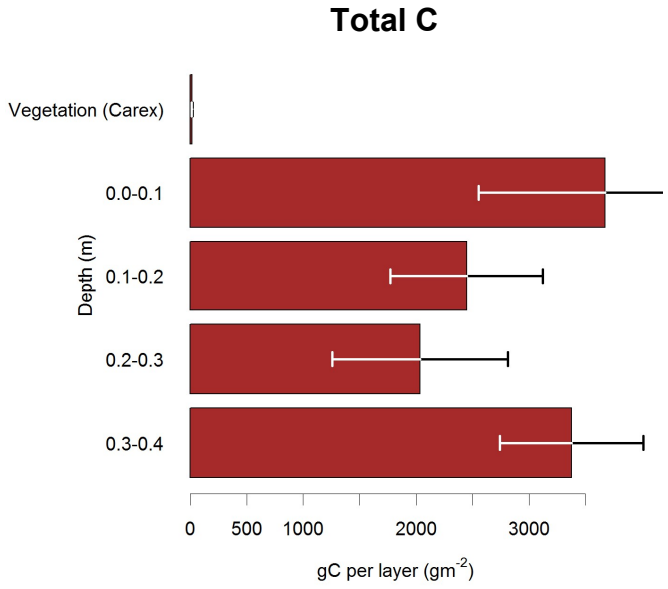

Figure 15. The total amount of carbon in vegetation and four soil depths is shown. The error bars represent one standard deviation (n=5, for 0.3-0.4 m n=3).

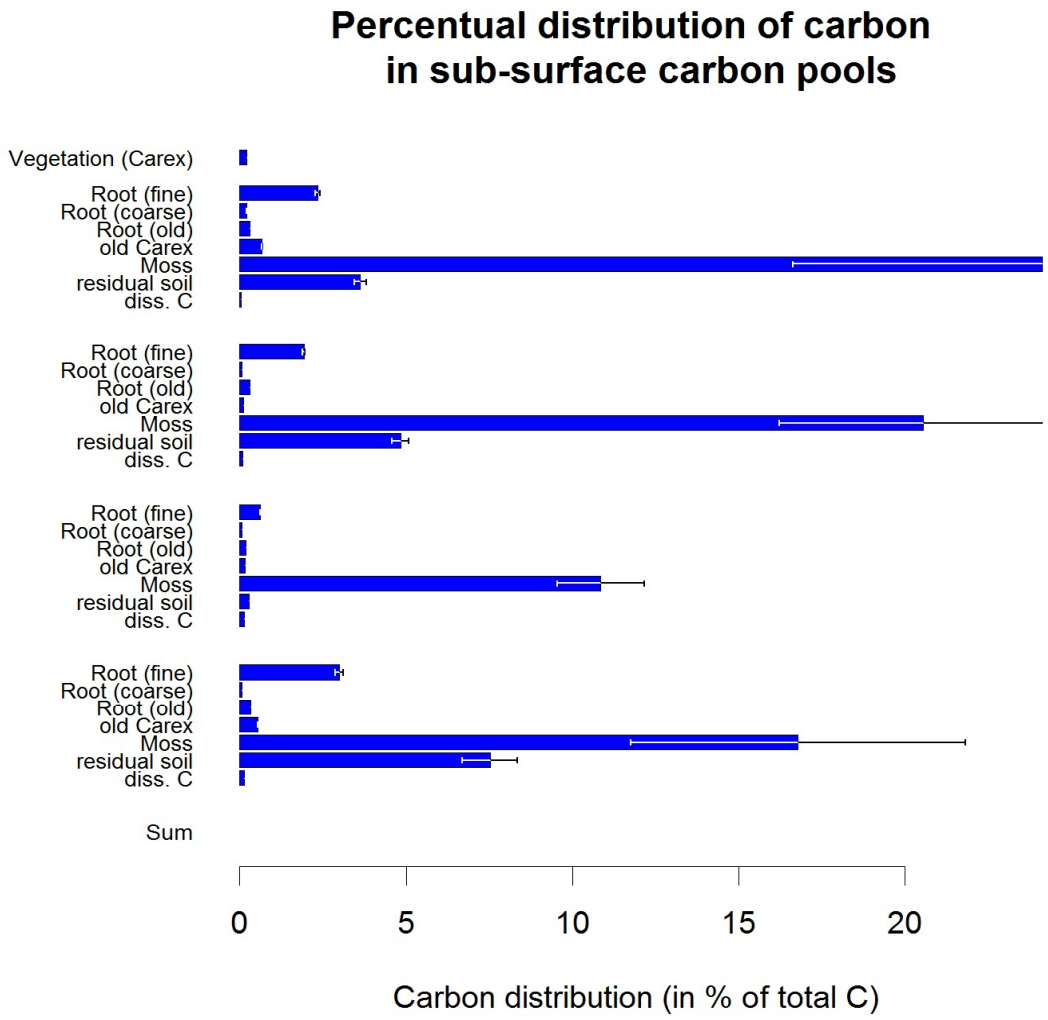

Figure 16. Carbon distribution in the polygonal center. Carbon pools are divided into sub-carbon pools. The error bars represent one standard deviation. The dissolved carbon (DIC, CH_4, and DOC) are summed up and displayed for comparison reason as dissolved C in this graph.

The roots represent small carbon pools (2.8 % of total found C in the first and 2.3 % of total C in the second layer; even less is found in the depth beneath 20 cm). In Figure 16 it is shown that the dissolved organic carbon content is small in comparison to the largest carbon pools carbon pools (the ratio of C % moss to C % dissolved organic carbon is 602 in the first layer and 256.65 in the second layer). In the dissolved organic carbon pool are three carbon pools combined: dissolved CH_4, DIC,

and dissolved organic carbon (DOC). These carbon pools are important for the tracer dynamic investigations in consecutive sections. Figure 17 shows the major sub-surface carbon pools in the soil system. Three roots categories (old, coarse, and fine) have been identified, together with *Carex*-remainders and moss. In general, the DIC concentration increases with depth and shows some variance. However, the concentration remains relatively stable over time – which is an important precondition for the compartmental analysis. The CH_4 concentration displays a similar stable pattern during the sampling period, which is displayed in Figure 19. The Cox-and-Stuart trend test results for each depth and time series show that a directed trend is statistically unlikely ($p>0.025$) in the dissolved carbon pools (compare to Table 29, Table 30, and Table 31 in Appendices). Therefore, the carbon concentration in the sub-surface carbon pools can be regarded as stable – an important pre-condition for the stationarity of the system. The CH_4 concentration and the DOC concentration are displayed in Figure 19 and Figure 20. The concentration of these sub-surface carbon pools does not display a clear time-dependent trend and, as DIC, can be regarded as constant.

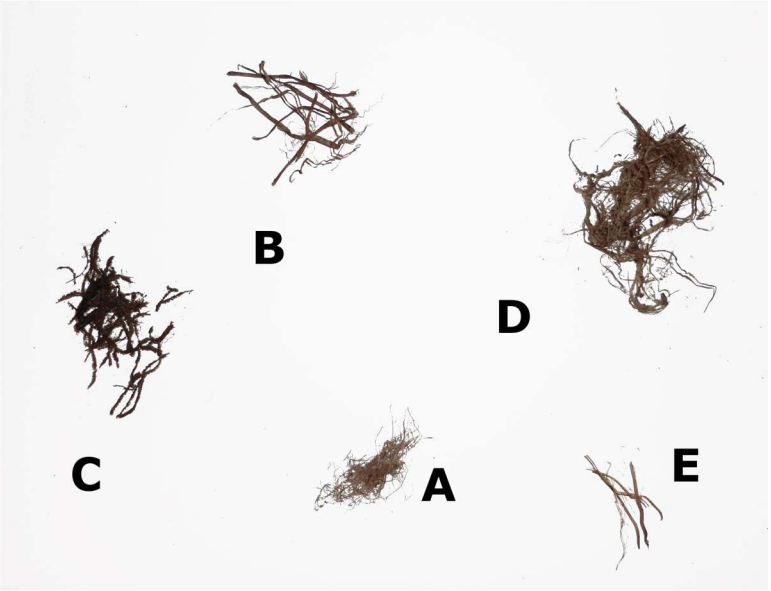

Figure 17. The major sub-surface carbon pools. A are the finest roots (Ø ≤ 1 mm), B are larger roots, brownish, beginning of decay, C are Scorpidium moss thalli, D are decayed *Carex* remainder, and E are fresh, coarse roots.

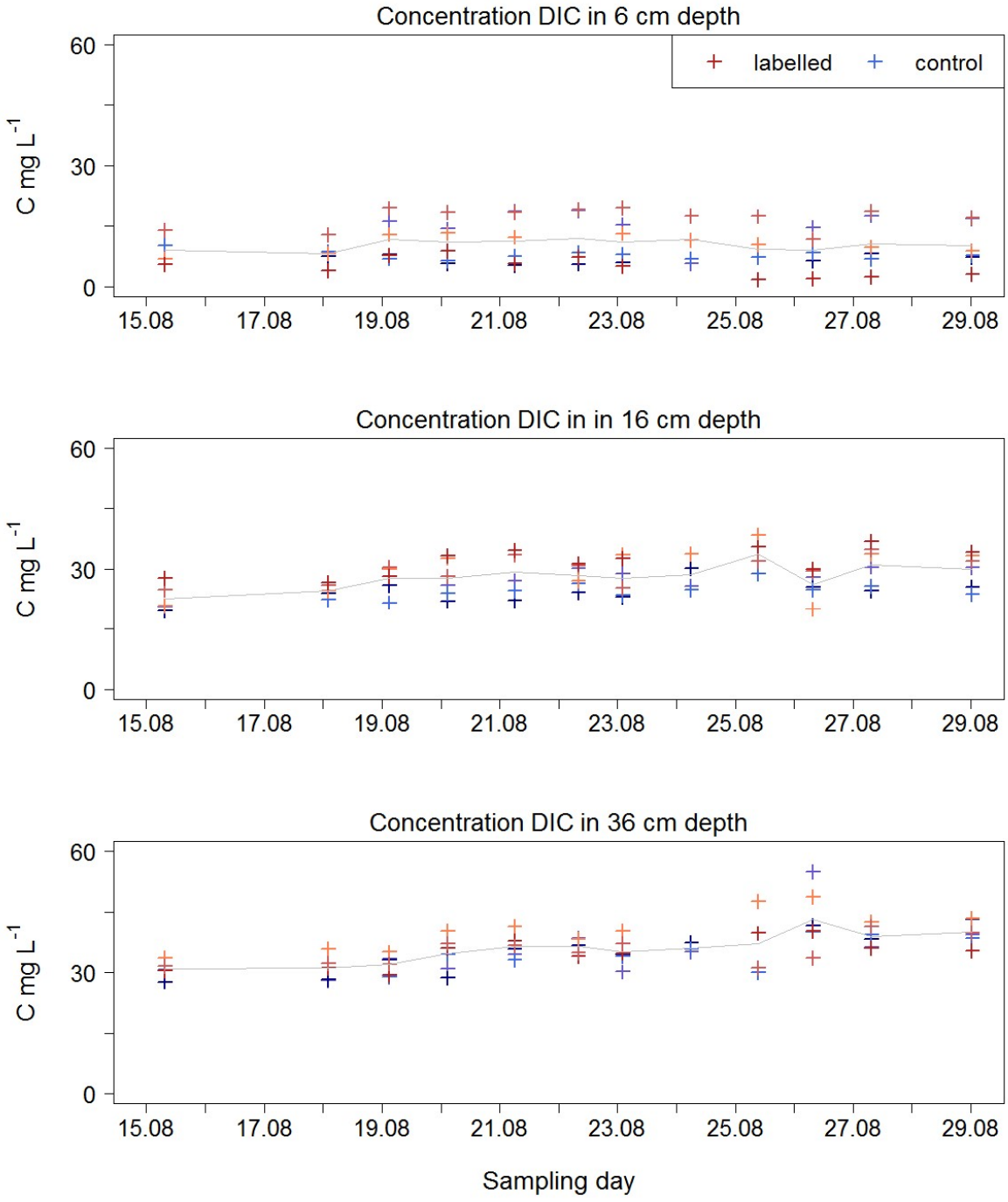

Figure 18. In three graphs, the concentration of DIC in three soil depths is depicted. The control (unlabeled) samples are in shown in bluish colors; the labeled samples are hold in reddish. The x-axis unit is dd.mm.2013, the x-tick is always set at 00:00 UTC for each day.

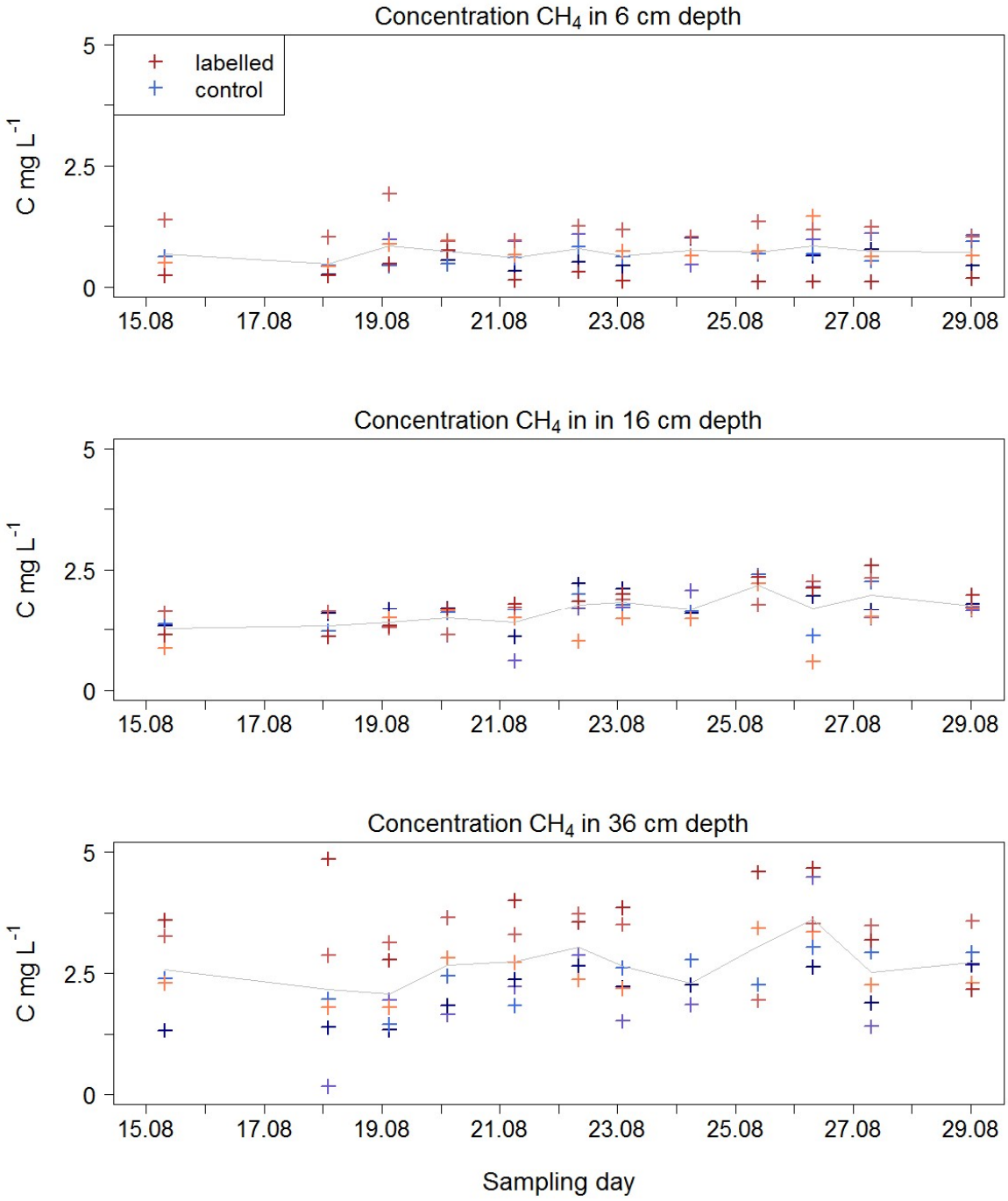

Figure 19. CH_4 concentration in three different soil depths. The control (unlabeled) samples are in shown in bluish colors; the labeled samples are hold in reddish. The x-axis unit is dd.mm.2013, the x-tick is always set at 00:00 UTC for each day.

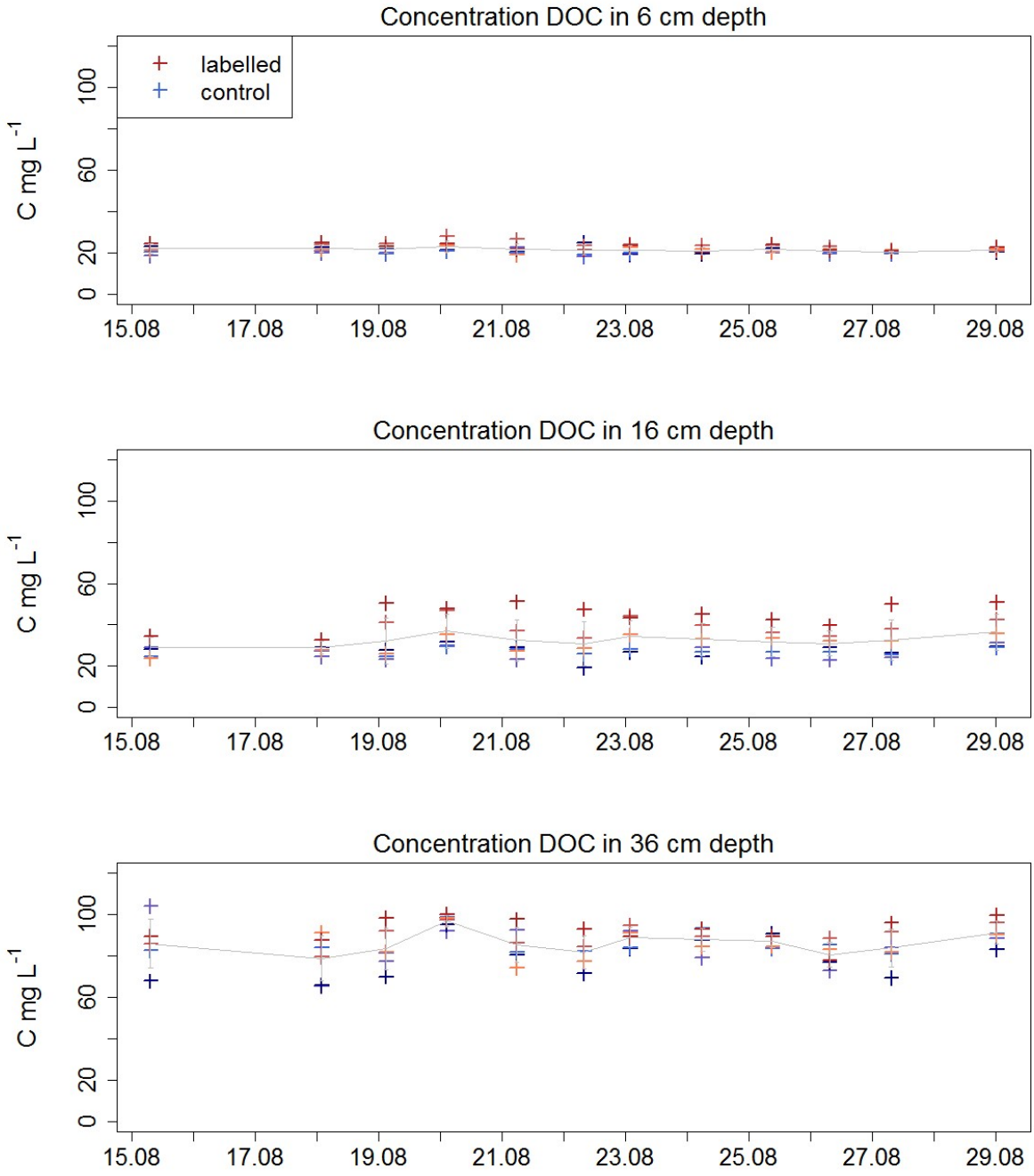

Figure 20. DOC concentrations in 3 different soil depths. The control (unlabeled) samples are in shown in bluish colors; the labeled samples are hold in reddish. The x-axis unit is dd.mm.2013, the x-tick is always set at 00:00 UTC for each day.

Potential amount of tracer in the system

The maximum amount of tracer given to the system is shown in table Table 11. During the labeling process repeatedly amounts of 10 to 180 ml of 99 % ^{13}C-CO_2 were injected into the chamber.

Table 11. The total amount of tracer exposed to the system.

	^{13}C addition (ml)	mol	mg
Sum	872	about 0.03893 mol STC	0.467 g ^{13}C

In total, about 0.5 g ^{13}C was exposed to the total system, i.e. assuming it is all found in the first 10 cm of the soil system, with an area of 0.63 m^2 or 63 dm^2, about 0.00794 g or 0.7 mg ^{13}C-tracer L^{-1}.

4.3 Tracer concentration in solid carbon pools

The pattern of tracer incorporation in the system shows is an altogether different compared to the total carbon content. The most active parts of the ecosystem incorporate most of the tracer per mass unit. The highest amount of tracer is found in the *Carex* -pool (see Figure 21), with 0.034 ± 0.0014 ^{13}C-excess %. The tracer incorporation in the first soil layer (living moss) is already an order of magnitude lower (0.0042 ± 0.0016). The label concentration shows generally a high variance. Even in the deepest investigated soil depth, 30-40 cm below surface and only 10 cm from the permafrost-table, there is still

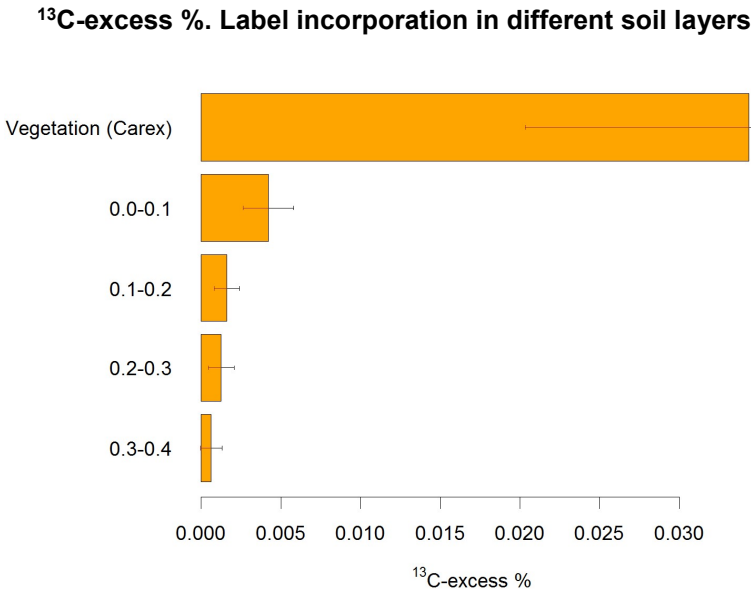

Figure 21. The ^{13}C-excess % values are shown. The ^{13}C-excess % is interpreted as the tracer. It is clearly visible that the highest tracer incorporation per mass C in the pool is observed in the supra-surface carbon pools (*Carex*). The near-surface sub-surface pools exhibit higher tracer concentrations than the lowest sub-surface pools ("Lowest" means close to the frozen layer surface), n_{carex} = 6, $n_{layer1\text{-}layer3}$ = 5, n_{layer4} = 3).

label presence observable. The label concentration shows generally a high variance. Even in the deepest investigated soil depth, 30-40 cm below surface and only 10 cm from the permafrost-table, there is still label presence observable.

The solid sub-surface carbon pools (*Carex* roots, moss, total soil organic matter) were sampled after sampling period had been stopped (29/08/2013, 12 days after the second and last label had been applied). The $\delta^{13}C$ data, used to calculate the label concentration at that time in the samples, therefore do not represent the most labile ADC in those pools. Those carbon compounds are likely to be respired already.

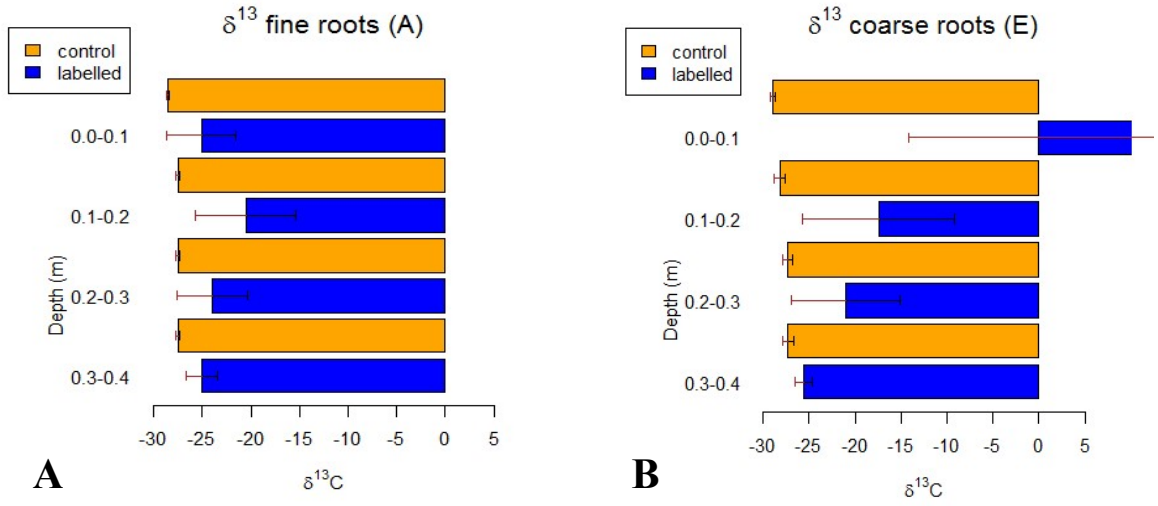

Figure 22. Label concentration in fine (A) and coarse roots (B) is shown. The fine roots show a clear label incorporation. However, per gram material, the highest concentration is displayed in coarser roots. This roots are hence the most prominent tracer storages.

The boxplot in Figure 24 shows in general high variances in labeled replicas and low variances for the unlabeled replicas. The box plot diagram in Figure 24 gives an overview about the medians and the quantiles of labeled and unlabeled $\delta^{13}C$ signatures in the investigated sub-surface carbon pools.

While the label is significantly incorporated in fine roots, coarse roots and the *Scorpidium* moss in the first 10 cm, a significant difference between $\delta^{13}C$ signatures is rejected by the t-test for example in the *Scorpidium* pool in 10-20 cm depth (for statistics compare Table 36 to Table 41 in Appendices). Observed increased variance still indicates the label's existence. Tracer, i.e. artificially increased $\delta^{13}C$ signatures in investigated carbon pools, is found in all types of sub-surface carbon

pools, even in the "dead"-root-pool. The highest tracer incorporation in the first layer, 0-10 cm below the water level/moss thalli is mainly directed into the coarse roots (up to 17.29 ± 31 $\delta^{13}C$). The control ^{13}C – values of the lower layers, 20-30 cm and 30-40 cm, are not available. Only the labeled site values are investigated and can be used for further comparison. The percentages of tracer allocation in the total system show that most of the tracer (24.8 ± 7.2 % and 21.05 ±10.7 % in the depth of 0-10 and 10-20 cm, respectively) found in the moss in the upper layers (down to 20 cm

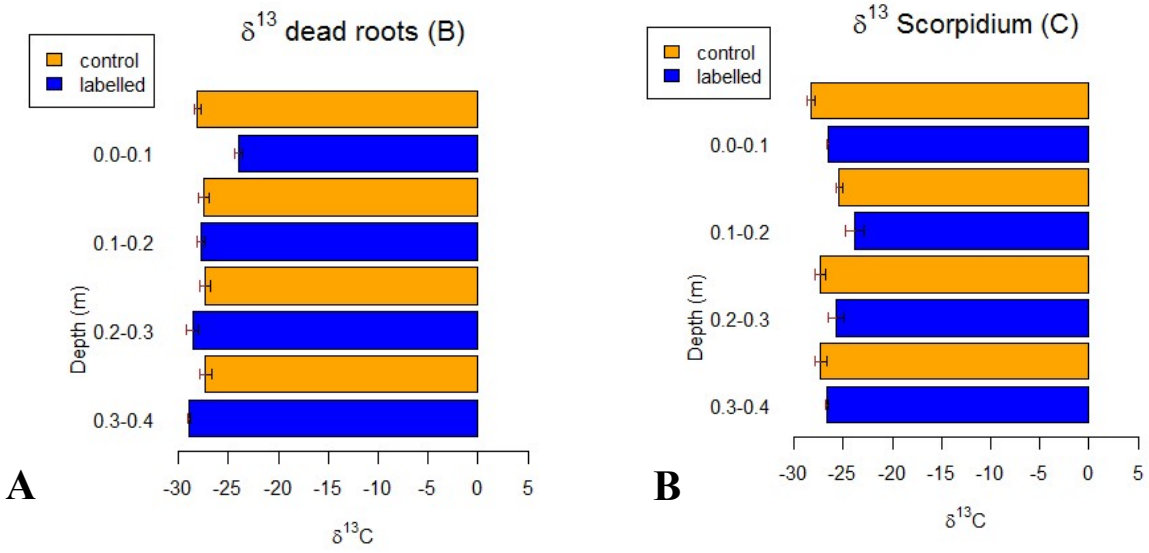

Figure 23. A) Tracer concentrations in "dead" *Carex* roots. Brownish-yellowish, as they appeared in the separation process, they were labeled "dead". However, it turns out that they were actively participating in plant's metabolic cycle, witnessed by the tracer incorporation. B) Tracer concentrations in the *Scorpidium* moss. The tracer is doubtless found in the first soil layer. It remains questionable, whether it is found in *Scorpidium* of the lower layers. The higher standard deviation of the labeled replicas indicates a slight incorporation, which is statistically (T-test) not feasible.

depth). The fine root in depth 0.3-0.4 still incorporates 4.2 ± 5.5 % of the total label (see Figure 25 and Table 12).

Total ^{13}C signatures in labelled and control carbon pools

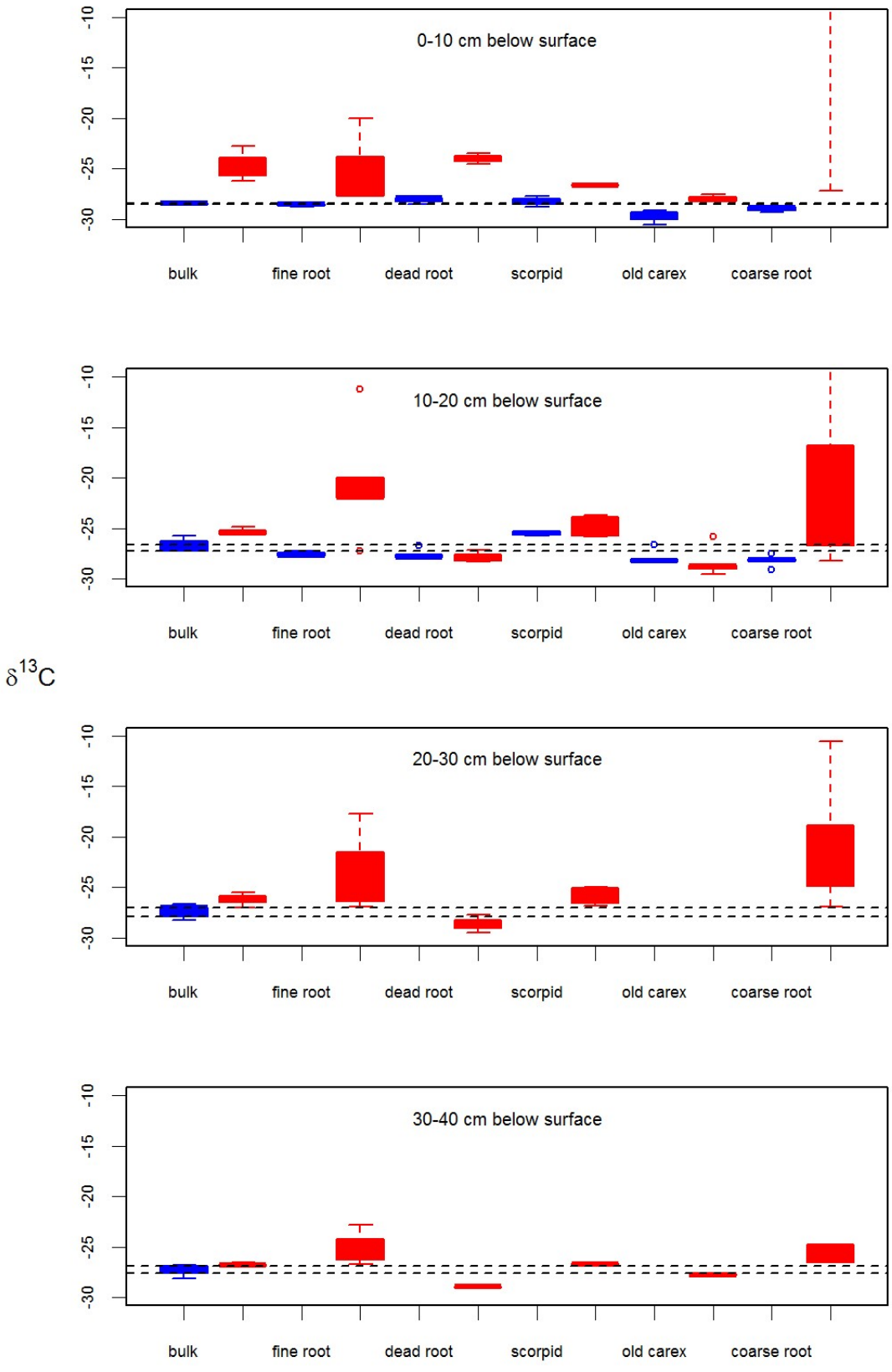

Figure 24. $\delta^{13}C$ signatures in different sub-surface carbon pools, labeled (red), control sites (blue). N is 3-5. The whiskers with dotted lines represent the upper and the lower quartile. Single dots above or below a box are extreme values (larger than 1.5 times the respective quartile value). In the depths 20-30 and 30-40 cm below surface, no natural background site data is available, only label site data is shown (except for bulk soil carbon). The red error bar in the 0-10 cm depth for the labeled coarse roots shows that the value of coarse roots is very high, beyond the limit of this graph and clearly indicate label incorporation.

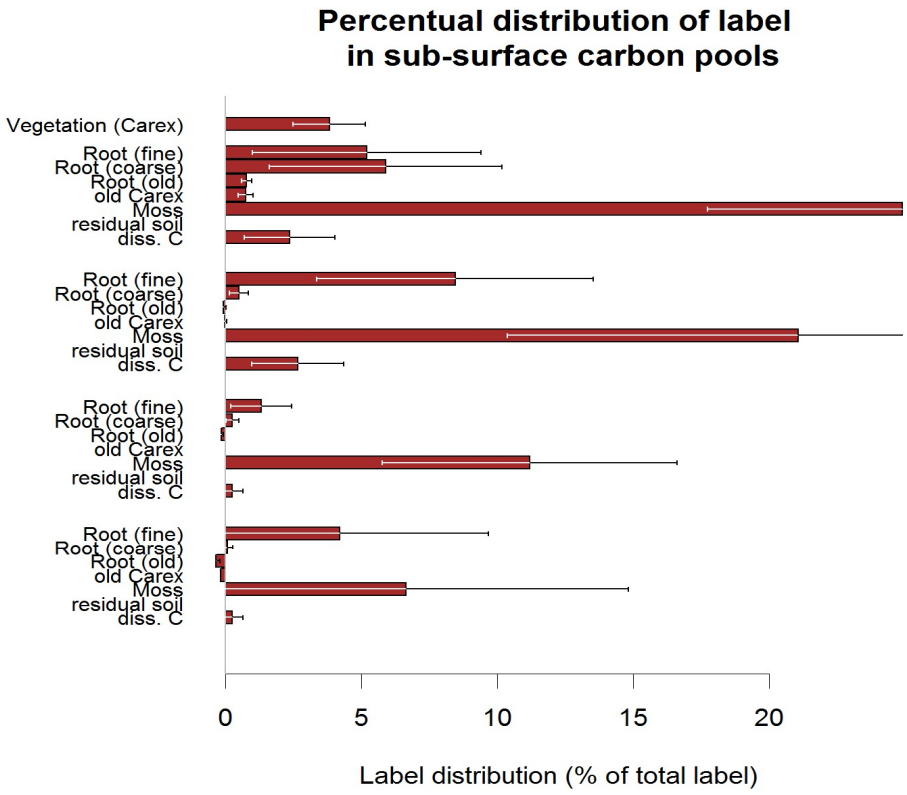

Figure 25. Total label distribution in the system. In comparison with Figure 21, where the label concentration per mass of carbon pool was presented, here the total label found in the system is the labeled sub-pool ^{13}C- concentration and the ^{13}C-concentration of the bulk soil C compared to the label found in each of the sub-carbon pools. Because the natural background $\delta^{13}C$-signatures for the two lower horizons where not available, the ^{13}C-excess values is calculated based on the difference between the bulk soil $\delta^{13}C$-signature and the labelled $\delta^{13}C$-signatures of the sub-pools.

Table 12. Percentage of label found in various carbon pools of the investigated tundra soil. The value for dissolved C represents the amount of label at the end of the experiment, i.e. after the concentration seems to level out for the observational period. The dissolved C-pools encompasses the sum of tracer found in DIC, DOC, and dissolved CH_4.

Depth	Carbon Pool	Percent of total label (%)	sd
Vegetation	Vegetation (*Carex*)	3.83	1.3
0.0-0.1	Root (fine)	5.21	4.2
	Root (coarse)	5.9	4.3
	Root (old)	0.79	0.2
	old *Carex*	0.76	0.3
	Moss	24.88	7.2
	residual soil		
	diss. C	2.37	1.7
0.1-0.2	Root (fine)	8.46	5.1
	Root (coarse)	0.51	0.3
	Root (old)	0	0.1
	old *Carex*	0	0.1
	Moss	21.05	10.7
	residual soil		
	diss. C	2.67	1.7
0.2-0.3	Root (fine)	1.33	1.1
	Root (coarse)	0.27	0.2
	Root (old)	0	0.1
	old *Carex*		
	Moss	11.2	5.4
	residual soil		
	diss. C	0.27	0.4
0.3-0.4	Root (fine)	4.22	5.5
	Root (coarse)	0.07	0.2
	Root (old)	0	0.1
	old *Carex*	0	
	Moss	6.65	8.2
	residual soil		

diss. C	0.27	0.4

4.4 Tracer concentration time series in dissolved carbon pools

In this section, the tracer values (artificially enriched ^{13}C values) of dissolved carbon pools are displayed and interpreted as tracer incorporation into these pools.

Firstly, the actual ^{13}C values in the labeled and the control sites are presented. It is obvious from the figures above (Figure 27 to Figure 34) that the label is present in all sub-surface carbon pools, though with varying intensity. The highest values are measured in the DIC-pool in 6 cm depth with up to 1.4 ^{13}C-excess % (see Figure 26). The ^{13}C-excess % in the first layer (6 cm) CH_4 pool is high as well, reaching about 0.2 ^{13}C-excess %. The tracer concentration is generally high in the 6 cm depth.

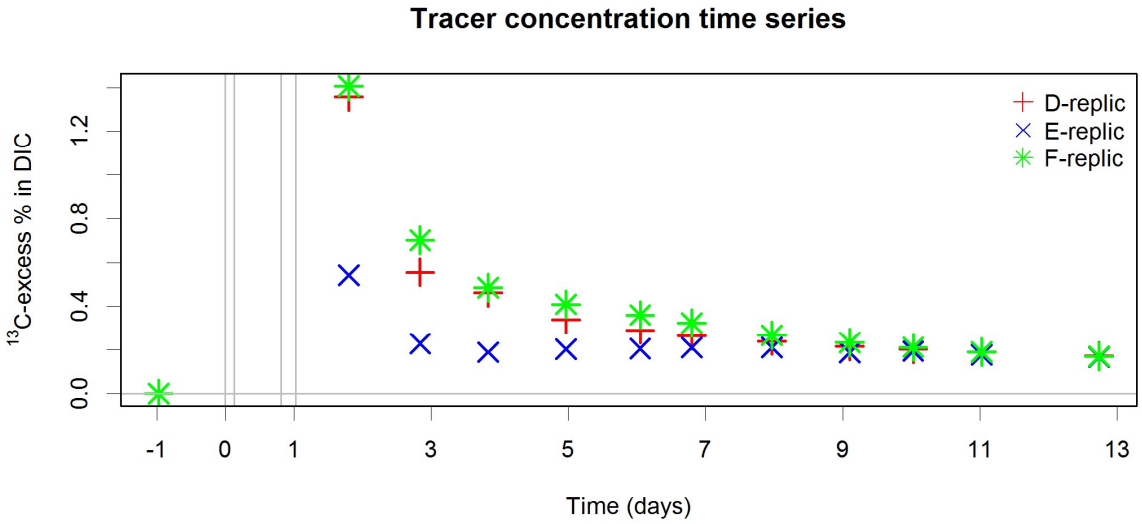

Figure 26. ^{13}C-excess % values of DIC in three labeled sites (Depth: 6 cm). The three sampled replica are denoted as D-, E-, and F-replica. The light-grey vertical lines represent the pulse-labeling periods. The time axis is normalized to the first tracer contact with the system. The data point at -1 represents the not-labeled ^{13}C concentration prior to the experiment, which is equal to the natural background and therefore 0 in the ^{13}C-excess graph. The gray vertical lines symbolize the both labeling periods.

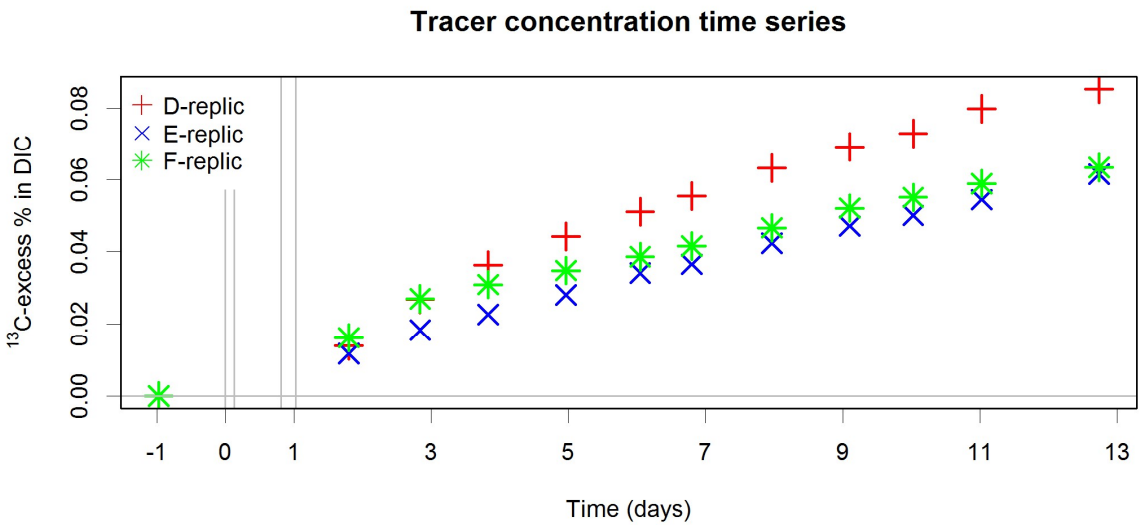

Figure 27. ^{13}C-excess % values of DIC in three labeled sites (Depth: 16 cm). The three sampled replica are denoted as D-, E-, and F-replica. The light-grey vertical lines represent the pulse-labeling periods. The time is normalized to the first tracer contact with the system. The data point at -1 represents the not-labeled ^{13}C concentration prior to the experiment, which is equal to the natural background and therefore 0 in the ^{13}C-excess graph. The gray vertical lines symbolize the both labeling periods.

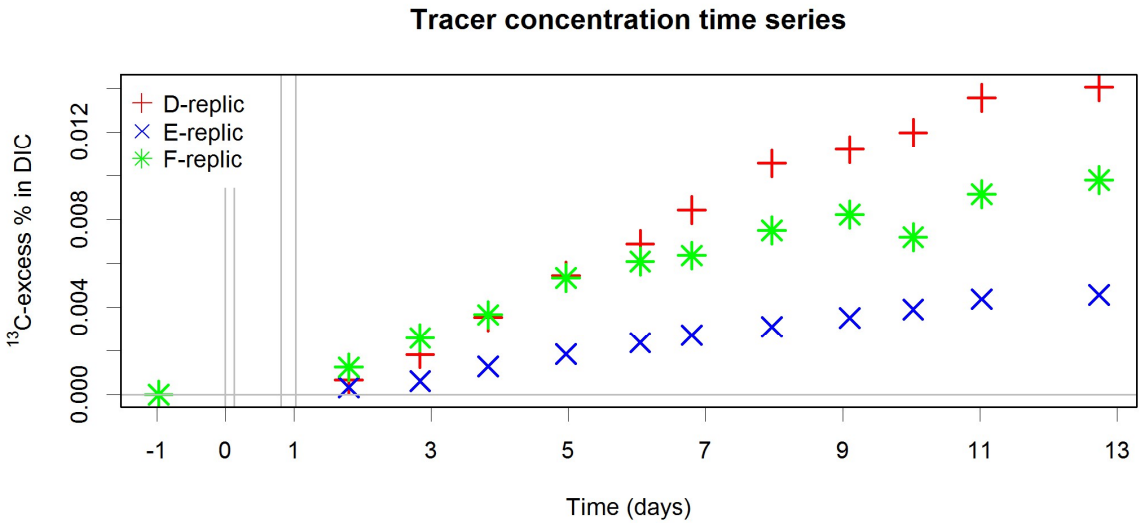

Figure 28. ^{13}C-excess % values of DIC in three labeled sites (Depth: 36 cm). The three sampled replica are denoted as D-, E-, and F-replica. The light-grey vertical lines represent the pulse-labeling periods. The time is normalized to the first tracer contact with the system. The data point at -1 represents the not-labeled ^{13}C concentration prior to the experiment, which is equal to the natural background and therefore 0 in the ^{13}C-excess graph. The gray vertical lines symbolize the both labeling periods.

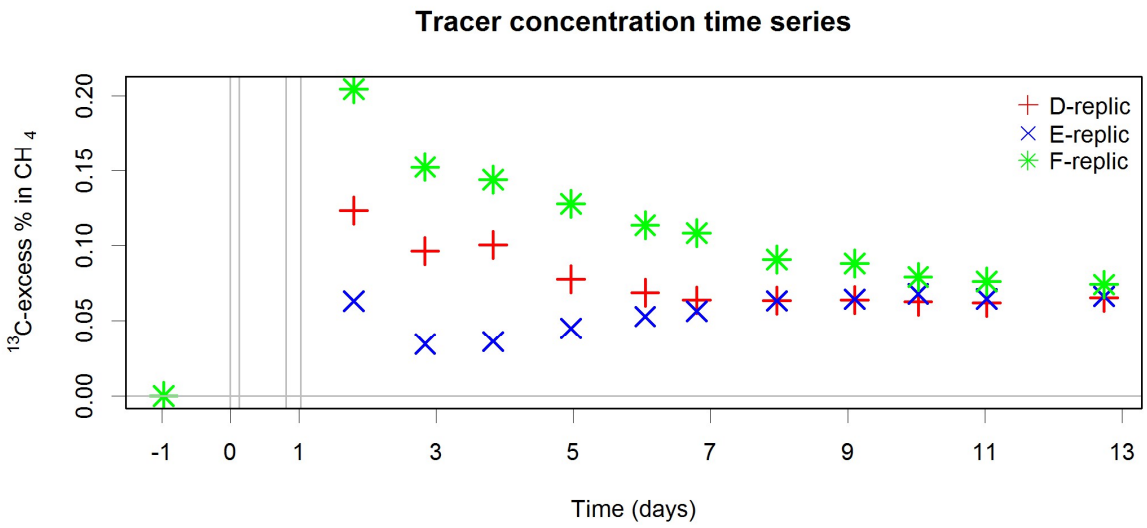

Figure 29. ^{13}C-excess % values of CH_4 in three labeled sites (Depth: 6 cm). The three sampled replica are denoted as D-, E-, and F-replica. The light-grey vertical lines represent the pulse-labeling periods. The time is normalized to the first tracer contact with the system. The data point at -1 represents the not-labeled ^{13}C concentration prior to the experiment, which is equal to the natural background and therefore 0 in the ^{13}C-excess graph. The gray vertical lines symbolize the both labeling periods.

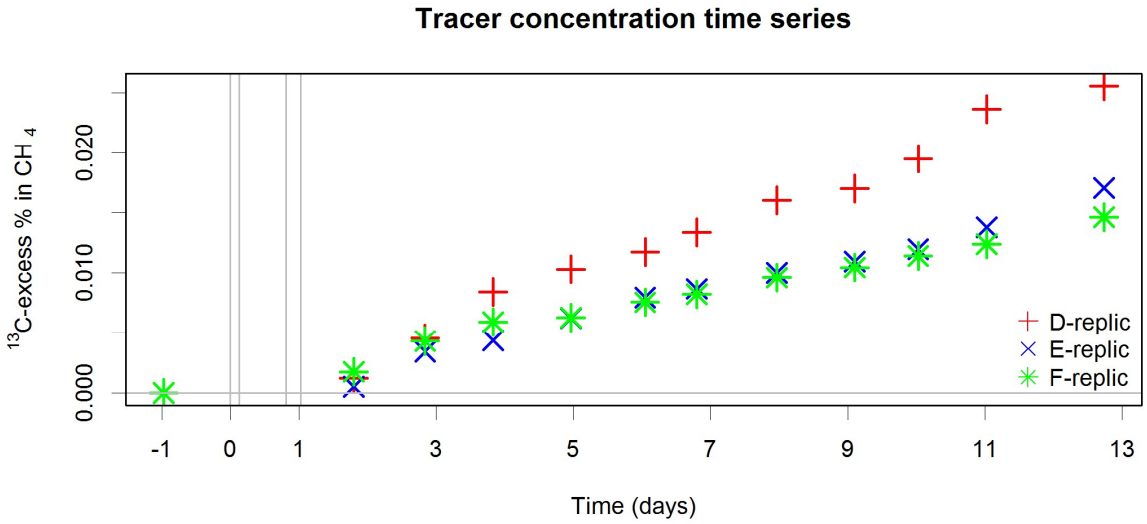

Figure 30. ^{13}C-excess % values of CH_4 in three labeled sites (Depth: 16 cm). The three sampled replica are denoted as D-, E-, and F-replica. The light-grey vertical lines represent the pulse-labeling periods. The time is normalized to the first tracer contact with the system. The data point at -1 represents the not-labeled ^{13}C concentration prior to the experiment, which is equal to the natural background and therefore 0 in the ^{13}C-excess graph. The gray vertical lines symbolize the both labeling periods.

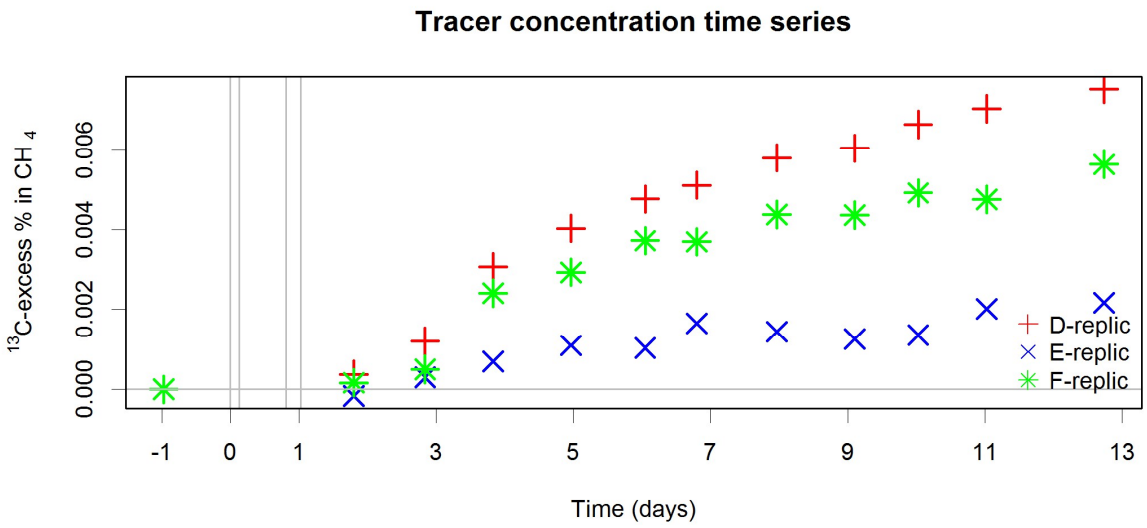

Figure 31. ^{13}C-excess % values of CH_4 in three labeled sites (Depth: 36 cm). The three sampled replica are denoted as D-, E-, and F-replica. The light-grey vertical lines represent the pulse-labeling periods. The time is normalized to the first tracer contact with the system. The data point at -1 represents the not-labeled ^{13}C concentration prior to the experiment, which is equal to the natural background and therefore 0 in the ^{13}C-excess graph. The gray vertical lines symbolize the both labeling periods.

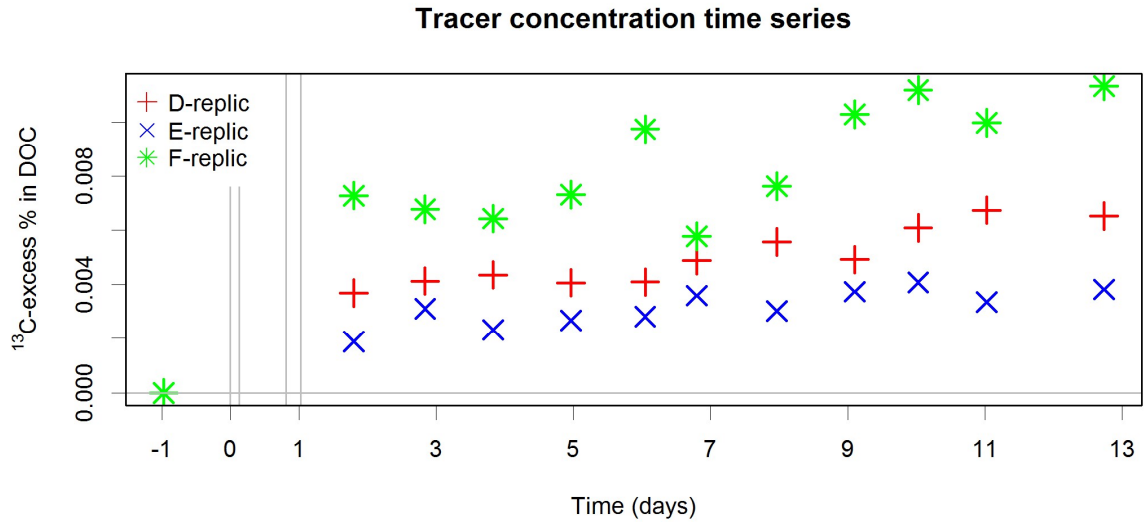

Figure 32. ^{13}C-excess % values of DOC in three labeled sites (Depth: 6 cm). The three sampled replica are denoted as D-, E-, and F-replica. The light-grey vertical lines represent the pulse-labeling periods. The time is normalized to the first tracer contact with the system. The data point at -1 represents the not-labeled ^{13}C concentration prior to the experiment, which is equal to the natural background and therefore 0 in the ^{13}C-excess graph. The gray vertical lines symbolize the both labeling periods.

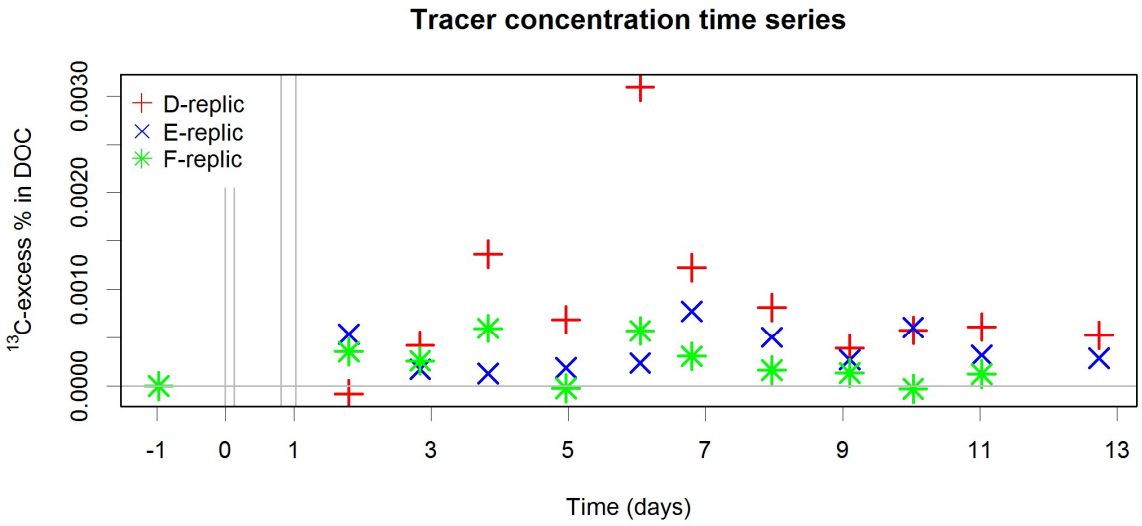

Figure 33. ^{13}C-excess % values of DOC in three labeled sites (Depth: 16 cm). The three sampled replica are denoted as D-, E-, and F-replica. The light-grey vertical lines represent the pulse-labeling periods. The time is normalized to the first tracer contact with the system. The data point at -1 represents the not-labeled ^{13}C concentration prior to the experiment, which is equal to the natural background and therefore 0 in the ^{13}C-excess graph. The gray vertical lines symbolize the both labeling periods.

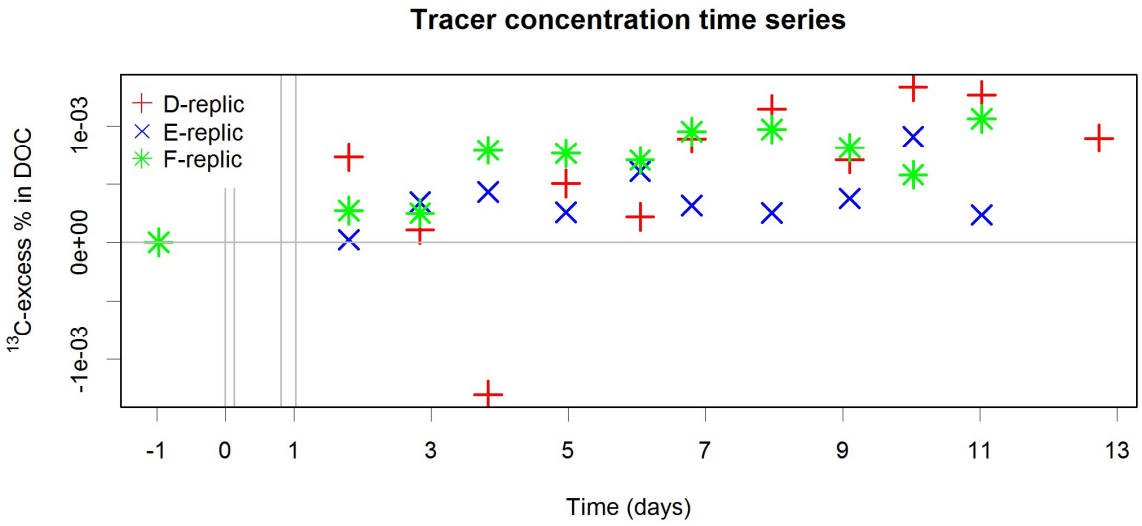

Figure 34. ^{13}C-excess % values of DOC in three labeled sites (Depth: 36 cm). The three sampled replica are denoted as D-, E-, and F-replica. The light-grey vertical lines represent the pulse-labeling periods. The time is normalized to the first tracer contact with the system. The data point at -1 represents the not-labeled ^{13}C concentration prior to the experiment, which is equal to the natural background and therefore 0 in the ^{13}C-excess graph. The gray vertical lines symbolize the both labeling periods.

The lowest concentration of tracer is observed in the DOC pools of all depths (when compared to the other carbon pools of the same depth). The DIC and CH_4 carbon pools in 6 cm depth show a distinctly declining tracer signal (see Figure 26 and Figure 29), while the DOC in the same depth is rising and levels out at the end of the two week sampling period (Figure 32). In the lower depths, 16 and 36 cm below surface, both in DIC- and CH_4 pools the tracer concentrations are increasing, almost linearly, as it seems, while DOC seems to show similar trace dynamics in all three pools. Additionally, it appears to be characteristic for the DIC and CH_4 tracer dynamics that they are clearly distinct from the natural background tracer concentration. In contrast, the DOC pools tracer signal, although the trend of a tracer induced ^{13}C concentration change over time is obvious, it never reaches more than 0.001 % ^{13}C-excess in the 6 cm DOC-pool.

4.5 LM (lognormal TCTS modelling) and CM (compartmental TCTS modelling)

Two type of models have been applied to reproduce the observed tracer concentration in three selected sub-surface carbon pools: DIC, CH_4, and DOC. In Figure 35, Figure 36, and Figure 37 the LM modelled and observed values for tracer in three sub-surface carbon pools in 6 cm depth is depicted. In Figure 38 the 20 best-fitted CM results are plotted. In three replicas, optimizing the lognormal model, the GA algorithm found good-fitting log-normal realizations. The TCTS of DIC is reproduced with R^2 – values of 0.94, 0.75, and 0.98 in three replicas. CH_4-TCTS reproduction reaches similar values, while DOC-TCTS R^2 is usually lower, reaching only values between R^2 = 0.76 and R^2 = 0.88.

Figure 38 shows the results of the compartmental modelling experiment. The 20 best-fitted solutions as found by the GA algorithm are represented and their mean is taken to show the ability of the model to reproduce the system.

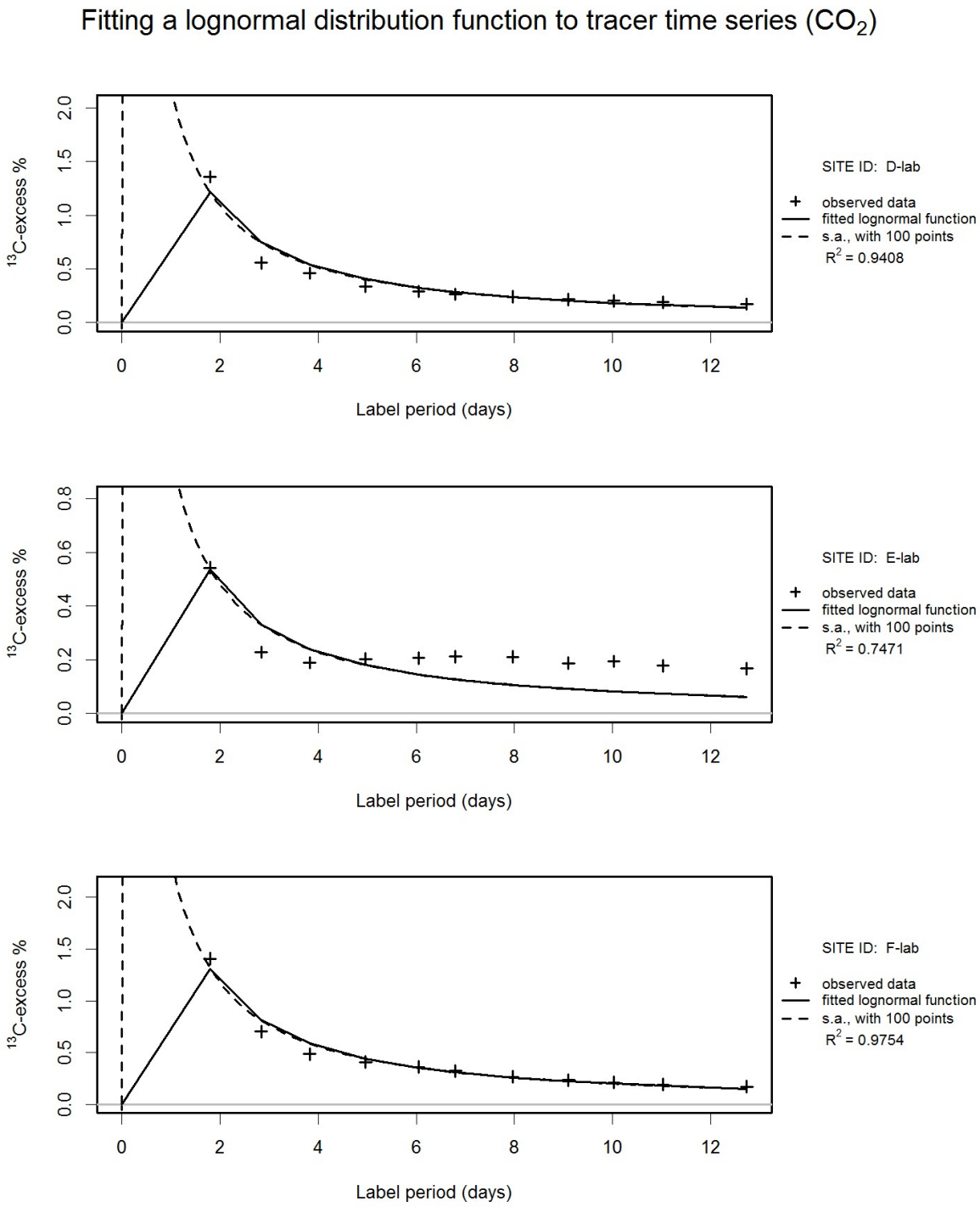

Figure 35. The observed tracer time series and the best-fitted lognormal distribution function for dissolved DIC are displayed. The baseline (grey) is based on the first, unlabeled data point of the tracer series. The x_0-point relates to the first time when the label was exposed to the system.

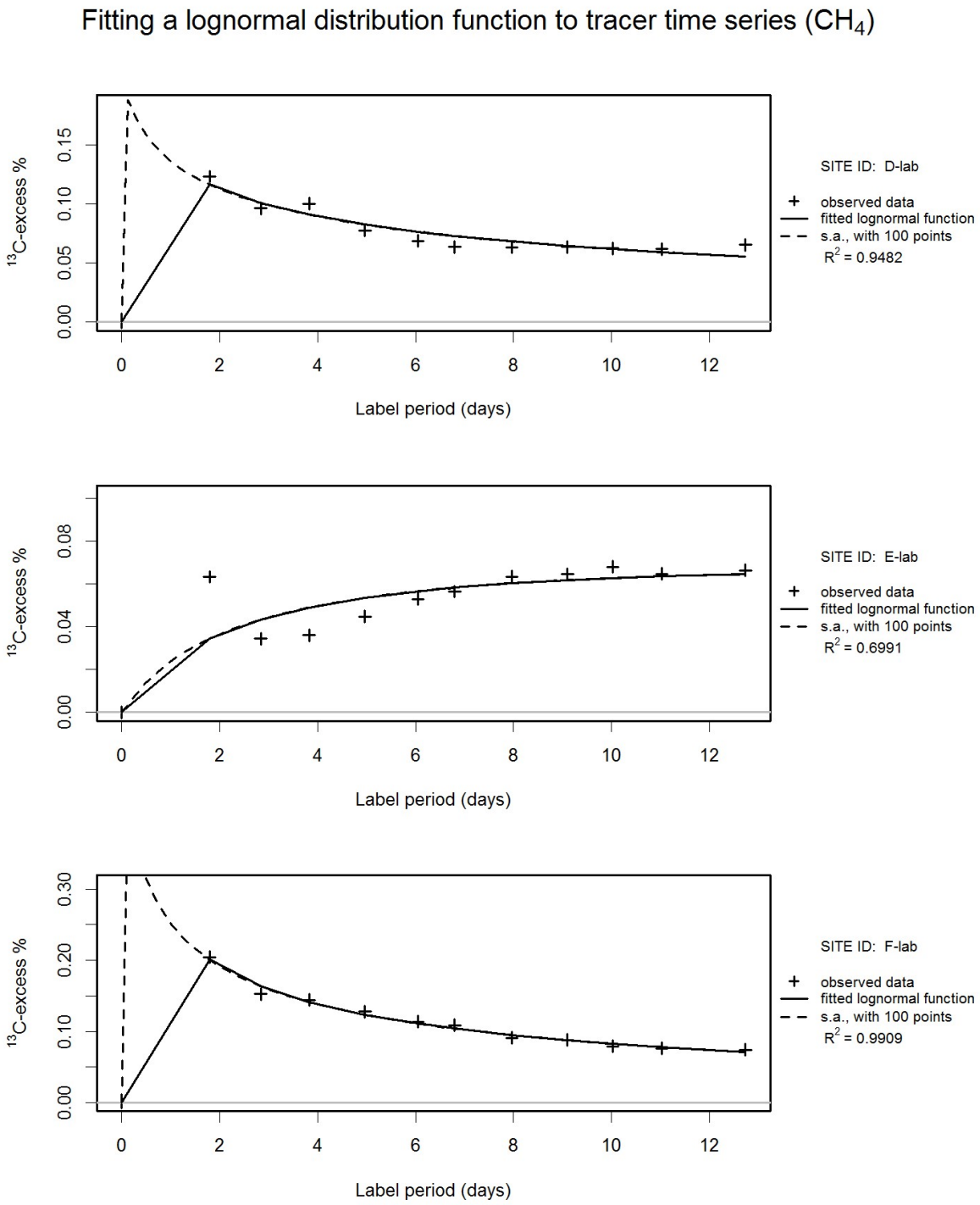

Figure 36. The observed tracer time series and the best-fitted lognormal distribution function for CH_4 are displayed. The baseline (grey) is based on the first, unlabeled data point of the tracer series. The x_0-point relates to the first time when the label was exposed to the system.

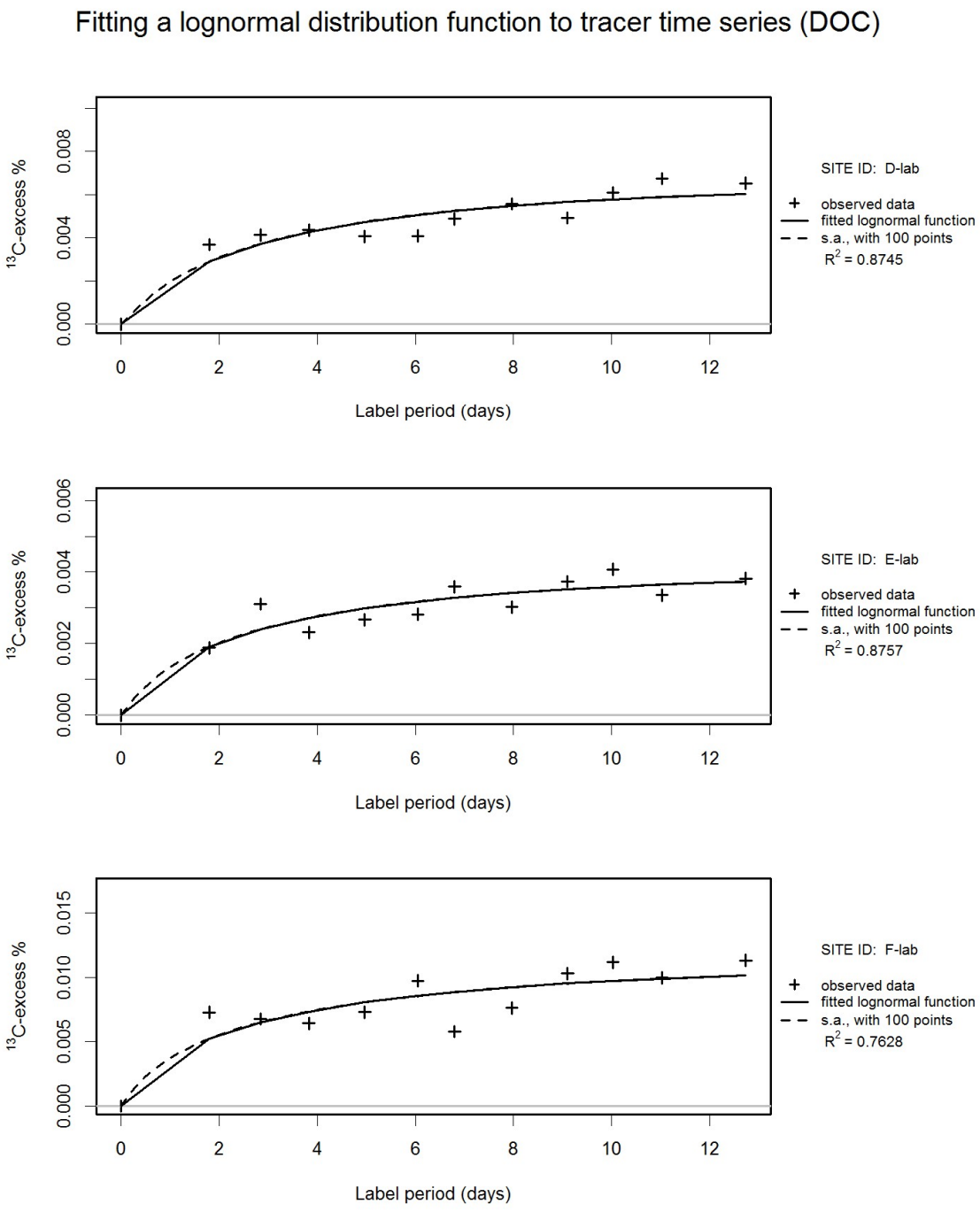

Figure 37. The observed tracer time series and the best-fitted lognormal distribution function for DOC are displayed. The baseline (grey) is based on the first, unlabeled data point of the tracer series. The x_0-point relates to the first time when the label was exposed to the system.

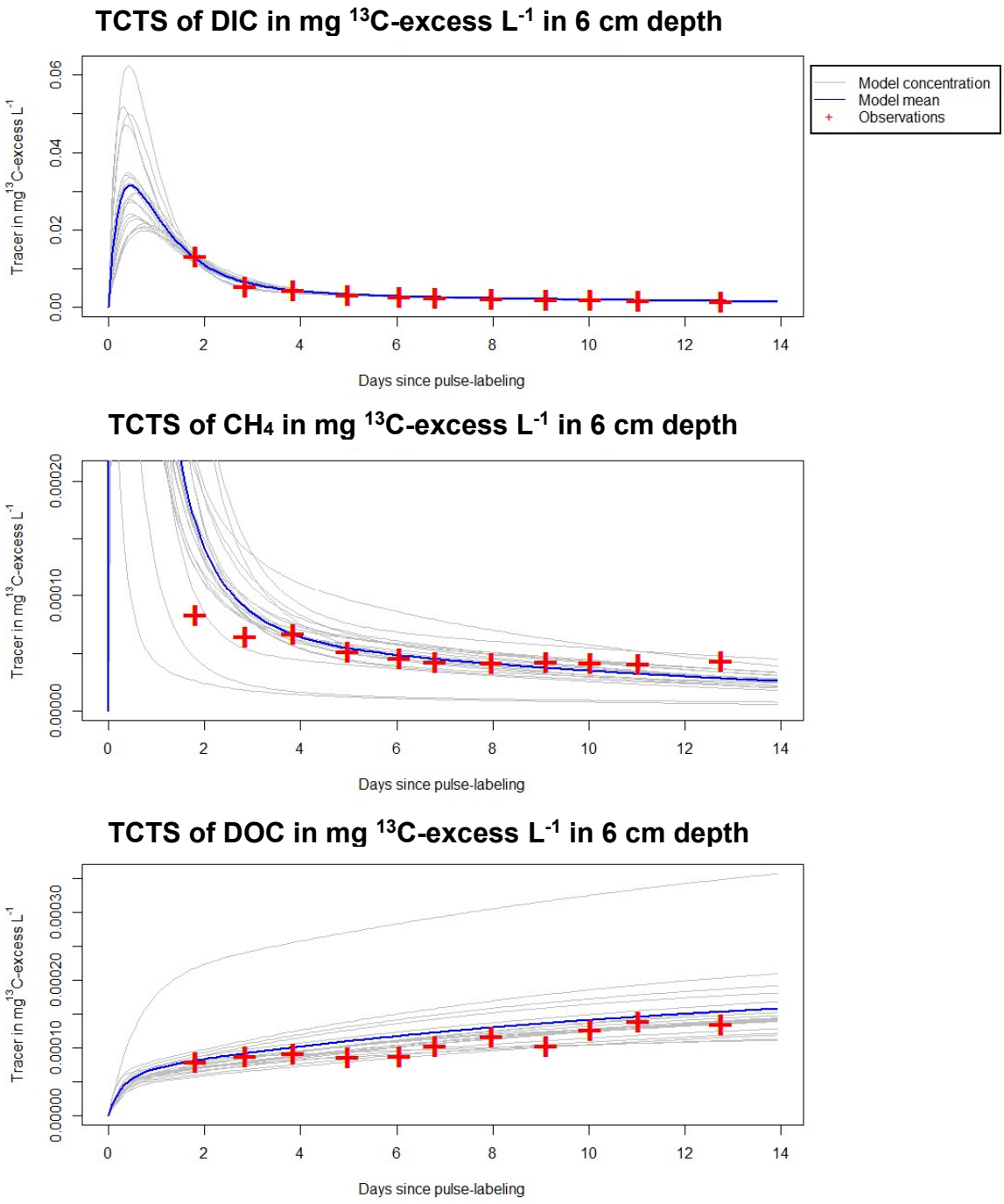

Figure 38. The 20 best-fitting TCTS reproductions by the compartmental model (grey). The blue line represents the simple mean of all good-fit time series (n=20). The grey lines represent different ensembles of model parametrization and are interpreted as the ensemble spread of the system realizations.

4.6 Mean residence time

In this study three different ways to calculate the mean residence time are applied. MRT is calculated by applying the equations 10, 11, and 12 on the CM and LM model-produced TCTC. These results allow an extrapolation into the part of the time axis where no observational record is available, and hence allow calculating MRT beyond the observational period. Furthermore, the MRT can be calculated based on the information of pool sizes and fluxes, the latter produced by the CM.

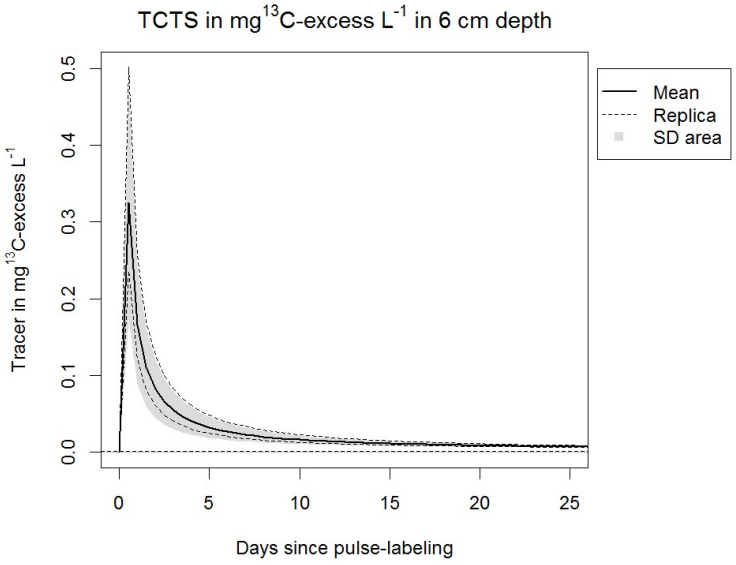

Figure 39. Mean tracer concentration (mg ^{13}C-excess L^{-1}) remaining in the upper 6 cm of a tundra soil as produced by the lognormal model. The graphs depicts the lognormally modelled tracer decline (black lines). The data represents the combination of the modelled tracer concentration time series of tracer in DIC, CH_4, and DOC (sum of tracers).

MRT calculated with the lognormal model

Figure 39 shows the extrapolated LM-modelled tracer concentration time series which is applied for calculating the MRT in this section. The mean MRT obtained by the lognormal model is 306.9 ± 41 days. The median MRT is only slightly different (312. 8, the range in the 0.15-0.85 quantiles is 264 – 350).

MRT calculated with compartmental model (with the E(t) function)

The mean MRT obtained by the compartmental model is 3.0 ± 0.2. The median MRT is in the same range (3.0, the range between the 0.15-0.85 quantiles is 2.9 –3.1). The mean residence time, as calcu-

lated by the compartmental-model produced TCTS, is more than 4-fold shorter than calculated by the normally modelled data series. Both approaches give a modelled TCTS which is strikingly similar, however, it is notably that the LM produces about 10 times as much initial tracer concentration for the system (in the extrapolated area between labeling and the first measured data point). Thus, the obtained E(t) function, which includes an integral of the C(t) function depicted here, produces larger numbers with the LM data and hence the MRT calculated from them vary significantly.

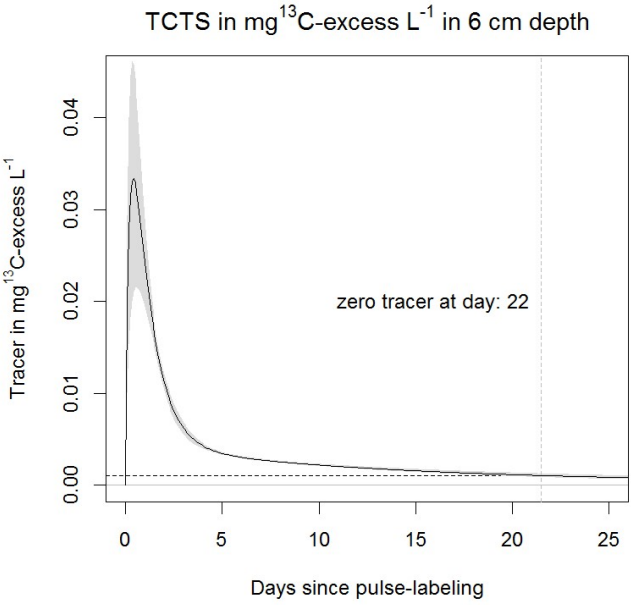

Figure 40. Tracer (mg ^{13}C-excess L^{-1}) remaining in the upper 6 cm of a tundra soil. The graphs depict the compartmental model- calculated tracer decline (black lines). The data represents the combination of the modelled tracer concentration time series of tracer in DIC, CH_4, and DOC. Zero tracer is assumed when the modelled tracer concentration becomes lower than the simple standard deviation of the zero-line (grey-shaded).

MRT calculated with compartmental model (with V_{in}/V_{pool})

The compartmental model allows calculating the mean residence time in the carbon pool not only by applying equations 10, 11, and 12, but also by using the model data produced while fitting the parameter set to the observed data by taking the reciprocal of the turnover rate (tr = V_{flux}/V_{pool}; V stands for volume or mass). In Table 14 the modelled system fluxes are presented. The pool size of replica D is found in Table 20 (for DIC), Table 23 (for CH_4), and in Table 26 (for DOC).

Table 13. Pool size, fluxes and mean residence time calculated from the transfer coefficients and the pool size as given in Table 14. The flux values given in this table are the sum of the inbound fluxes into the respective carbon pool per day. Error estimation is explained in section 3.10.

Pool	Pool size (mg C L^{-1})	Flux (mg $CL^{-1}d^{-1}$)	MRT $(V_{flux}/V_{pool})^{-1}$ / 24 (unit: day)
DIC	10.83 (± 2.1)	11.66 (± 3.2)	0.98 (± 0.3)
CH_4	0.75 (± 0.3)	7.68 (±1.4)	0.10 (± 0.06)
DOC	21.62 (± 1.1)	0.069 (± 0.03)	379.9 (±182.7)
Total	33.2 (± 2.4)	12.77 (± 3.2)	2.74 (± 0.6)

4.7 Intrafluxes and CH_4/C_{in} and CO_2/C_{in} ratios

The fluxes between the sub-surface carbon pools can be quantified with the CM model. In Figure 38 the intrafluxes of the soil system are displayed. The depicted values represent the 20 best-fitted CM-produced fluxes for the soil system. Table 14 shows, that most of the carbon enters the system via the DIC pool (*a41*, *a51*, and *a63* with 0.132, 0.146, and 0.127 mg $CL^{-1}h^{-1}$), about 81 % of the total carbon which enters the current-season carbon cycle system. Only 0.5 % enters the system via the DOC pathway. The complete list of the 20 best-fitting flux values is given in A IV.

The total mean modelled C flux into the soil system is 0.53 (± 0.15) mg C $L^{-1}h^{-1}$, from which 0.26 (± 0.05) mg $CL^{-1}h^{-1}$ exit from the CH_4 pool and 0.27 (± 0.14) mg C $L^{-1}h^{-1}$ from the CO_2 (DIC) pool. Thus, the model suggests an average C_{CO2}/C_{In} ratio of 0.51 (± 0.12) and C_{CH4}/C_{In} ratio of 0.49 (± 0.12), i.e. the model suggests a CH_4 production from root exudates which is in the same order of magnitude as the CO_2 (DIC) production in the current-season photosynthate carbon cycle (mainly driven by root exudates and root respiration). The flux entering the system from pool X_6 (encompasses all carbon that enters the system, which are not labeled) is about 0.19 (± 0.06) mg$CL^{-1}h^{-1}$, which is about 36 % (± 10 %) of the total C incorporated in the system. This suggests that 36 % of the material incorporated into the system origin-

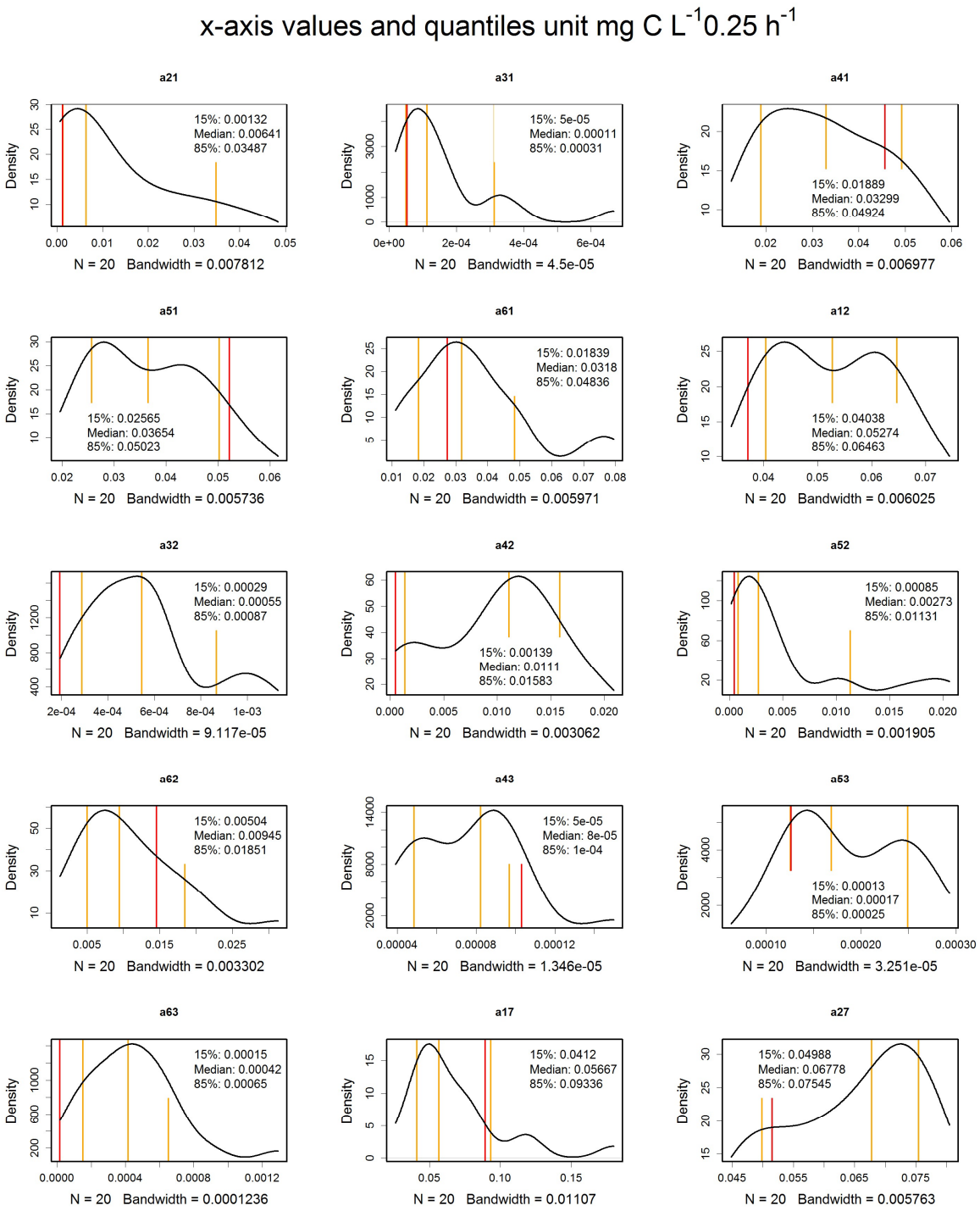

Figure 41. Good-fit parameters of the compartmental model. The distribution probability of values for each parameter is modelled with the kernel density function from the R software. The data represents the 20 well-fitted model parametrizations with respect to their ability to reproduce the DIC-tracer concentration. The orange lines represent the 0.15, 0.5 (=median), and the 0.85 quantiles of each parameter set. The red line represents the respective variable-value for the best-fit. The tracer concentration time series produced by these 20 well-fit model parametrizations are shown in Figure 38.

Table 14. Soil system carbon fluxes in 6 cm depth. Calculated with best-fitted compartmental model data. The flux is given in mg C $L^{-1}h^{-1}$. The flux is the median of the 20 best-fitted model realizations, the variance is expressed by the 0.15 and the 0.85 quantile (this range covers 70 % of the data, which is in the same range of the 68.2 % covered by the Gaussian distribution standard deviation).

Model parameter	Flux direction	Median-Flux (mg $CL^{-1}h^{-1}$)	Range (0.15 and 0.85 quantiles)
a21	dissCH4-DIC	0.002564	0.00528 -0.13948
a31	DOC-DIC	0.00044	0.0002-0.000124
a41	fast Pool-DIC	0.13196	0.07556-0.19696
a51	slowPool-DIC	0.14616	0.1026-0.20092
a61	noTracer-DIC	0.1272	0.07356-0.19344
a12	DIC-dissCH4	0.21096	0.16152-0.25852
a32	DOC-dissCH4	0.00022	0.00116-0.00348
a42	fastPool-CH4	0.0444	0.00556-0.06332
a52	slowPool-CH4	0.01092	0.0034-0.04524
a62	noTracer-CH4	0.0378	0.02016-0.07404
a43	fastPool-DOC	0.00032	0.0002-0.0004
a53	slowPool-DOC	0.00068	0.00052-0.001
a63	noTracer-DOC	0.00168	0.0006-0.0026
a17	DIC-atmosphere	0.22668	0.16508-0.37344
a27	DIC-atmosphere	0.27112	0.19952-0.3018

nates from not-labeled sources. The average CH_4 flux is 0.26 (± 0.05) $mgCL^{-1}h^{-1}$, from which 21 $mgCL^{-1}h^{-1}$ are obtained by the DIC pool, thus suggesting 68 % (± 16) of methane being produced by hydrogenotrophic methanogenesis (CO_2 reduction).

4.8 Model comparison and model data summary

In Table 15 some results of the model comparison are given.

Table 15. Summary of lognormal and compartmental modelling of the current-season carbon cycle.

Property	GA lognormal model	GA-fitted compartmental model
Computation time	+	-

TCTS tracer reproduction	+	+
internal system parameter information	not possible	+
user-friendly	++	-
mean residence time (MRT) with E(t)	306.9 -49.1/+37.5	3.0 ± 0.2
mean residence time (model parameters)	-	2.74 ± 0.6
R^2 - adjusted	DIC: 0.9408, 0.7464, 0.9754 CH_4: 0.9476, 0.6962, 0.9909 DOC: 0.8774, 0.8754, 0.7541	DIC: 0.9811 CH_4: 0.8569 DOC: 0.7808
$\frac{CH_4}{C_{in}}, \frac{CO_2}{C_{in}}$	not possible	0.49, 0.51
n	3	1
future work	very high initial concentration	finer time-step resolution, sensitivity test of influence of different pools (exclude certain pools)

5 Discussion

5.1 Carbon allocation into the belowground

Discussion of research question Q1) *How does recently incorporated atmospheric-derived carbon redistribute in carbon pools of a high-latitude tundra plant-soil system?*

The allocation of label into the belowground is mainly depending on the season and on the plant association at the site. In section 4 is shown that tracer – and hence atmospheric carbon – is found in all depths of the active layer. The roots are the prominent distributor of freshly incorporated carbon into the deepest part of the active layer, but the largest amount of label is found in the moss of the first few centimeters soil substrate. Furthermore, dissolved organic carbon was affected by incorporated tracer in all investigated soil layers.

Table 16. Different data of tracer distribution after labeled carbon is incorporated into the plant-soil system. For further explanation and discussion see text.

Plant association	Geography	Labeling event	carbon pool compared	Percentage of total tracer recovered at day$_x$	Time passed since labeling	Study
Carex-Scorpidium	Polygonal tundra wetland, Lena delta	16-17 August	Above ground Below ground Living roots** mosses (6 cm) mosses (all depths)	3.8 ± 1.3 96.6 ± 19 27.4 ± 9.7 45.9 ± 12.9 63.8 ± 16.2	13-12 days	**This study**
Kobresia humilis meadow	Qingha-Tibet-Plateau (3250 m)	July, 29	Shoots Living roots Dead roots Soil C_{org}	33.6 ± 24 69.7 ± 12 7.9 ± 1 6.1 ± 2	15 days	(Wu et al., 2010)
Agropyron-Koeleria.	Saskatchewan-Prairie	18-20, May	Above ground Below ground	65 35	11-13 days	(Warembourg and Paul, 1977)

Agropyron-Koeleria	Saskatchewan-Prairie	31 May-4 June	Above ground Belowground	65.5 34.5	28-24 days	(Warembourg and Paul, 1977)
Agropyron-Koeleria	Saskatchewan-Prairie	21-25 June	Above ground Belowground	56 44	~ 30 days	(Warembourg and Paul, 1977)
Agropyron-Koeleria	Saskatchewan-Prairie	7-10 Sept.	Above ground Belowground	57 43	11-14 days	(Warembourg and Paul, 1977)
Betula nana-Empetrum nigrum-Vaccinium vitis-Pleuzerium schreberi-Sphagnum	At northern treeline, tundra Finland	7 July	Mosses Vascular plants (above and belowground)	27.5 ± 23 72.6 ± 23	19 days	(Street et al., 2013)*
Eriophorum-Carex-Drepanocladus	wet tundra mesocosm, Toolik, Alaska	mid-season	aboveground roots soil rhizome and porewater emit CO_2	~35.7 14.3-28.6 14.3 7.1 21.4	15 days	(King and Reeburgh, 2002)*

* Originally, data is given as percentage of total label and modified by the author to be percentage of total label recovered at day_x.
** As also observed by Wu et al. (2010) the "dead roots" appeared not to be always dead, because they showed sometimes tracer incorporation. For this study, as soon as a root showed tracer incorporation, it was included into the statistics done for living roots

In Table 16 the tracer distribution 13-12 days after the pulse-labeling in the plant-soil-system is shown in comparison to data from different tracer experiments. The tracer concentrations used for calculating the tracer distribution in the sub-surface carbon pools are partly not significantly (on a 95 % confidence level) different from the unlabeled control value. Yet, due to their higher variance and the presence of nature-unlike sample ^{13}C-values, the label is considered to be present and the calculation is based on the mean of the trace concentration in those samples[3]. For the amount of

[3] Generally, the labeled pools show a wider sample distribution, i.e. a higher variance, which is undoubtedly a sign of label incorporation, even though the difference between the signatures might not significantly different (when tested with the t-test). Therefore, whenever the labeled C pool displays a higher variance as the control C pool, the label is assumed to be

tracer found in the depths of 20-30 and 30-40 centimeters, the natural background values, necessary to calculate the tracer enrichment in relation to the natural background ^{13}C-concentration (see equation 4), were available only for the bulk soil C.

The tracer incorporation into mosses obtained by this study falls in the same range as given by Street et al. (2013), the tracer incorporated into living roots is lower as given by Wu et al. (2010) for the Qinghai-Tibet plateau at mid-season and lower as reported by King and Reeburgh (2002) for an Alaskan tundra wetland (all data from the here quoted studies is given in Table 16), also during mid-season. Since the "aboveground" term in this study means only the vascular *Carex*-shoots, but in the study of King and Reeburgh (2002) obviously the uppermost moss-layer and the vascular grasses, which comprise a small percentage of the total tracer incorporation, the "mosses"-percentage can be compared with the "aboveground"-term of King and Reeburgh (2002) and hence falls into the same range of the data given by King and Reeburgh (2002; compare also discussion page 108 of this study). Based on the data for *Carex* in Miller et al. (1980), which shows a decline in leaf area index for August in 1970 and 1971 in Barrow, Alaska, and taking into account the partly yellowish-greenish *Carex* shoots in Samoylov in August 2013, it can be concluded that the ecosystem was already preparing for senescence, i.e. the current experiment for this was conducted just right during the peak of the phenological plant cycle. This has implications for the interpretation, because according to data given by Warembourg and Paul (1977), it can be assumed that the tracer incorporation during the peak of the phenological plant cycle represent the average tracer incorporation during the entire phenological plant cycle. When comparing the data of the current investigation in a Siberian wetland tundra polygon to King and Reeburgh (2002) in an Alaskan tundra wetland, to Street et al. (2013) in a quasi-tundra system in Finland and to the in-situ high-altitude pasture study of Wu et al. (2010), it seems to be the case that in higher latitudes – and high

---

present and used for the calculation of the label percentage distribution in the sub-surface carbon system. This approach is feasible, because although the significance of the difference of $\delta^{13}C$ in the control-label pairs of question is rejected by the t-test, the probability value p in the case of the Scorpidium is 0.15 (still only 15 % chance of a random test result), which, given the assumption that a tracer incorporation is the only possible reason for a higher $\delta^{13}C$ value, is considerable.

altitudes- the major part of the synthesized carbon is directed into the belowground. Contrasting, the study of Warembourg and Paul (1977) showed that in lower latitudes (but continental climate), in Saskatchewan, most of the tracer is found in aboveground plant parts.

Street et al. (2013) showed that mosses are important parts of the carbon cycle in high latitudes – their experiment was conducted at the northern tree border line. For the Samoylov tundra, where the tundra is tree-less - in comparison to Street et al. (2013) - this finding is also true, because, at least in the upper few centimeters, huge amounts of atmospheric-derived carbon is found in mosses. As demonstrated by Street et al. (2013) for high latitudes, but also by Fenner et al. (2004) for *Sphagnum* (after 23 days still 64 % of the initially measured label was detected), mosses work like a sponge for ADC: rapidly incorporation and slow release. Although the tracer concentration time series is not measured for this study, but only the value at day 12 after the labeling stopped, the total tracer incorporation to the mosses is high as well and supports the findings of Street et al. (2013) and Fenner et al. (2004).

These findings have two implications for any attempt to set up a compartmental carbon flux model of the system:

1. Mosses act as a potentially huge tracer source with a low turnover rate – this has to be taken into account when modelling the tracer dynamics of wetland soil systems
2. They might prevent tracer diffusion into the soil, because they seem to take up any atmospheric-derived CO_2 readily and fast, so they might deplete the uppermost centimeters of soil-pore water by traced CO_2. This means that the tracer concentration detected some centimeters lower already represents photosynthetically-synthesized tracer. The tracer diffusion problem can be assumed negligible.

Furthermore, any studies that aim to model wetland soil carbon cycle, especially of high latitudes (and altitudes), should consider the special tracer retention induced into the carbon cycle system by the presence of mosses. It seems to make no difference, which moss species are present at the experiment site, because similar retention effects have been observed for different moss species in this study, by Street et al. (2013) and by Fenner et al. (2004).

This study aims to follow the tracer as deep as possible into the active layer. At 36 cm depth, about 10 cm above permafrost table, the roots of the plants were still affected by the tracer. This means that not only is the belowground of the active layer in a shrub-less tundra polygon by far the most active part of the ecosystem (if belowground is defined as everything below the water level), but that the influence of vascular plant carbon incorporation impacts the soil system as deep as the permafrost table. Any attempt to process-oriented model the active layer should take this into account. The distribution of recently-incorporated atmospheric-derived carbon is hence possible in the total active layer and the most important carbon pool in the uppermost centimeters is the moss.

5.2 Tracer concentration time series and modelling

Discussion of research question Q2) *Does the ^{13}C tracer display a tracer concentration time series in sub-surface carbon pools that allows modelling the sub-surface carbon cycle in a permafrost-affected tundra soil?*

The soil system of the low-center polygon shows distinct tracer concentration time series. The shape of this tracer concentration is comparable with the data presented by King and Reeburgh (2002), and indicates, for the upper centimeters of the soil, that the tracer concentration has a similar shape as reported for tracer concentration in mosses by Street et al. (2013) and Street et al. (2011). From a more general perspective, these tracer concentration functions are similar to a number of tracer outwash curves reported in several studies on plant carbon allocation (Luo and Nobel, 1992; Kuzyakov, Kretzschmar, and Stahr, 1999). This supports the hypothesis that the in-situ tundra wetland soil-plant carbon cycle system can be modelled with a simple tracer model and hence supports the basic assumption of this study. The lognormal distribution can be fitted to the observed TCTS quite good (R^2 = 0.71 – 0.91). Norwich (1997) suggested the modelling of tracer washout curves with the lognormal function. A comparison with King and Reeburgh (2002) - there is data shown in Figure 42 – shows the tendency of sub-surface carbon pools to show distinctive tracer time series after photosynthetically incorporated isotope carbon migrates through the system. Depending on the system's turnover times in those carbon pools, which mainly govern the carbon emission, the actual observed tracer concentration time series can be different from the idealistic shape of a single

pool well-mixed tracer concentration decay function. Kuzyakov (2001) – see Figure 43 – demonstrated that the shape of the emission tracer concentration time series curve is mainly governed by plant respiration and microbial activity, i.e. the tracer outwash curve is mainly controlled by two major soil carbon pools. Luo and Nobel (1992) also successfully modelled the ^{14}C-tracer concentration in *Opuntia ficus* cladodes by assuming two mainly controlling carbon pools, mobile and immobile plant organic molecules. Hence, there is reason to assume that natural systems, which are mainly influenced by plant and soil carbon cycle processes can be sufficiently modelled with a low number of carbon pools. It seems to be the case that photo assimilated ^{13}C as tracer in a tundra wetland soil-plant system shows a reliable, in the sense of repeatable, tracer pattern. This is an important finding for the system investigation and compartmental modeling of the system, since a tracer-based investigation method for the lower soil parts is possible, not only with radioactive ^{14}C as tracer, as applied by King and Reeburgh (2002), Dorodnikov et al. (2011),

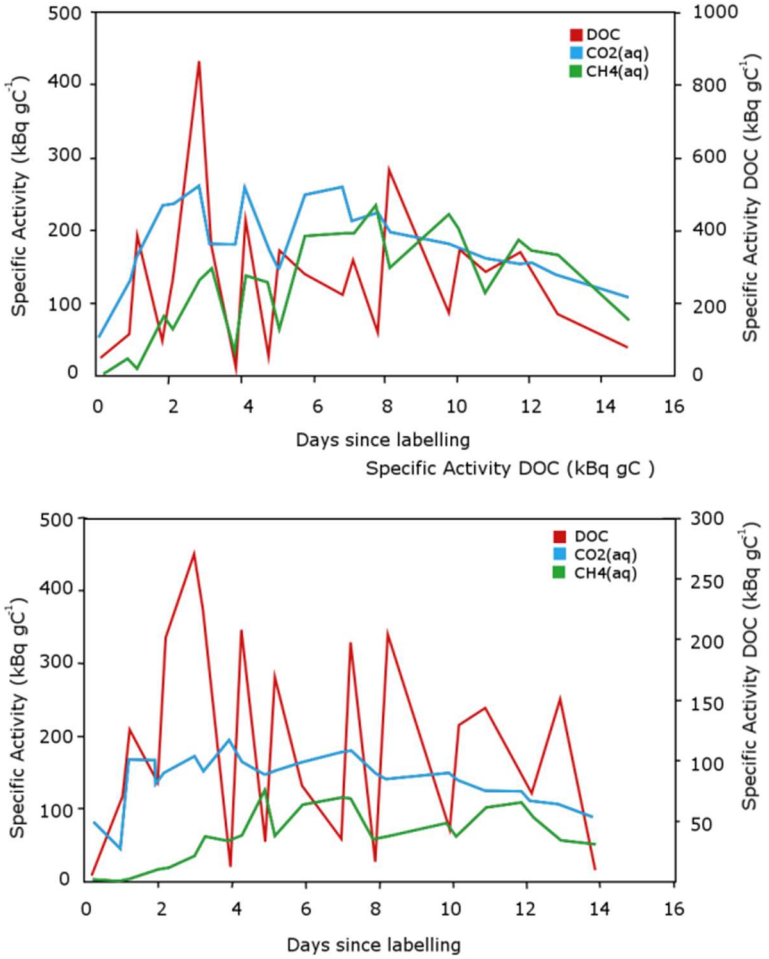

Figure 42. Activity of ^{14}C in different sub-surface carbon pools as observed by King and Reeburgh (2002). The tracer time series show generally a higher variance than the ^{13}C-tracer time series of this study. However, the general shape of tracer outwash curves is obvious. Graph adapted and modified from King and Reeburgh (2002).

and others, but also on the base of ^{13}C as tracer and the system shows comparable tracer concentration pattern.

Conclusively, this study, backed by the tracer concentration time series graphs published by King and Reeburgh (2002) and Fenner et al. (2004), indicates that tracer behavior in current-season carbon cycle in tundra soil systems can be interpreted the same way as TCTS are interpreted in human or animal bodies or chemical reactors. The "washout" curve of freshly incorporated carbon was obvious from those studies and could be observed in this study as well, with the help of ^{13}C instead of ^{14}C.

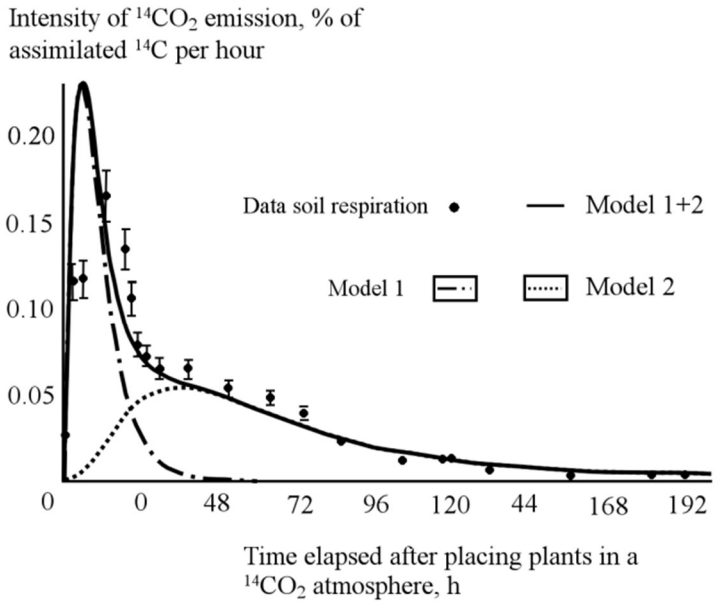

Figure 43. Modelled and observed $^{14}CO_2$-tracer time series from a grassland soil. The data points represent measurements, the solid line the combination and the dashed and dotted line the ^{14}C – release from plant (model 1) and microbial activity (model 2). Aadapted and slightly modified from Kuzyakov (2001).

The tracer concentration time series observed as a result of a ^{13}C-CO_2 labeling experiment show similar dynamics as have been observed by previous authors. Firstly, these findings support the application of ^{13}C in soil-system studies in remote areas, because ^{13}C as tracer produces TCTS comparable to ^{14}C-TCTS in plant-soil systems. Secondly, the finding of ^{13}C-TCTS in this system strongly encourage the further development and application of modelling methods in combination with TCTS for describing small-scale wetland soil system carbon cycles, which are not quantifiable by other means. Last, but no least, theses time series show the close connection between recently incorporated atmospheric carbon and small-scale belowground carbon dynamics.

TCTS produced by the model in relation to natural observed TCTS

The encompassing study of Street et al. (2013) showed that while in mosses the tracer decline in about three weeks is relatively small, the tracer decline in leaves of vascular plants can be very fast (about 50 percent in leaves after 19 days as published by Street et al. (2013)). In this study's CM model results the tracer concentration time series in the "artificial" pre-pools X_4 and X_5 was a free variable (i.e. subject to optimization) and the system seemed to adapt to two pre-tracer pools which have different tracer declines.

Kuzyakov, Kretzschmar, and Stahr (1999) published modeling results where they successfully simulated the total $^{14}CO_2$ emission from grassland with a combination of two compartments (in the study the compartments stand for plant respiration and microbial respiration). Luo and Nobel (1992) simulated the ^{14}C-dynamics in roots, basal and daughter cladode (cladode: photosynthetic shoots, for example in some Cactacea and Asparagacea members) with an immobile and a respiration compartment. In both cases, in the first more than in the latter, because of its similarity to the investigated system in this study, it seems plausible to assume that two major carbon pools with different turnover times are suitable for modeling the system. The BT model, published by Street et al. (2013), uses six fitted parameters – exponential temperature response of respiration, basal rates for both photosynthetic and stem tissue, an exponent, as well as three linear coefficients – comparable to transfer coefficients – which steer the fluxes into different moss tissue parts. Both approaches, from Street et al. (2013) and from Kuzyakov, Kretzschmar, and Stahr (1999), require a number of ambient parameters which control the model output so they model the entire plant-soil system based on their physical parameters.

Therefore, such model approaches are only partly comparable with the CM model applied in this study, because this model is independent from ambient influence and assumes a steady-state of the carbon cycle system, i.e. the system pools are unchanged in size during the observation time. The advantage of this approach is the possibility to investigate the system in total, with a reduced complexity. However, short-term changes of the system, i.e. the violation of the steady-state assumption, remain subject for future studies and must be taken into account when modelling soil systems following the technique given in this study.

Allessio and Tieszen (1975) published that ^{14}C tracer is appearing in an Arctic soil system already hours after the labeling occurred. This supports the approach in this study, where turnover rate of all soil carbon cycle compartments is very fast.

One of the problem areas of this project is the comparison of model values to observation data. Yes, this model to some degree of agreement describes the observed tracer concentrations in the sub-surface carbon pools. However, the feasibility of the results is to be interpreted with care, just because of the lack of observation data to compare to. Therefore, it is important to compare the model results to other data sets, which, partly at least, are similar to the model-produced data of this project. Many authors published CH_4 and CO_2 data for different sites and geographical regions. There exist a number of studies that investigate flux partition from both methane and CO_2 from wetlands and tundra soils, which can be used for comparison (refer to sections 5.3 and section 5.4).

For this study, stable isotope tracers are used as proxies for carbon transfer and mean residence time among and in carbon pools. The short-term pulse-labeling tracer applied in this study aims to investigate carbon pools composed by recently incorporated ADC. Among other questions, an obvious task of tracer application is to find mean residence time of the tracer – and hence the ADC – in the respective carbon pools. For calculating the mean residence time according to equations 10 to 12 (Fogler, 2016), a more encompassing observational TCTS, is required to shorten the period of time for which a model-based extrapolation is required. Obtaining the observed TCTS in situ in remote areas is usually challenging – incomplete TCTS are the result. Therefore, a model which can be fitted and used to extrapolate the TCTS data into the non-observed time interval is required. For this study, a lognormal model (LM) and a multi-compartmental model (CM) were used for extrapolating the limited data points of the TCTS. The LM was chosen because Norwich (1977) mentioned its usefulness for modelling TCTS without any physical basis. The CM was chosen, because Norwich (1977) and Anderson (1983) explained that more complex systems are usually sufficiently modelled by multi-compartmental models. Manzoni, Katul, and Porporato (2009) already showed that soil-carbon transfer and residence times are preferably modelled with multi-compartmental models. A polynomial fit-model was ruled out, because of the tendency of polynomial fits to significantly deviate from the real data set when extrapolated beyond the

observational data. Other models, which produce curve shapes similar to TCTS are gamma distribution models and a number of multi-compartment models with various structures (Norwich 1977).

To summarize, the TCTS observed in the soil pore water carbon pools shows a clear tracer "washout" trend, i.e. enabling the application of compartmental models for investigation of system carbon fluxes and system pool turnover times in a wetland tundra soil. However, there is still work to be done in order to fully establish the theoretical and methodological foundations to foster future studies of this type in similar plant-soil systems.

The biggest advantage of the compartmental model with numerical optimization parameter fitting is its potential to model not only a range of mean residence times and fluxes for the observed tracer compartments (in this study DIC, DOC, and CH_4). It also gives information about the actual tracer concentration and the flux of tracer-bearing carbon from fast-, medium-, and slow turnover pools, which are difficult to estimate in ^{13}C tracer studies.

5.3 Mean residence time of atmospheric-derived carbon

Discussion of research question Q3) *What is the mean residence time of freshly incorporated carbon a tundra wetland soil?*

The mean residence time calculations, based on the equations 10, 11, and 12 (all from Fogler, 2016), are applied to the complex soil system, although they are supposed to be used with simple chemical reactors. In contrast to neatly lined up chemical reactor-compartments, the soil compartments (pools) are intertwined on a microscopic scale. However, in this study the soil system is assumed to behave like a series of chemical reactors, because it can be seen as a box, into which tracer is introduced and its concentration decline is observed and measured in distinct chemical pools (DIC, CH_4 and DOC). Conceptually, these pools can be separated as is demonstrated with Figure 14. The equations 10, 11, and 12, as given by Danckwerts (1953) and Fogler (2016) usually require a complete observed tracer concentration time series, which is not realized in this study. Therefore, the not-observed part of the TCTS is extrapolated by two different models (LM and CM). This study's results show that they give

very different MRT for the soil system: While the LM-extrapolated TCTS has a MRT of about 300 days, the CM-extrapolated MRT is about 3 days.

The reasons for this difference can be concluded from the type of model and its TCTS-curve, respectively.

The LM model fits only one lognormal function to the observational data, the fitting of 2-parameters is done by a GA-numerical optimization. Although the result of this fitting process is repeatable, there might still be a "better fitting", which the optimization is missing.

The total amount of tracer exposed to the system (about 0.45 g per 0.63 m^2) allows a theoretical concentration of more than 10 mg tracer per liter – so the modelled tracer concentrations of both models is lower than the maximum amount of tracer possibly entered the system. The MRTs produced by both models appear to be feasible when compared to similar investigations (Brown et al. 1980, p. 192) give turnover rates (turnover rate = 1/mean residence time) of 0.13 y^{-1} (i.e. an MRT of 7.7 y^{-1}) for a belowground biomass *Carex-Eriophorum* meadow; mosses in the same ecosystem are published with a turnover rate of 0.23 yr^{-1} (i.e. an MRT of 4.35 years). Although, conceptually, the total belowground biomass is probably more than the current-season photosynthates, the comparison shows that the model results seem to be feasible.

Raich and Schlesinger (1992) give MRT of 490 years for tundra soils and 520 years for swamps and marshes. Such data sets encompass the total carbon in soils, from which the current-season carbon is only a small pool. The mean residence time of current-season photosynthates is shorter. The MRT of carbon in a temperate forest plant-soil system is reported with 4 ± 1 years and 8 ± 1 years for the recent photosynthates and longer-term stable carbon, respectively (Gaudinski et al., 2000). These values are slightly different from the 2.5 years for MRT of C in pine forest floor published by Schlesinger and Lichter (2001). In a very impressive compartmental modelling approach of different carbon mean residence times in the framework of the Duke-Forest FACE-experiment, Luo et al. (2003) estimated the residence time of microbial biomass and metabolic litter with 0.321 and 0.128 years, respectively.

Of course, the published data of other studies used here for comparison describe the total soil system (i.e. the bulk carbon cycle processes of the sites) while the current study aims to in-situ quantify the fluxes in the current-season carbon cycle.

Compared to the polygonal tundra soil system current- season photosynthate- MRT of 3 ± 0.2 days (CM) and 307 ± 41 days (LM) in this study, the other authors' soil-plant system carbon MRTs are longer. However, only the freshest and most labile part of the carbon cycle is modelled in this study (current-season photosynthates) and this might explain the very short MRTs observed. Moreover, this shows that the investigation of carbon turnover in-situ with ^{13}C-tracer-based modelling might actually open a more detailed understanding of such soil systems and might help to improve the understanding of the short-term or current-season carbon cycle processes.

These comparisons with other author's data shows that the CM –calculated MRT is orders of magnitude shorter, an indication that the CM model actually depicts only the freshest, most active and labile carbon pools of the soil system. Especially the DIC and the CH_4 pools show turnover times in the range of hours to days (Kuzyakov, 2001; Jones, Nguyen, and Finlay, 2009), which keeps the model MRT still in the feasible range. The model DOC pool, however, might represent already more stable carbon pools in the system, because the MRT of the total system tracer is, after day 25, basically only controlled by the DOC-TCTS, i.e. the fastest, most-labile carbon compounds are respired and emitted from the system and only the DOC-pool receives a steadily declining input of tracer.

The comparison with the ^{13}C-excess % found in the other, solid soil carbon pools (stems, roots, mosses) shows that at, the end of the observation period, a lot of carbon is still incorporated into the soil system. Together with the still-rising tracer concentrations in the DOC-pool, this shows that the tracer is far from being removed from the system at the end of the observation time.

This backs the assumption that the LM- produced MRT of 312 days, which is closer to the real-world MRT, because, judged by the still increasing amount of tracer in DOC and the high amount of tracer still stored in the system, there is little reason to assume that the MRT of 3 days produced by the CM is feasible. However, both values are calculated by the produced graph, transferring this value into an E(t) function and subsequently calculating the MRT. And it is obvious that the LM produces 10 times

higher tracer concentrations as does the CM, which might explain the huge difference in MRT produced by both models.

However, besides the transformation of the model produced C(t) – function to the MRT (compare to section 4.6), the compartmental model allows estimating the MRT from the best-fitting parameters. Here, the MRT for DOC is 380 days, which is comparable to the LM-produced MRT.

Summarizing, it could be shown that different mean residence times are obtained, depending on which model is applied (LM or CM), and whether the model TCTS is simply transferred to a E(t) function or whether the compartmental model parameters are used to calculate MRT. More research is essential to further establish this method.

5.4 Intrafluxes and CH_4/C_{in} and CO_2/C_{in} ratios of incorporated carbon and quantification of intra-fluxes

Discussion of research question Q4) *What is the ratio of both produced methane and produced carbon dioxide to up taken atmospheric carbon in the emission from the current-season carbon cycle (root exudates and respired carbon)? Are the fluxes among sub-surface carbon pools quantifiable by a compartmental model?*

Each carbon atom that enters a tundra wetland soil system via the photosynthetic pathway has a system-dependent probability to end up in one of the four major states: 1) in a recalcitrant or structural carbon compound, 2) discharged from the system as a DOC-carbon compound, 3) as re-emitted CO_2 or 4) as emitted CH_4. The experimental set-up suggests excluding the states 1) and 2)[4], so the remaining states for a carbon molecule is to be emitted as either CO_2 or CH_4. While in the system, a carbon atom is transferred from one system carbon pool to another. Quantifying both the CH_4/C_{in} – CO_2/C_{in} ratio and the intrafluxes is done with the compartmental model. In this study, the CH_4/C_{in} ratio is estimated with 0.51, and the CO_2/C_{in} ratio with 0.49. King and Reeburgh (2002) and Dorodnikov et al. (2011) report that less than 1 % of the totally incorporated ^{14}C-label is found in emitted CH_4 (in mesocosm experiments for boreal *Eriophorum-Sphagnum* association in the study by

[4] It is assumed that the ^{13}C-tracer which went into structural carbon pools does so far not appear in the sampled dissolved carbon pools, which excludes 1). Since the polygonal centre is assumed to be hydrological contained, i.e. DOC-based excretion (2) from the system can be excluded as well.

Dorodnikov et al. (2011) and in a *Carex-Eriophorum-Drepanocladus*-association in the study by King and Reeburgh (2002)). The difference between those both experiments and the current-study results is striking (50 % CH_4-fraction to less than 1%). However, this can be explained: In this study, the tracer was not measured in the emitted methane but in methane in 6 cm depth. The results of this study represent the CH_4-fraction in close vicinity to the roots, i.e. root exudates and their by-products. At least a part of that methane is possibly later oxidized to CO_2 on its way into the atmosphere. Roslev and King (1996) report a methane oxidation of up to 76 % in temperate pond. Preuss et al. (2013) demonstrate that the water-logged tundra soils on Samoylov island can foster methane oxidation of 50 % in the first centimeters of soil. Moreover, methane oxidation is likely due to the presence of the *Scorpidium* moss, which is reported to foster methane oxidation with symbiont microbes (Liebner et al., 2011). Knoblauch et al. (2015) even reported up to 99 % of CH_4 oxidation in water logged polygon centers.

However, these are only theoretical interpretations and the results of this study strongly suggest further investigation of the topic.

Generally, the modelled intra-fluxes of the undisturbed soil system are difficult to compare because comparable data is lacking. Still, they can be compared to atmosphere-soil fluxes from similar soil-systems, to learn whether they are in the same order of magnitude.

Based on the transformation method explained in the section 3.10 and Figure 14, the carbon fluxes obtained by this modelling experiment become comparable to carbon fluxes from other soil carbon cycle investigations. Kutzbach et al. (2007) gave respiration fluxes (i.e. CO_2 emitted by the system, comparable to flux a_{17}) between 0.025 g C h^{-1} m^{-2} and 0.03 g C $h^{-1}m^{-2}$. The transformed flux a_{17} corresponds to ecosystem respiration and has a value of 0.0274 g C h^{-1} m^{-2} (transformed from 0.274 mg C h^{-1} L^{-1}) and hence falls into the same range as the data given by Kutzbach et al. (2007) for September 2003. Wille et al. (2008) reported methane fluxes between 9.8 and 22.5 mg C m^{-2} d^{-1}. The methane flux obtained by this study (flux a_{27}) is 619.2 mg C d^{-1} (transformed from 0.258 mg C $h^{-1}L^{-1}$) and hence about 30 times larger than the fluxes reported by Wille et al. (2008). This discrepancy is explainable with a potential oxidation of the high methane flux obtained in the current study and hence the transformation of methane to carbon dioxide in the aerobic uppermost centimeters of the

soil. However, this comparison shows that the model produces flux values which are in the same range as reported fluxes from similar areas (both studies, Wille et al. (2008) and Kutzbach et al. (2007) were conducted in the Samoylov tundra, just like the current study).

Additionally, it has to be noted that each flux value obtained by the CM belongs to a certain solution. Each of these solutions is constraint-satisfying, i.e. it satisfies the constraints imposed by the mathematical model formulation. Hence, a flux value of one solution (each solution consists out of the fluxes a_{21}, a_{31}, a_{41}, a_{51}, a_{61}, a_{12},…., a_{ij}) cannot be directly compared with a flux value of another solution, because the constraint-satisfaction would not hold. The values given in this study, the median and the 0.25 and 0.85 quantiles of the flux values are to be only interpreted as ranges, because they do not represent underlying probability distributions. The only statement that can be done is that all solutions found by the optimization procedure fall into a certain range, thus limiting the range of possible solutions of the system.

The fluxes furthermore show that the GA algorithm favors CM model realizations where most of the CH_4 produced by the system is produced by hydrogenotrophic methanogenesis (CO_2 reduction), which is in the same order of magnitude as given by Nakagawa et al. (2002) for Siberian alasses (51-68 %), Quay et al. (1991. In: Nakagawa et al. (2002)) for Alaskan tundra CH_4 (80 %), and Martens et al. (1992. In: Nakagawa (2002)) for Alaskan Pingo ponds (70 %).

5.5 Methodology and further aspects of this study

Diffusion as main tracer transport?

Among the biggest issues related to the tracer time series development and its relation to the sub-surface soil system processes is the possibility that the observed amounts of tracer might be an artefact produced by simple downward-directed diffusion through the system. It is argued here that the diffusional tracer allocation in the system plays a minor role in comparison to the carbon cycle processes. In the following, the argumentation supporting this assumption is developed.

According to Crank (1975), the diffusion concentration function of time and space is

$$15) \qquad C\,(x,t) \;=\; \frac{M}{2\,(\pi D t)^{\frac{1}{2}}}\, exp\left(-\frac{x^2}{4D}\right),$$

where D is the diffusion coefficient of CO_2 in water ($1.97 \cdot 10^{-5}$, according to Frank, Kuipers, and van Swaaij (1996)), t is the time since the introduction of the amount M of the substance, x is the distance from the point of insertion. In Figure 44 the hypothetical tracer increase at the depths of 6 cm is depicted. The surface layer tracer concentration is unknown[5], hence values between 2 to 30 % tracer concentrations are assumed. It cannot be denied that the calculated tracer concentrations are in the same order of magnitude as the measured tracer time series. Therefore, an influence of diffusion introduced tracer concentration cannot be simply excluded. However, the predicted diffusion-related tracer concentration time series graph does not resemble the observed tracer time series graph (fast increase, very slow decline in the calculated diffusion tracer time series in comparison to relatively fast and mediate decline in the observational data graphs).

Moreover, if tracer diffusion plays an important role in the tracer concentration time series, it would – according to the calculated concentration changes, show a more stable, less declining concentration in at the end of the observed time series. In Figure 44, the green lines display the integral of calculated tracer time series concentrations. The hypothetical diffusion-induced tracer concentration is a function of time (time passed since tracer introduction) and the depth (distance from the location of tracer introduction (see equation 15). The sample represents about 100 ml from around the sampling point (6 cm) and hence represents an integral over the area (sample plume, refer to A VI, page xxvi).

This does not rule out the possibility of an advective tracer allocation rather than diffusion or a combination of both. Wind and precipitation might possibly cause eddies and particle motions at least in the first centimeters of the system. It remains unclear, whether or not they do affect the chemistry down to a depths of 6 and more centimeters. Judged by the shape of the calculated diffusion-based tracer concentration time series and the observed tracer concentration data points, it can be assumed that diffusion does not impact the tracer concentration time series significantly, since

[5] The concentration of tracer in the depth of 6 cm is known for DIC. However, the tracer concentration in the uppermost surface layer can be higher (or lower), because the DIC-tracer in 6 cm depth is already influenced by carbon cycling processes. Equation 15 gives the DIC concentration in 6 cm depth, hence a possible diffusion-affected tracer concentration depends on the tracer concentration in surface DIC.

the concentration curve shape would be a different one. This assumption is possibly backed by the observation in an additional in-vitro labeling experiment with *Eriophorum* spec. and *Sphagnum* spec., which has been conducted to show the effect of mosses on the tracer behavior in the plant-moss-soil system and is shown in Appendix A V . The mosses seem to readily incorporate any carbon dioxide available to them in the upper few centimeters and hence might inhibit a diffusion-controlled downward migration, simply by removing the diffusion substance (i.e. the tracer $DI^{13}C$). However, this topic should be scrutinized in further investigations because the fact that both the calculated diffusion-tracer concentration curve and the observed data points range over the same order of magnitude. This might impact the tracer concentration time series. An additional experimental set-up and the results are given in the appendix. Summarizing, the experiment explained there shows that the moss-*Sphagnum* plant community strongly promotes the label incorporation in the soil system, when the plants and the mosses photosynthesize unhampered. If the mosses are "switched" of (in the experiment achieved by simply banning them from the ^{13}C-enriched CO_2), the label transportation in the system is significantly less. Hence this experiment supports the approach to simplify this study's conceptual model (grouping vascular plants and mosses in the same compartment).

The label could have penetrated into the belowground via diffusion processes via plant or soil surface. This possibility cannot be ruled out completely. However, the soil surface is covered photosynthetic active mosses (*Scorpidium*) which would incorporate CO_2 and thus prevent it from directly entering the soil belowground (inhibition of CO_2 diffusion). This theory is supported by the CO_2 diffusion coefficient into water and soil, both of which would suggest a high CO_2 concentration of labeled DIC in depth of interest (6 cm), which was not observed. DOC in this soil layer was only observed after several days, and increased more and more until the end of the sampling period, affected by ^{13}C-label. Previous literature suggests an immediate increase in ^{13}C-DOC in (*Sphagnum*-) moss-produced DOC after a label experiment (Fenner et al., 2004), which supports the hypothesis that mosses, due to their high affinity to ADC, prevent tracer diffusion through water by quickly taking up any tracer molecules that are around in the first few centimeters. Plants itself can serve as a pathway for diffusive CO_2 transportation and there is no reason to assume that label ^{13}C-CO_2 could

not be transported downward via this pathway. In this case the DIC would not only represent plant-respired CO_2 but also directly air-delivered DIC. This possibility allows still the deduction of CO_2 mean residence time in the belowground, since the label is washed out by subsequently incorporated newly derived CO_2, and thus allows interpreting plant-root-released CO_2 behavior in context with CH_4 production at the same site. The CO_2 in the system reaches – at least for the observation period – a new, higher $^{13}C/^{12}C$ ratio. This can be explained by the observation that ^{13}C is incorporated into the young roots and plant stems and that its concentration was still higher than natural background concentration when the experiment was terminated. This means that the plants serve as "label trap", in which enough of the label ^{13}C is stored in order to supply the sub-surface system with a constant stream of labeled carbon (in forms of CO_2 and DOC), still days and weeks after the pulse-labeling took place. The new, higher $^{13}C/^{12}C$ ratio indicates a "baseline" of the system, now contaminated with label material that is brought into the system. The outwash-behavior of CO_2 (and CH_4, partly) suggests that sub-pool of the CO_2 pool is directly influenced by plant metabolic activity. Thus there are two parallel processes that lead to a modified (in comparison with natural background values) $\delta^{13}C$ signature. The tracer interpretation, as applied in this study, requires information of the natural background site concentration of ^{13}C, which needs to be subtracted from the label site ^{13}C. The difference is the “tracer” – part of the ^{13}C concentration. Unfortunately, for the depths 20-30 and 30-40 cm, the $\delta^{13}C$ signature of the solid natural sub-surface carbon pools (fine roots, coarse roots, dead roots, *Scorpidium* moss and old *Carex* remainders) is not available. Hence, the tracer amount for these deeper sub-surface carbon pools is calculated from natural background ^{13}C value.

Representativeness of pore water sample and label concentration in carbon pools

In general, a tracer interpretation is difficult in systems such complex as a soil. The difficulty arises since the tracer, which is inserted into the system (in this study by photosynthesis), is immediately diluted and fixed in carbon pools with different turnover times (sugars, organic acids, amino acids, lipids, lignin etc.). The technology available does not allow detecting the tracer concentration in all this sub-pools. What can be done is to give a value for the average tracer concentration in the compartment. This is fine for the compartment where the tracer enters first (in this case, the plants

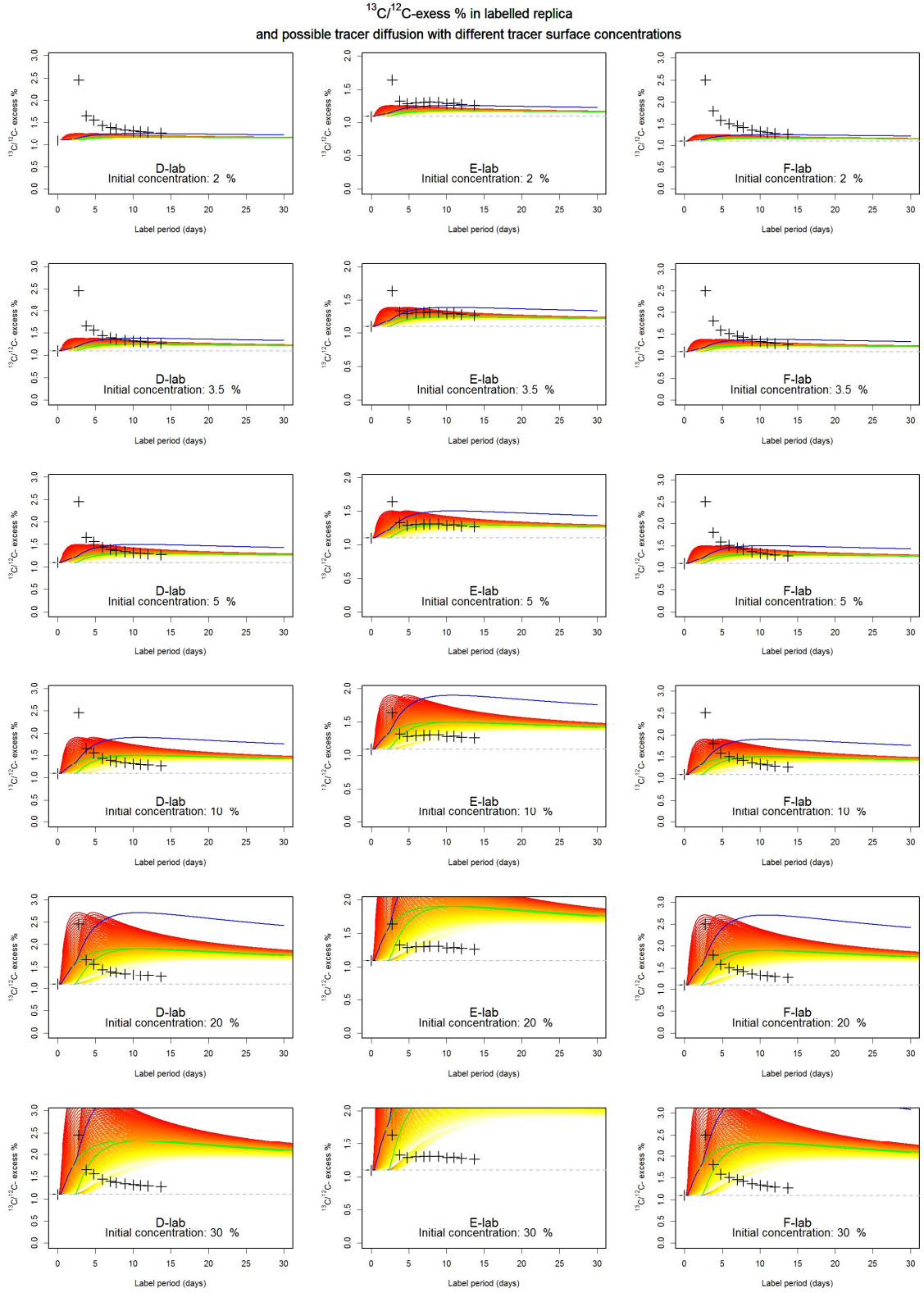

Figure 44. The modelled (with equation 15) tracer concentration increase in the sample area 6 cm below surface due to diffusion tracer allocation in DIC. The integral (green) of an hypothetical tracer time series in

1 (red), 2, 3,4, 5, 6, 7, 8, 9, 10, 11 (yellow) cm is shown. The calculated hypothetical diffusion-induced tracer concentration time series is plotted for day 0 (before the labeling) and day 2 (afte the labeling). The blue line represent the sum of both concentration time series. The assumed initial surface concentration of tracer (in % ^{13}C) is annoted in each sub-figure. The observed ^{13}C-excess % concentrations for CO_2 are depicted with black crosses.

and roots). However, as soon as the next compartment (the compartment into which the tracer finds its way after leaving the plant, e.g. CO_2 or DOC) is interpreted, the situation is a different. The observed tracer concentration can always represent either a very little portion of the previous pool with a high tracer concentration or a huge portion with a low tracer concentration – and all steps in-between.

This simple problem impacts the interpretation of tracer experiment significantly, because, in comparison to blood tracer experiments in the medical sector (Norwich 1977; Anderson 1983), where the tracer is homogeneously mixed in the compartment, the label in this study is probably heterogeneously mixed. Therefore, any correlation between tracer concentration and matter flux has to be done with keeping this problem in mind.

The label concentration is a vector pointing into the zones of activity in the carbon cycle system. Conceptually expected, in this study quantified, atmospheric-derive carbon, i.e. carbon incorporated 12 days earlier than the 29th of August 2013 (end of experiment), was mostly allocated into the moss, which forms the substrate in which the *Carex* roots grow. The homogeneous label distribution in the mosses shows that the mosses incorporate atmospheric carbon which is dissolved in the upper surface layers together with carbon dioxide released by root respiration and by breakdown of dead organic matter. This is an explanation for the higher $\delta^{13}C$ value of the DIC (natural background) in 6 cm depth in comparison to 16 cm and 36 cm depth. The carbon incorporation in the *Carex* stems, as well as the *Carex* roots, displayed high variations. This is explicable with the structure of the vascular plants. Each plant is further separated into several compartments, with differing mean residence time of carbon. Some parts, roots and stem parts as well, are less or not maintained by plant metabolic processes and hence produce and receive less freshly-produced photosynthates. This could lead to

parts of the roots and stems that show very high label incorporations and others that did not incorporate the label at all.

Comparing the *Carex* plants and the bryophytes, it becomes obvious that in this system the moss plays the most important role when it comes to the incorporation of label in the system. The label distribution pattern is similar to the total carbon distribution pattern, slightly preferring the carbon incorporation into the *Carex* plant. *Carex* is important, because it shows activity until the very depth of the active layer, which has been observed by Brown et al. (1980) for *Eriophorum* as well. The plant roots are likely to follow the active layer lower border and hence release freshly incorporated atmospheric-derived C also in the deepest parts of the active layer. The mosses, naturally, are constrained to that part of the active layer, in which enough sun insulation still enables photosynthesis (Glime, 2014).

Interesting is the label incorporation in some of the "dead" roots. According to literature (Wu et al., 2010), black roots has been chosen as dead roots, whitish-yellowish roots as living, or short-term dead roots. However, having found label in the "dead" roots indicates that some of the black roots might still incorporate significant amounts of ADC.

As shown in section 4, the tracer signal is very prominent in the DIC pool and the CH_4 carbon pool of 6 cm. The tracer is generally higher in both DIC and CH_4 pools across all depths. In CH_4 and DIC pools, the tracer concentration follows a similar pattern of change over time, although the tracer concentration in CH_4 is generally lower (about an order of magnitude, when transformed into ^{13}C-excess %). The close similarity of CH_4 and DIC shows the close interconnection between both carbon pools. The CH_4 in the carbon pool is produced either with the hydrogenotrophic pathway (meaning, the C originates in the CO_2 pool) or the acetoclastic pathway (meaning, the C originates from the DOC and other soil compartments). Since the DOC is not displaying a comparable tracer concentration behavior, this tracer concentration of the methane can be only influenced by the tracer concentration of CO_2. This is the first qualitative indication about the connections among the sub-surface carbon pools: at least some fraction of the CH_4 pool is produced by hydrogenotrophic methanogenesis and this carbon is transferred from DIC to CH_4. To assume that the methane is at least partly produced by hydrogenotrophic methanogenesis corresponds to observations of Beer et al.

(2008) from peat underlying a beaver pond and Zhang et al. (2011) in a rice field. The threshold, which decides whether the hydrogenotrophic or the acetoclastic pathway is more feasible seems to be highly variable with season in those studies. The samples used here to measure $\delta^{13}C$ of DIC and CH_4, and DOC are taken at a single point but represent a volume plume of about 100 m, which corresponds to a plume with about 3 cm^{-3} [6]. This is important to keep in mind for the interpretation, because it means that each pool represents an integrated sample of different processes in the root-soil environment. Since many carbon transportation processes at the root-soil interface happen with different reaction speeds (Jones, Nguyen, and Finlay, 2009), the reader has to keep in mind that there exists always the possibility that the tracer behavior is governed by a process which is not taken into account or which is impossible to define.

Numerical optimization and the problem of the adequate objective function

Numerical optimization methods, such as GA, Simulated Annealing, Firefly-Algorithms etc., might generally miss the "perfect", the global optimum. Applying numerical optimization methods, especially when the solution has a constrained search space, bears the risk to miss the actual solution of the optimization process. However, due to the infinite search space of such problems, such methods are usually the only option one has to meet the requirement of optimization (e.g. Yang, 2014). The performance of the algorithm applied, be it GA, SA, or any other, depends on the skills of the program developer and the understanding of the system – at least in rather complex problems as met in this study. Tuning the algorithm is a time-consuming endeavor. In this case, the case of a simple GA Algorithm, a multi-level (bi-level) constrained-satisfying optimization program is applied. The search space is divided in the free-search space, consisting of the variables X_1, X_2, X_3, and the variables that control the tracer concentration and tracer decline in the pre-pools, $X_{4\text{-tracer concentration}}$, $X_{5\text{-tracer concentration}}$, $X_{4\text{-tracer concentration decline}}$, and $X_{5\text{-tracer concentration decline}}$, and the sub-search space of the transfer fluxes among the carbon pools of the system a_{ij}. The plan was to define the seven free-search parameters and then use a numerical algorithm to find the optimal combination of a_{ij}, assuming free-

[6] For further explanation refer to the sample plume concept, in A VI xxxii)

search parameters as constant for this sub-parameter optimization problem. The idea was to use the value of the sub-level optimization problem and find the free-search variable combination that produces the best sub-level optimization. It turned out that there are some pit falls, which make life trickier for the experimenter. The free-search parameters search ended in something I considered a local minimum. There was simply no trend observable in the development of the values of the objective function, and the parameters produced model outputs that did not represent the CH_4 tracer function well.

It became obvious that this first objective function was less suited than previously thought for finding a best-fitted solution. And the first assessment of the produced tracer-curves made it obvious that some factors were not taken into account.

Therefore, a workaround was tried. A file was created, into which manually chosen model products are stored, namely those that have a worse optimization value in comparison with the best values found so far, but which showed a graph which resembled the natural system closer than the graphs produced by the so far best-fitted parameter combinations. The algorithm treated these manually chosen model-products with high priority when selecting new parameter combination-species for modification.

Another aspect, the variance of data, is a problem that can be solved only with high-resolution data sets and/or the definition of some degree of variance in the model (deviation from the actual fluxes by a defined probability and inside a defined range). Defining this in the stiff-framework of constraint-satisfying conditions was found to be not a simple task. High-resolution data sets are challenging to be received from soil pore water in such small-scale changing system as the heterogenic tundra landscape, because the higher the sample frequency, the more water is removed from the system. Removing water from the system, without replenishing, constantly changes the chemistry of the system and probably has an effect on the systems behavior. The advantage of a low-resolution data set is the reasonability of the assumption that one gets a nicely averaged tracer sample (averaged over time and space), so the systems variability is reduced ("smeared") already to a certain, but unknown degree.

The “curse of dimensionality” and the constrained-imposed complexity of the problem showed the need for more computational power. The standard desktop PC produced only several hundred solutions of the system per day and the R software was susceptible for unforeseen crashes so the application of the GA was lengthy. The model resolution had to be reduced from 0.25 hour time step to 2 hour time step. This enhanced the time performance of the GA procedure. Yet, the slow performance and hence the time-consuming development required an adaptation of the work schedule. Moreover, the data produced during the optimization procedure requires storage volumes of more than 2 GB. The time-consuming approach is – with additional research – improvable.

Compartmental modelling and compartmental model analysis

One major point of criticism, when it comes to compartmental model analysis, is the lack of physical laws in the approach. There are no physical laws ore stoichiometric dependencies included that govern the matter fluxes among the compartments (or pools). Norwich (1977) picked up this point of criticism and still recommends the method for simple input-output studies, because "[…], the results obtained should be correct because they can be shown to be in agreement with the predictions of linear systems theory which *does* have a firm physical base. […]" (from Norwich, 1977). The author shares this opinion, because although the physical laws govern the matter transfer in the pools, if the pool sizes do not change (significantly) during the experimental time, the matter transfer can be described by the compartmental approach. Of course, for this assumption it is essential that there are no large unknown carbon pools. The simple structure of this plant-soil system allows assuming that all important pools are known.

Time step sensitivity test

The chosen compartmental model reproduces tracer concentrations in the soil system environment in the depths of 6 cm. It is a discrete time step model, i.e. each tracer concentration at time step t_i depends on the previous step. With other words, the differential equation function $\frac{dC}{dt}$ is solved numerically for each defined discrete time step. The performance of the model depends on the length of the chosen time step, i.e. the smaller the selected time step interval, the closer the numerical

solution is to the "real" solution of the equation (Anderson, 1983). A first time step sensitivity test showed that, while the model is very reliable in reproducing the TCTS of DIC-tracer and DOC-tracer, the reproduction of the CH_4-tracer was dependent on the time step-size (no data given).

Discussion of the label-experiment

There is no standardized method to do in-situ pulse-labeling, so every study uses its own method. In comparison with this study's method, Dorodnikov et al. (2011) and King and Reeburgh (2002) labeled for shorter periods with $^{14}CO_2$. The sensitivity of ^{14}C label should be compensated by the longer label period with ^{13}C in this experiment. Ostle et al. (2000) applied a longer, $^{13}CO_2$, pulse-label (10 daylight hours during two days), which seems to work fine for labeling a *Sphagnum* site.

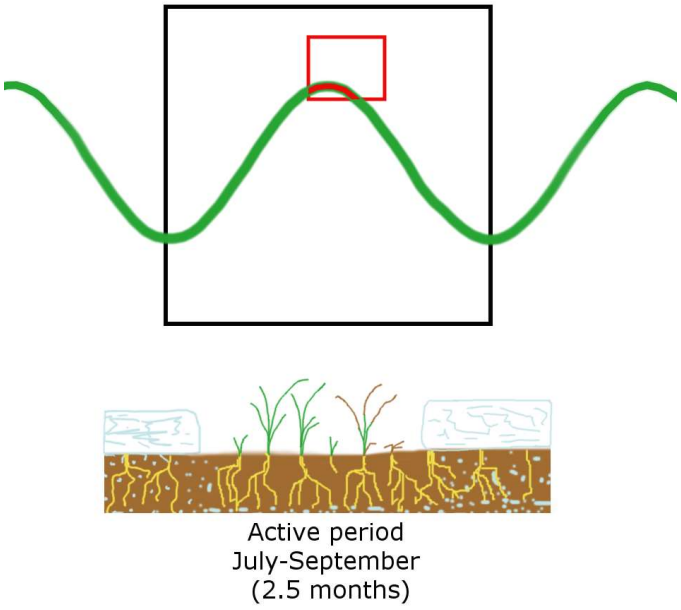

Figure 45. Schematic experiment time in the context of the circannual model of the phenological plant cycle. The experiment represents the period where the vegetative growth is ceded and the senescence about to begin. Since the Arctic summer is very short, this time window is very narrow and the experimenter must be aware of the possibility that the experiment represents a transitional phase, i.e. it might be biased.

Temporal resolution, spatial resolution, limitations, and implications for longer observational periods

The temporal resolution of the in-situ ^{13}C isotope labeling experiment is about two weeks. On such a short period, most probably some aspects of the tracer dynamics remain unobserved, because they happen afterwards. Of course, ideally, it would be advisable to just observe for a longer period. However, the limited time budget at the Samoylov research station made this impossible.

Therefore, each system's simulation can be compared only with the observational time period. The challenge is that there are carbon pools with a slow turnover rate – slow enough to show only a very small section of their potential tracer outwash function. This is due to long-living plant-produced organic molecules, which contain tracer. The degradation of such organic molecules (e.g proteins, lignins) can be delayed for weeks, months or even years. The respiration rate – and hence the tracer mean residence time of such molecules depends, especially in permafrost-affected areas, on ambient parameters such as temperature and soil water content. Therefore, in this study, the tracer signal's fraction that is related to dying and decomposition of *Carex* stems, as well as older moss thalli appear in the system only as background signal. However, in the Arctic ecosystem wetland, and generally in wetlands, the net loss might be either positive (i.e. accumulation of organic matter and little to no decomposition by organisms) or negative (i.e. decomposition) and it must be taken into account, if the tracer loss happening via this pathway is significant compared to the total tracer loss and incorporation, respectively.

Another important factor is the temperature, sun insolation and precipitation regime, because these parameters are a direct threat to the assumption of system stationarity (compare modelling approaches based on environmental parameters (e.g. Street et al., 2011). All three investigated carbon pools display seasonal changes, which in Arctic regions tend to appear within weeks rather than months. In theory, the existence of parameters that change the stationarity of a system is barely sufficient for an observation-based interpretation of the tracer concentration function in the system. This is, because the steady-state assumption is violated when drastic changes of environmental parameters cause a forced change of system fluxes and pool sizes. A violation of the steady-state assumption results in transfer coefficients and pool sizes, which are no longer constants, but functions of time. Such a change dramatically increases the number of variables in the system and complicates the mathematical solution for the system pools' tracer concentration differential equations (Anderson, 1983), making the system's equation system unsolvable if no further data can be used to find specific solutions for it. Furthermore, the temporal scale has to be included.

However important these questions are, it could be assumed that in the present study, short-term changes variation of stationarity makes the system states wobble around an ideally system response

curve but still represent the general shape of the system's tracer outwash function. Minor violations of stationarity would then appear only as variance of the simulated system parameters. Any observed trend could still be used for analysis.

Finally, it has to be mentioned, that the current experimental approach and the CM model is limited to water-stained soils, because a TCTS is difficult to measure in soil gas (i.e. in aerated soil types). Obtaining tracer signals from not-water saturated soils requires usually the destruction of the soil material and so the method turns into an invasive one. In principle, as the amount of pore water, also an amount of pore gas could be sampled and measured for tracer concentrations.

Vegetation association

For the study of King and Reeburgh (2002) a ^{14}C-pulse-labeling experiment was conducted in Toolik, Alaska, in a similar ecosystem type (wet tundra). The vascular plants and the mosses are different species, which still might be regarded as physiologically close enough for a direct comparison. The Samoylov association is a *Carex-Scorpidium* plant association, while their Toolik-counterpart was an *Eriophorum-Carex-Drepanocladus* association (personal communication J. King, 2016).

Only 17.3 g m^{-2} is bound in shoots (764 tillers m^{-2}), which is slightly more as the 689 in the mesocosm experiment from King and Reeburgh (2002), but less than in their natural sites (1108-1145). Since in our study site the aboveground biomass solely consists out of *Carex* (i.e. all mosses are considered to end at the water level), we have comparatively low aboveground C (17.29 g C m^{-2}, or 37.94 g biomass m^{-2}), compared to 399.9 g biomass m^{-2} in King and Reeburgh (2002), but it is in the range of aboveground *Carex*-association biomass (28-42 g m^{-2}) as given for coastal tundra in Alaska by Miller et al. (1980). Based on the data for *Carex* in Miller et al. (1980), which shows a decline in leaf area index for August in 1970 and 1971 in Barrow, Alaska, and taking into account the partly yellowish-greenish *Carex* shoots in Samoylov in August 2013, it can be concluded that the ecosystem was already preparing for senescence. In general, it can be stated that the experimental site data is comparable to data from King and Reeburgh (2002), which would allow repeating the compartmental modelling with the data from that study. The two plant species found in the polygonal center represent tracheophytae, (*Carex aquatilis*) and bryophytae (*Scorpidium scorpidioides*). They

have different roles in the biogeochemical process, controlling the carbon cycle in the polygonal tundra center. The sedge *Carex* utilizes atmospheric-CO_2 for the photosynthetic process. The aerenchyma enables swapping oxygen and methane between atmosphere and rhizosphere (Allessio and Tieszen, 1975), carbon dioxide can be directed to the leaves from the rhizosphere (Constable, Grace, and Longstreth, 1992).

The moss Scorpidium can take up carbon dioxide from the atmosphere, but also dissolved carbon dioxide (Glime, 2014) from the pore water and open water in the polygon center. Moreover, Scorpidium hosts methanotrophic symbionts that convert methane to carbon dioxide which then is utilized by the moss (Liebner et al., 2011). Glime (2014) states that carbon dioxide represents a limiting factor for aquatic mosses in summer months, when the competition for carbon dioxide with phytoplankton is highest.

The close interactions between plant roots and moss thalli in all layers support the compartmental model assumption that the mosses and plants can be conceptually combined in one "plant pool", because they cannot be separated into different carbon pools without more tracer incorporation data.

The interaction of both plants allows drawing a conceptual model of the night and day carbon dioxide uptake-allocation, which in return helps to understand conceptually the path of the label into plant compartment of the system.

Day: When the system is exposed to atmospheric carbon dioxide, the vascular plant and the tips of the bryophytes photosynthetically utilize carbon dioxide and produce photosynthates, which will be used in respiration processes (oxidation of photosynthates and subsequently emission as carbon dioxide) or excreted into the soil as acids, lipids, dead cell walls and other short-term carbon compounds that are quickly released into the soil pore water environment. Some of the carbon dioxide label (!) will cross the atmosphere-water surface and will be readily dissolved, forming CO_2 (aq). This dissolved carbon dioxide will be consumed by those parts of the bryophytes, which are located in the pore water column. It is assumed that this process happens quickly, because the moss thalli are everywhere in the pore water.

Night: carbon dioxide is released from all parts of the system. The label can diffuse into all compartments, depending on concentration gradient and compartment borders. This is the only

situation in which the label – theoretically – could migrate into the pore water without representing a product of the plant metabolic process, but simply an experimental artefact. However, in mid-August the night is very short and photosynthesis is clearly reduced, but not completely stopped. Moreover, the label diffuses only some centimeters per day into the water column, meaning that any label still freely dissolved in the system will by then be taken up by mosses from within the water column. Hence, the label detected later represents plant-produced carbon compounds.

In this system, we can assume that the label is incorporated entirely by plant processes (which means by both *Scorpidium* and *Carex*, forming a "single" plant organism) and hence truly represent only ADC dioxide.

By far the largest carbon pool is represented by the mosses. The mass of supra-surface *Carex*, in comparison to the mosses is rather small. The second largest pool is formed by the fine roots, everywhere entangled with the mosses on a semi-macroscale. The most active pools, the dissolved carbon dioxide, the dissolved organic matter and the dissolve methane represent only very small pools. The size of the carbon pools is important in this study for two main reasons. Firstly, it is important to know the size in order to formulate a model of the system. The size of the compartments which exchange matter among themselves and the outer-system environment only makes the model formulation and application possible. Secondly, in order to check whether the assumption of stationarity is true, the concentration of carbon (i.e. the pool size) should stay the same during the observation period.

The observation that significant amounts of (about 4 %) label are found in an undefined carbon pool of small grain size and did not fall into one of the defined carbon pools shows that a deeper investigation of all carbon pools is required and should be done in further studies.

The roots are not a huge carbon pool in the system, but an active one, which is demonstrated by their small contribution to the total C found in the system (between 2.8 and 3 %) and their relatively high contribution to the total label found in the system (between more than 11 % in the first and about 9 % in the second layer).

The assumption, that the high variance of the label-site $\delta^{13}C$ values generally indicates a label incorporation is backed by the observation that even in the lowest layer (36 cm below the surface),

the dissolved Carbon pools show ^{13}C-concentrations that indicate label incorporation into roots even in this depth. Because the natural background ^{13}C values are only available for the total soil C, not for the sub-pools, - to calculate the ^{13}C-excess % values in the pools in the depths of 0.2-0.3 and 0.3-0.4 cm, the average soil ^{13}C-concentration was used as background value.

6 Conclusion and Outlook

Conclusion

This study addresses the information gap about the high-latitude soil carbon cycle. The outcome of this study gives valuable information about the soil carbon cycle in the polygonal tundra. In detail, the following findings are made:

- (related to Q1) – The distribution of atmospheric-derived carbon in a tundra wetland soil is presented and compared to similar studies, enhancing the understanding of carbon allocation patterns in high-latitude wetland soils. Particularly, it was demonstrated that most of the incorporated carbon (namely 45.9 ± 13 %) is found in the mosses in the upper 20 cm of soil. Furthermore, the label is found in the *Carex*- rhizosphere in a depth of 36 cm, which shows that the entire active layer is affected by root-driven carbon allocation.
- (related to Q2) – This study suggests that tracer experiment evaluation methods, well established in medical, chemical and biological science, have a potential for wide-spread application in wetland soil carbon cycle investigation. Tracer concentration time series can be reproduced by properly set up compartmental models of the carbon cycle. However, depending on the type of model applied, the calculated MRT values differ and further research on the topic is required. The major challenge is to obtain continuous tracer concentration time series, because the fitted model performance depends on the available tracer concentration curves. So for further studies it is strongly recommended to produce data sets that meet this requirement. In general, at least for tundra and high-latitude soils, the time series should cover a time period of more than 2 weeks after the pulse-labeling, because the 2-week observation time of the current study show that the tracer concentration time series in the DOC-pool started to decline (the $\delta^{13}C$-values were still rising), while it was sufficient for tracer dynamic investigations in both DIC and CH_4 in 6 cm depth. The TCTS in all deep-layer carbon pools were also still rising.

- (related to Q3) – The mean residence time of recently incorporated atmospheric-derived carbon in the soil system is estimated by a lognormal and compartmental model with 306.9 ± 41 days and 3.0 ± 0.2 days, respectively. Although in the range of previously published values for turnover rates in comparable soil systems, these contrasting results require further research. Probably, they are obtained by using two different models (LM and CM) for extrapolating the TCTS beyond the observed data points. Moreover, the LM is limited in its ability to produce a tracer concentration curve of a multi-compartment system.
- (related to Q4) – The fraction of emitted CH_4 and CO_2 for each incorporated carbon atom in the current-season carbon cycle is given with 0.51 ± 0.12 for CO_2 and 0.49 ± 0.12 for CH_4. These values correspond to CO_2 and CH_4 production in 6 cm depth – further oxidation of CH_4 is likely, but not captured by this study. The unlabeled soil carbon pools (X_6) contribute 36 ± 10 % to the current-season carbon cycle. The CM model suggest that 68 ± 16 % of the methane is produced by CO_2 reduction.

General conclusion: A compartmental model with 7 sub-surface carbon pool-compartments reproduced naturally observed TCTS in DIC, CH_4, and DOC pools and gives information about the intrafluxes of different sub-surface carbon pools. Without ignoring the doubtless existing challenges, the overall conclusion of the current study is that the further development of tracer-based compartmental modelling of the small-scale carbon cycle in wetland rhizospheres has a great potential to significantly increase the understanding and the ability to investigate such systems. It is applicable with relatively ease and in remote areas, thus having advantages in comparison with large-scale labeling studies like FACE-studies. An improved understanding of the tundra soil carbon cycle would eventually allow a reliable prediction of the future state of the important carbon pools in the permafrost-affected landscapes. Yet, the conceptual challenges and the methodological questions should be addressed in further studies (see Outlook).

Outlook

The current study gives interesting insight into the sub-surface carbon cycle of a tundra soil. However, many questions are unsolved and other questions arose in the course of this study.

Investigating the following points could improve both the understanding of the carbon cycle and of the methodology:

- Further development of the method is essential. Therefore, more replica and experiment repetitions are required. In the beginning, existing data sets of the current study, so far not used for this study so far, could be used to increase the number of replicas in the CM experiment from n=1 to n=3.
- Sensitivity tests of time-step size, variance, reproducible model application in other soil systems, and the influence of environmental parameters (e.g. radiation, temperature, precipitation, wind stress) on the tracer concentration time series data point variance are among the points that need to be investigated.
- Different study sites, both in comparable ecosystems and in differing ones would help to understand whether and how the methodology is generally applicable.
- Improvement of the compartment model, more case studies, implementation in the framework of ongoing EC and chamber measurement campaigns for direct comparison.
- Comparison with alternative labeling methods and established modelling methods (such as FACE, ^{14}C-labeling, etc.).
- A mesocosm setup in the square meter scale (artificial ecosystem) is necessary, which allows investigating the soil carbon cycle under natural-like conditions to understand how changing environmental parameters influence the tracer concentration time series. Furthermore, the model performance and the model output like MRT and intrasystem fluxes could be compared to measurement data in a controlled laboratory environment.
- This type of soil investigations have a great potential, especially in combination with ever-improving measurement technology – such methods could be standardized (so far every research group has their own methods and data analytical procedures) and the discussion should be tread lose how tracer experiments can be integrated into long-term carbon cycle measurement campaigns in Arctic soil research (for improved understanding of the processes going on).

7 References

Ainsworth, E. A., and S. P. Long. 2005. 'What Have We Learned from 15 Years of Free-Air CO2 Enrichment (FACE)? A Meta-Analytic Review of the Responses of Photosynthesis, Canopy Properties and Plant Production to Rising CO2:Tansley Review'. *New Phytologist* 165 (2): 351–72. doi:10.1111/j.1469-8137.2004.01224.x.

Allessio, M. L., and L. L. Tieszen. 1975. 'Patterns of Carbon Allocation in an Arctic Tundra Grass, Dupontia Fischeri (Gramineae), at Barrow, Alaska'. *American Journal of Botany* 62 (8): 797. doi:10.2307/2441890.

Anderson, D. H. 1983. *Compartmental Modeling and Tracer Kinetics*. Edited by S. Levin. Lecture Notes in Biomathematics 50. Berlin Heidelberg New York: Springer Verlag. doi:10.1007/978-3-642-51861-4.

Anderson, D. H., J. Eisenfeld, S. I. Saffer, J. S. Reisch, and C.E. Mize. 1977. The Mathematical Analysis of a Four-Compartment Stochastic Model of Rose Bengal Transport through the Hepatic System. Edited by V. Lakshmikantham. *Nonlinear Systems and Applications*, Academic Press, New York. doi:10.1016/B978-0-12-434150-0.50033-3.

Anderson, G.M. 1976. 'Error Propagation by the Monte Carlo Method in Geochemical Calculations'. *Geochimica et Cosmochimica Acta* 40 (12): 1533–38. doi:10.1016/0016-7037(76)90092-2.

Are, F., and E. Reimnitz. 2000. 'An Overview of the Lena River Delta Setting: Geology, Tectonics, Geomorphology, and Hydrology'. *Journal of Coastal Research* 16 (4): 1083–1093. http://www.jstor.org/stable/4300125.

Avagyan, A., B. R.K. Runkle, and L. Kutzbach. 2014. 'Application of High-Resolution Spectral Absorbance Measurements to Determine Dissolved Organic Carbon Concentration in Remote Areas'. *Journal of Hydrology* 517 (September): 435–46. doi:10.1016/j.jhydrol.2014.05.060.

Bassingthwaighte, J. B., and D. A. Beard. 1995. 'Fractal ^{15}O-Labeled Water Washout from the Heart'. *Circulation Research* 77 (6): 1212–1221. doi: 10.1161/01.RES.77.6.1212.

Beer, J., K. Lee, M. Whiticar, and C. Blodau. 2008. 'Geochemical Controls on Anaerobic Organic Matter Decomposition in a Northern Peatland'. *Limnology and Oceanography* 53: 1393–1407. doi: 10.4319/lo.2008.53.4.1393.

Bellman, R.. 2003. *Dynamic Programming*. First Dover Edition, 6 Princeton University Press Edition (from 1957). Mineola, New York: Dover Publications, Inc.

Beven, K.J., and P.C. Young. 1988. 'An Aggregated Mixing Zone Model of Solute Transport through Porous Media'. *Rapid and Far-Reaching Hydrologic Processes in the Vadose Zone* 3 (2): 129–43. doi:10.1016/0169-7722(88)90028-9.

Blodau, C, and M. Siems. 2012. 'Drainage-Induced Forest Growth Alters Belowground Carbon Biogeochemistry in the Mer Bleue Bog, Canada'. *Biogeochemistry* 107 (1–3): 107–23. doi:10.1007/s10533-010-9535-1.

Brown, J., P. C. Miller, L. L. Tieszen, and F. L. Bunnell, eds. 1980. *An Arctic Ecosystem : The Coastal Tundra at Barrow, Alaska*. Stroudsburg, Pennsylvania: Dowden, Hutchinson & Ross : http://www.biodiversitylibrary.org/item/23552.

Butler, J.. 1982. *Carbon Dioxide Equilibria and Their Applications*. Michigan: Lewis Publishers, Inc.

Christensen, T. R., T. Johansson, H. J. Åkerman, M. Mastepanov, N. Malmer, T. Friborg, P. Crill, and B. H. Svensson. 2004. 'Thawing Sub-Arctic Permafrost: Effects on Vegetation and Methane Emissions'. *Geophysical Research Letters* 31 (4): L04501. doi:10.1029/2003GL018680.

Christiansen, H. H., B. Etzelmüller, K. Isaksen, H. Juliussen, H. Farbrot, O. Humlum, M. Johansson, et al. 2010. 'The Thermal State of Permafrost in the Nordic Area during the International Polar Year 2007–2009'. *Permafrost and Periglacial Processes* 21 (2): 156–81. doi:10.1002/ppp.687.

Ciais, P., C. Sabine, G. Bala, L. Bopp, V. Brovkin, J. Canadell, A. Chhabra, et al. 2013. 'Chapter 6: Carbon and Other Biogeochemical Cycles'. In *Climate Change 2013: The Physical Science Basis. Contribution of Working Group I to the Fifth Assessment Report of the Intergovernmental Panel on Climate Change*, edited by T.F. Stocker, D.

Qin, G.-K. Plattner, M. Tignor, S.K. Allen, J. Boschung, A. Nauels, Y. Xia, V. Bex, and P.M. Midgley. Cambridge-New York: Cambridge University Press.

Constable, J. V. H., J. B. Grace, and D. J. Longstreth. 1992. 'High Carbon Dioxide Concentration in Aerenchyma of Typha Latifolia'. *American Journal of Botany* 79 (4): 415–418. http://www.jstor.org/stable/2445153.

Crank, J. 1975. *The Mathematics of Diffusion*. 2nd ed. Oxford: Oxford University Press.

Cui, L., Y. Zhang, M. Zhang, W. Li, X. Zhao, S. Li, and Y. Wang. 2012. 'Identification and Modelling the HRT Distribution in Subsurface Constructed Wetland'. *Journal of Environmental Monitoring* 14 (11): 3037–44. doi:10.1039/c2em30530e.

Danckwerts, P. V. 1953. 'Continuous Flow Systems'. *Chemical Engineering Science* 2 (1): 1–13.doi:10.1016/0009-2509(53)80001-1.

Dorodnikov, M., K.-H. Knorr, Y. Kuzyakov, and M. Wilmking. 2011. 'Plant-Mediated CH_4 Transport and Contribution of Photosynthates to Methanogenesis at a Boreal Mire: A ^{14}C Pulse-Labeling Study'. *Biogeosciences* 8 (8): 2365–75. doi:10.5194/bg-8-2365-2011.

Dorrepaal, E., S. Toet, R. S. P. van Logtestijn, E. Swart, M. J. van de Weg, T. V. Callaghan, and R. Aerts. 2009. 'Carbon Respiration from Subsurface Peat Accelerated by Climate Warming in the Subarctic'. *Nature* 460: 616–19. doi:10.1038/nature08216.

Fenner, N., N. Ostle, C. Freeman, D. Sleep, and B. Reynolds. 2004. 'Peatland Carbon Efflux Partitioning Reveals That Sphagnum Photosynthate Contributes to the DOC Pool'. *Plant and Soil* 259 (1): 345–354.doi: 10.1023/B:PLSO.0000020981.90823.c1.

Fogler, H. S. 2016. *Elements of Chemical Reaction Engineering*. 5th ed. Boston-Columbus-Indianapolis-New York: Prentice Hall.

Frank, M. J. W., J. AM Kuipers, and W. PM van Swaaij. 1996. 'Diffusion Coefficients and Viscosities of CO_2+ H_2O, CO_2+ CH_3OH, NH_3+ H_2O, and NH_3+ CH_3OH Liquid Mixtures'. *Journal of Chemical & Engineering Data* 41 (2): 297–302. doi: 10.1021/je950157k.

Gaudinski, J. B., S. E. Trumbore, E. A. Davidson, and S. Zheng. 2000. 'Soil Carbon Cycling in a Temperate Forest: Radiocarbon-Based Estimates of Residence Times, Sequestration Rates and Partitioning of Fluxes'. *Biogeochemistry* 51 (1): 33–69. doi:10.1023/A:1006301010014.

'Genetic Algorithm'. 2016. *Wikipedia*. https://en.wikipedia.org/w/index.php?title=Genetic_algorithm&oldid=755327894.

Gill, R A., and R. B. Jackson. 2000. 'Global Patterns of Root Turnover for Terrestrial Ecosystems'. *New Phytologist* 147 (1): 13–31. 10.1046/j.1469-8137.2000.00681.x.

GIMP developer team. 1997. *GIMP 2.8.4*. http://www.gimp.org.

Glime, J. M. 2014. 'Photosynthesis in Aquatic Bryophytes'. In *Photosynthesis in Bryophytes and Early Land Plants*, edited by T. David Hanson and K. Steven Rice, 201–31. Dordrecht: Springer Netherlands. doi:10.1007/978-94-007-6988-5_12.

Gould, J., D. Roemmich, S. Wijffels, H. Freeland, M. Ignaszewsky, X. Jianping, S. Pouliquen, et al. 2004. 'Argo Profiling Floats Bring New Era of in Situ Ocean Observations'. *Eos, Transactions American Geophysical Union* 85 (19): 185–91. doi:10.1029/2004EO190002.

Hearon, J. Z. 1968. 'The Washout Curve in Tracer Kinetics'. *Mathematical Biosciences* 3 (0): 31–39. doi:10.1016/0025-5564(68)90070-9.

Hicks Pries, C. E., E. A. G. Schuur, and K. G. Crummer. 2012. 'Thawing Permafrost Increases Old Soil and Autotrophic Respiration in Tundra: Partitioning Ecosystem Respiration Using δ13C and Δ14C'. *Global Change Biology* 19 (2): 649-661. doi:10.1111/gcb.12058.

Holland, J. H. 1992. *Adaptation in Natural and Artificial Systems. An Introductory Analysis with Application in Biology, Control and Artificial Intelligence*. First MIT Press edition. Complex Adaptive Systems. Cambridge, Massachusetts, London, England: The MIT Press.

Hongve, D. 1987. ‘A Revised Procedure for Discharge Measurement by Means of the Salt Dilution Method’. *Hydrological Processes* 1 (3): 267–270. doi:10.1002/hyp.3360010305.

Hope, D., J. J.C. Dawson, M. S. Cresser, and M. F. Billett. 1995. ‘A Method for Measuring Free CO2 in Upland Streamwater Using Headspace Analysis’. *Journal of Hydrology* 166 (1–2): 1–14. doi:10.1016/0022-1694(94)02628-O.

Hugelius, G., J. Strauss, S. Zubrzycki, J. W. Harden, E. A. G. Schuur, C.-L. Ping, L. Schirrmeister, et al. 2014. ‘Estimated Stocks of Circumpolar Permafrost Carbon with Quantified Uncertainty Ranges and Identified Data Gaps’. *Biogeosciences* 11 (23): 6573–93. doi:10.5194/bg-11-6573-2014.

IPCC. 2013a. *Climate Change 2013: The Physical Science Basis: Working Group I Contribution to the IPCC Fifth Assessment Report of the Intergovernmental Panel on Climate Change*. Edited by T. F. Stocker, D. Qin, G.-K. Plattner, M. Tignor, S. K. Allen, J. Boschung, Y. Nauels, Y. Xia, V. Bex, and P.M. Midgley. Cambridge: Cambridge University Press.

———. 2013b. Annex I: Atlas of Global and Regional Climate Projections [van Oldenborgh, G.J., M.Collins, J.Arblaster,J.H. Christensen, J.Marotzke, S.B. Power, M.Rummukainen and T. Zhou (Eds.)].’ In *Climate Change 2013: The Physical Science Basis. Contribution of Working Group I to the Fifth Assessment Report of the Intergovernmental Panel on Climate Change*, edited by T.F. Stocker, D. Qin, G.-K. Plattner, M. Tignor, S.K. Allen, J. Boschung, A. Nauels, Y. Xia, V. Bex, and P.M. Midgley. Cambridge-New York: Cambridge University Press.

Johnson, D., J. R. Leake, N. Ostle, P. Ineson, and D. J. Read. 2002. ‘In situ $^{13}CO_2$ Pulse-Labelling of Upland Grassland Demonstrates a Rapid Pathway of Carbon Flux from Arbuscular Mycorrhizal Mycelia to the Soil’. *New Phytologist* 153 (2): 327–334. doi:10.1046/j.0028-646X.2001.00316.x.

Jones, D. L., C. Nguyen, and R. D. Finlay. 2009. ‘Carbon Flow in the Rhizosphere: Carbon Trading at the Soil–root Interface’. *Plant and Soil* 321 (1–2): 5–33. doi:10.1007/s11104-009-9925-0.

Jørgensen, S. E., and B. D. Fath. 2011. *Fundamentals of Ecological Modelling*. 4th ed. Developments in Environmental Modelling. Amsterdam-Boston-Heidelberg: Elsevier.

Kaiser, S., M. Göckede, K. Castro-Morales, C. Knoblauch, A. Ekici, T. Kleinen, S. Zubrzycki, T. Sachs, C. Wille, and C. Beer. 2017. ‘Process-Based Modelling of the Methane Balance in Periglacial Landscapes (JSBACH-Methane)’. *Geoscientific Model Development* 10 (1): 333–58. doi: 10.5194/gmd-10-333-2017.

King, J. Y., and W. S. Reeburgh. 2002. ‘A Pulse-Labeling Experiment to Determine the Contribution of Recent Plant Photosynthates to Net Methane Emission in Arctic Wet Sedge Tundra’. *Soil Biology and Biochemistry* 34 (2): 173–180. doi: 10.1016/S0038-0717(01)00164-X.

Knoblauch, C., C. Beer, A. Sosnin, D. Wagner, and E.-M. Pfeiffer. 2013. ‘Predicting Long-Term Carbon Mineralization and Trace Gas Production from Thawing Permafrost of Northeast Siberia’. *Global Change Biology* 19 (4): 1160–72. doi:10.1111/gcb.12116.

Knoblauch, C., O. Spott, S. Evgrafova, L. Kutzbach, and E.-M. Pfeiffer. 2015. ‘Regulation of Methane Production, Oxidation and Emission by Vascular Plants and Bryophytes in Ponds of the Northeast Siberian Polygonal Tundra: Methane Turnover in Siberian Ponds’. *Journal of Geophysical Research: Biogeosciences* 120 (12):2525-2541. doi:10.1002/2015JG003053.

Kuntze, H., G. Roeschmann, and G. Schwerdtfeger. 1994. *Bodenkunde*. 5th ed. Stuttgart: Verlag Eugen Ulmer.

Kutzbach, L., J. Schneider, T. Sachs, M. Giebels, H. Nykänen, N. J. Shurpali, P. J. Martikainen, J. Alm, and M. Wilmking. 2007. ‘CO_2 Flux Determination by Closed-Chamber Methods Can Be Seriously Biased by Inappropriate Application of Linear Regression’. *Biogeosciences Discussions* 4 (4): 1005–1025. doi: 10.5194/bg-4-1005-2007.

Kutzbach, L., D. Wagner, and E. M. Pfeiffer. 2004. ‘Effect of Microrelief and Vegetation on Methane Emission from Wet Polygonal Tundra, Lena Delta, Northern Siberia’. *Biogeochemistry* 69 (3): 341–362. doi: 10.1023/B:BIOG.0000031053.81520.db

Kutzbach, L., C. Wille, and E.M. Pfeiffer. 2007. ‘The Exchange of Carbon Dioxide between Wet Arctic Tundra and the Atmosphere at the Lena River Delta, Northern Siberia’. *Biogeosciences* 4 (3): 869–90. doi: 10.5194/bg-4-869-2007.

Kuzyakov, Y. 2006. 'Sources of CO_2 Efflux from Soil and Review of Partitioning Methods'. *Soil Biology and Biochemistry* 38 (3): 425–48. doi:10.1016/j.soilbio.2005.08.020.

———. 2011. 'How to Link Soil C Pools with CO_2 Fluxes?' *Biogeosciences* 8 (6): 1523–37. doi:10.5194/bg-8-1523-2011.

Kuzyakov, Y., A. Kretzschmar, and K. Stahr. 1999. 'Contribution of Lolium Perenne Rhizodeposition to Carbon Turnover of Pasture Soil'. *Plant and Soil* 213 (1–2): 127–136. doi:10.1023/A:1004566027237

Kuzyakov, Ya V. 2001. 'Tracer Studies of Carbon Translocation by Plants from the Atmosphere into the Soil (a Review)'. *Eurasian Soil Science* 34 (1): 28–42. https://www.researchgate.net/publication/279892329_Tracer_Studies_of_Carbon_Translocation_by_Plants_from_the_Atmosphere_into_the_Soil_A_Review.

Liebner, S., J. Zeyer, D. Wagner, C. Schubert, E.-M. Pfeiffer, and C. Knoblauch. 2011. 'Methane Oxidation Associated with Submerged Brown Mosses Reduces Methane Emissions from Siberian Polygonal Tundra: Moss-Associated Methane Oxidation'. *Journal of Ecology* 99 (4): 914–22. doi:10.1111/j.1365-2745.2011.01823.x.

Lin, Y., D. Liu, W. Ding, H. Kang, C. Freeman, J. Yuan, and J. Xiang. 2015. 'Substrate Sources Regulate Spatial Variation of Metabolically Active Methanogens from Two Contrasting Freshwater Wetlands'. *Applied Microbiology and Biotechnology* 99 (24): 10779–91. doi:10.1007/s00253-015-6912-7.

Luo, Y., and P. S. Nobel. 1992. 'Carbohydrate Partitioning and Compartmental Analysis for a Highly Productive CAM Plant, Opuntia Ficus-Indica'. *Annals of Botany* 70 (6): 551–559. doi:10.1093/oxfordjournals.aob.a088516.

Luo, Y., L. W. White, J. G. Canadell, E. H. DeLucia, D. S. Ellsworth, A. Finzi, J. Lichter, and W. H. Schlesinger. 2003. 'Sustainability of Terrestrial Carbon Sequestration: A Case Study in Duke Forest with Inversion Approach: Sustainability Of Terrestrial Carbon Sequestration'. *Global Biogeochemical Cycles* 17 (1). doi:10.1029/2002GB001923.

Manzoni, S., G. G. Katul, and A. Porporato. 2009. 'Analysis of Soil Carbon Transit Times and Age Distributions Using Network Theories'. *Journal of Geophysical Research* 114 (G4). doi:10.1029/2009JG001070.

Martens, C. S., C. A. Kelley, J. P. Chanton, and W. J. Showers. 1992. 'Carbon and Hydrogen Isotopic Characterization of Methane from Wetlands and Lakes of the Yukon-Kuskokwim Delta, Western Alaska'. *Journal of Geophysical Research: Atmospheres* 97 (D15): 16689–701. doi:10.1029/91JD02885.

Marushchak, M. E., T. Friborg, C. Biasi, M. Herbst, T. Johansson, I. Kiepe, M. Liimatainen, et al. 2016. 'Methane Dynamics in the Subarctic Tundra: Combining Stable Isotope Analyses, Plot- and Ecosystem-Scale Flux Measurements'. *Biogeosciences* 13 (2): 597–608. doi:10.5194/bg-13-597-2016.

Melton, J. R., R. Wania, E. L. Hodson, B. Poulter, B. Ringeval, R. Spahni, T. Bohn, et al. 2013. 'Present State of Global Wetland Extent and Wetland Methane Modelling: Conclusions from a Model Inter-Comparison Project (WETCHIMP)'. *Biogeosciences* 10 (2): 753–88. doi:10.5194/bg-10-753-2013.

Microsoft Corporation. 2010. *Microsoft Office Standard 2010*. Microsoft Corporation.

Miller, P. C., P. J. Webber, W. C. Oechel, and L. L. Tieszen. 1980. 'Biophysical Processes and Primary Production'. In *An Arctic Ecosystem: The Coastal Tundra at Barrow, Alaska*. Stroudsburg, Pennsylvania: Dowden, Hutchinson & Ross.

Munk, O. L., S. Keiding, and L. Bass. 2003. 'Impulse-Response Function of Splanchnic Circulation with Model-Independent Constraints: Theory and Experimental Validation'. *American Journal of Physiology - Gastrointestinal and Liver Physiology* 285 (4): G671–80. doi:10.1152/ajpgi.00054.2003.

Myhre, G., K. P. Shine, G. Rädel, M. Gauss, I.S.A. Isaksen, Q. Tang, M.J. Prather, et al. 2011. 'Radiative Forcing due to Changes in Ozone and Methane Caused by the Transport Sector'. *Atmospheric Environment* 45 (2): 387–94. doi:10.1016/j.atmosenv.2010.10.001.

Nakagawa, F., N. Yoshida, Y. Nojiri, and V. N. Makarov. 2002. 'Production of Methane from Alasses in Eastern Siberia: Implications from Its ^{14}C and Stable Isotopic Compositions: Methane From Alasses In Eastern Siberia'. *Global Biogeochemical Cycles* 16 (3): 14-1-14–15. doi:10.1029/2000GB001384.

Natali, S. M., E. A. G. Schuur, C. Trucco, C. E. Hicks Pries, K. G. Crummer, and A. F. Baron Lopez. 2010. 'Effects of Experimental Warming of Air, Soil and Permafrost on Carbon Balance in Alaskan Tundra'. *Global Change Biology* 17 (3): 1394–1407. doi:10.1111/j.13-2486.2010.02303.x.

Nocedal, J., and S. J. Wright. 2006. *Numerical Optimization*. 2nd ed. Springer New York.

Norwich, K. H. 1977. *Molecular Dynamics in Biosystems*. Oxford: Pergamon Press Ltd.

———. 1997. 'Noncompartmental Models of Whole-Body Clearance of Tracers: A Review'. *Annals of Biomedical Engineering* 25 (3): 421–39. doi:10.1007/BF02684184.

Ostle, N., P. Ineson, D. Benham, and D. Sleep. 2000. 'Carbon Assimilation and Turnover in Grassland Vegetation Using an in situ $^{13}CO_2$ Pulse Labelling System'. *Rapid Communications in Mass Spectrometry* 14 (15): 1345–50. doi:10.1002/1097-0231(20000815)14:15<1345::AID-RCM22>3.0.CO;2-B.

Preuss, I., C. Knoblauch, J. Gebert, and E.-M. Pfeiffer. 2013. 'Improved Quantification of Microbial CH_4; Oxidation Efficiency in Arctic Wetland Soils Using Carbon Isotope Fractionation'. *Biogeosciences* 10 (4): 2539–52. doi:10.5194/bg-10-2539-2013.

Preuss, I.-M. 2013. 'In-Situ Studies of Microbial CH_4 Oxidation Efficiency in Arctic Wetland Soils - Application of Stable Carbon Isotopes'. Hamburg: Staats- und Universitätsbibliothek Hamburg. http://ediss.sub.uni-hamburg.de/volltexte/2013/6331/pdf/Dissertation.pdf.

Qian, H., and J. B. Bassingthwaighte. 2000. 'A Class of Flow Bifurcation Models with Lognormal Distribution and Fractal Dispersion'. *Journal of Theoretical Biology* 205 (2): 261–68. doi:10.1006/jtbi.2000.2060.

Quay, P. D., S. L. King, J. Stutsman, D. O. Wilbur, L. P. Steele, I. Fung, R. H. Gammon, et al. 1991. 'Carbon Isotopic Composition of Atmospheric CH: Fossil and Biomass Burning Source Strengths'. *Global Biogeochemical Cycles* 5 (1): 25–47. doi:10.1029/91GB00003.

R Core Team. 2012. *R: A Language and Environment for Statistical Computing*. Windows 7. Vienna, Austria. http://www.R-project.org.

Raich, J. W., and W. H. Schlesinger. 1992. 'The Global Carbon Dioxide Flux in Soil Respiration and Its Relationship to Vegetation and Climate'. *Tellus B* 44 (2): 81–99. doi:10.1034/j.1600-0889.1992.t01-1-00001.x.

Romanovsky, V. E., D. S. Drozdov, N. G. Oberman, G. V. Malkova, A. L. Kholodov, S. S. Marchenko, N. G. Moskalenko, et al. 2010. 'Thermal State of Permafrost in Russia'. *Permafrost and Periglacial Processes* 21 (2): 136–55. doi:10.1002/ppp.683.

Ronkanen, A. K., and B. Kløve. 2007. 'Use of Stabile Isotopes and Tracers to Detect Preferential Flow Patterns in a Peatland Treating Municipal Wastewater'. *Journal of Hydrology* 347 (3–4): 418–429. doi:10.1016/j.jhydrol.2007.09.029.

Roslev, P., and G. M. King. 1996. 'Regulation of Methane Oxidation in a Freshwater Wetland by Water Table Changes and Anoxia'. *FEMS Microbiology Ecology* 19 (2): 105–15. doi:10.1111/j.1574-6941.1996.tb00203.x.

Sachs, L., and J. Hedderich. 2009. *Angewandte Statistik*. 13th ed. Berlin Heidelberg: Springer.

Sachs, T., C. Wille, J. Boike, and L. Kutzbach. 2008. 'Environmental Controls on Ecosystem-Scale CH_4 Emission from Polygonal Tundra in the Lena River Delta, Siberia'. *Journal of Geophysical Research* 113: 1-12. doi:10.1029/2007JG000505.

Schaetzl, R., and S. Anderson. 2007. *Soils - Genesis and Geomorphology*. Cambridge.

Schlesinger, W. H. 1997. *Biogeochemistry : An Analysis of Global Change*. 2nd ed. San Diego, London: Academic Press.

Schlesinger, W. H., and J. Lichter. 2001. 'Limited Carbon Storage in Soil and Litter of Experimental Forest Plots under Increased Atmospheric CO2'. *Nature* 411: 466-469. doi:10.1038/35078060.

Schneider, J., G. Grosse, and D. Wagner. 2009. 'Land Cover Classification of Tundra Environments in the Arctic Lena Delta Based on Landsat 7 ETM+ Data and Its Application for Upscaling of Methane Emissions'. *Remote Sensing of Environment* 113 (2): 380–91. doi:10.1016/j.rse.2008.10.013.

Schuur, E. A. G., B. W. Abbott, W. B. Bowden, V. Brovkin, P. Camill, J. G. Canadell, J. P. Chanton, et al. 2013. 'Expert Assessment of Vulnerability of Permafrost Carbon to Climate Change'. *Climatic Change* 119 (2): 359–74. doi:10.1007/s10584-013-0730-7.

Schuur, E. A. G., J. G. Vogel, K. G. Crummer, H. Lee, J. O. Sickman, and T. E. Osterkamp. 2009. 'The Effect of Permafrost Thaw on Old Carbon Release and Net Carbon Exchange from Tundra'. *Nature* 459 (7246): 556–559. doi:10.1038/nature08031.

Steffen, W., J. Grinevald, P. Crutzen, and J. McNeill. 2011. 'The Anthropocene: Conceptual and Historical Perspectives'. *Philosophical Transactions of the Royal Society A: Mathematical, Physical and Engineering Sciences* 369 (1938): 842-867. doi:10.1098/rsta.2010.0327.

Street, L.E., J.A. Subke, M. Sommerkorn, A. Heinemeyer, and M. Williams. 2011. 'Turnover of Recently Assimilated Carbon in Arctic Bryophytes'. *Oecologia* 167 (2): 325–37. doi:10.1007/s00442-011-1988-y.

Street, L. E., J. A. Subke, M. Sommerkorn, V. Sloan, H. Ducrotoy, G. K. Phoenix, and M. Williams. 2013. 'The Role of Mosses in Carbon Uptake and Partitioning in Arctic Vegetation'. *New Phytologist* 199 (1): 163–75. doi:10.1111/nph.12285.

Ström, L., A. Ekberg, M. Mastepanov, and T. Røjle Christensen. 2003. 'The Effect of Vascular Plants on Carbon Turnover and Methane Emissions from a Tundra Wetland'. *Global Change Biology* 9 (8): 1185–1192.

Subke, J.-A., A. Heinemeyer, H. W. Vallack, V. Leronni, R. Baxter, and P. Ineson. 2012. 'Fast Assimilate Turnover Revealed by in Situ 13CO2 Pulse-Labelling in Subarctic Tundra'. *Polar Biology* 35 (8): 1209–19. doi:10.1007/s00300-012-1167-6.

Subke, J.-A., I. Inglima, and M. Francesca Cotrufo. 2006. 'Trends and Methodological Impacts in Soil CO2 Efflux Partitioning: A Metaanalytical Review'. *Global Change Biology* 12 (6): 921–43. doi:10.1111/j.1365-2486.2006.01117.x.

Tagesson, T., M. Mölder, M. Mastepanov, C. Sigsgaard, M. P. Tamstorf, M. Lund, J. M. Falk, A. Lindroth, T. R. Christensen, and L. Ström. 2012. 'Land-Atmosphere Exchange of Methane from Soil Thawing to Soil Freezing in a High-Arctic Wet Tundra Ecosystem'. *Global Change Biology* 18: 1928–40. doi:10.1111/j.1365-2486.2012.02647.x.

Tan, K. H. 2005. *Soil Sampling, Preparation, and Analysis*. Second Edition. Boca Raton, Florida: Taylor & Francis.

Tarantola, A. 2005. *Inverse Problem Theory and Methods for Model Parameter Estimation*. Philadeplphia: Siam (Society for Industrial and Applied Mathematics).

'The Duan Group - Models - H_2O-CO_2-NaCl'. 2015. Accessed May 5. http://models.kl-edi.ac.cn/models/h2o_co2_nacl.

Tokida, T., M. Adachi, W. Cheng, Y. Nakajima, T. Fumoto, M. Matsushima, H. Nakamura, M. Okada, R.Sameshima, and T. Hasegawa. 2011. 'Methane and Soil CO_2 Production from Current-Season Photosynthates in a Rice Paddy Exposed to Elevated CO_2 Concentration and Soil Temperature'. *Global Change Biology* 17 (11): 3327–37. doi:10.1111/j.1365-2486.2011.02475.x.

Turner, J. V., and C. J. Barnes . 1998. 'Chapter 2 - Modeling of Isotope and Hydrogeochemical Responses in Catchment Hydrology'. In *Isotope Tracers in Catchment Hydrology*, edited by Carol Kendall and Jeffrey J. McDonnell, Amsterdam: Elsevier.

Vaughan, P., J.C. Comiso, I. Allison, J. Carrasco, G Kaser, R. Kwok, P. Mote, et al. 2013. 'Chapter 4: Observations Cryosphere'. In *Climate Change 2013: The Physical Science Basis. Contribution of Working Group I to the Fifth Assessment Report of the Intergovernmental Panel on Climate Change*, edited by T.F. Stocker, D. Qin, G.-K. Plattner, M. Tignor, S.K. Allen, J. Boschung, A. Nauels, Y. Xia, V. Bex, and P.M. Midgley. Cambridge-New York: Cambridge University Press.

Wania, R., J. R. Melton, E. L. Hodson, B. Poulter, B. Ringeval, R. Spahni, T. Bohn, et al. 2013. 'Present State of Global Wetland Extent and Wetland Methane Modelling: Methodology of a Model Inter-Comparison Project (WETCHIMP)'. *Geoscientific Model Development* 6 (3): 617–641. doi:10.5194/gmd-6-617-2013.

Warembourg, F.R., and E.A. Paul. 1977. 'Seasonal Transfers of Assimilated 14C in Grassland: Plant Production and Turnover, Soil and Plant Respiration'. *Soil Biology and Biochemistry* 9 (4): 295–301. doi:10.1016/0038-0717(77)90038-4.

Whiticar, M. J. 1999. ‘Carbon and Hydrogen Isotope Systematics of Bacterial Formation and Oxidation of Methane’. *Chemical Geology* 161 (1): 291–314.

Whiticar, M. J., E. Faber, and M. Schoell. 1986. ‘Biogenic Methane Formation in Marine and Freshwater Environments: CO_2 Reduction vs. Acetate fermentation—Isotope Evidence’. *Geochimica et Cosmochimica Acta* 50 (5): 693–709.

Whitley, D. 1994. ‘A Genetic Algorithm Tutorial’. *Statistics and Computing* 4 (2): 65–85. doi:10.1007/BF00175354.

Wille, C., L. Kutzbach, T. Sachs, D. Wagner, and Eva-Maria Pfeiffer. 2008. ‘Methane Emission from Siberian Arctic Polygonal Tundra: Eddy Covariance Measurements and Modeling’. *Global Change Biology* 14 (6): 1395–1408. doi:10.1111/j.1365-2008.01586.x.

Winter, J. C. F. de. 2013. ‘Using the Student’s T-Test with Extremely Small Sample Sizes’. *Practical Assessment, Research & Evaluation* 18 (10): 1–12.

Wu, Y., H. Tan, Y. Deng, J. Wu, X. Xu, Y. Wang, Y. Tang, T. Higashi, and X. Cui. 2010. ‘Partitioning Pattern of Carbon Flux in a Kobresia Grassland on the Qinghai-Tibetan Plateau Revealed by Field ^{13}C Pulse-Labeling’. *Global Change Biology* 16 (8): 2322–33. doi:10.1111/j.1365-2486.2009.02069.x.

Yang, X.-S. 2014. *Nature-Inspired Optimization Algorithms*. 1st ed. Amsterdam: Elsevier Science.

Zhang, G., X. Zhang, Y. Ji, J. Ma, H. Xu, and Z. Cai. 2011. ‘Carbon Isotopic Composition, Methanogenic Pathway, and Fraction of CH_4 Oxidized in a Rice Field Flooded Year-Round’. *Journal of Geophysical Research* 116: G04025. doi:10.1029/2011JG001696.

Zilversmit, D. B., C. Entenman, and M. C. Fishler. 1943. ‘On the Calculation of "Turnover Time" and "Turnover Rate" from Experiments Involving the Use of Labeling Agents’. *The Journal of General Physiology* 26 (3): 325–31.

Zubrzycki, S., L. Kutzbach, G. Grosse, A. Desyatkin, and E.-M. Pfeiffer. 2013. ‘Organic Carbon and Total Nitrogen Stocks in Soils of the Lena River Delta’. *Biogeosciences* 10 (6): 3507–24. doi:10.5194/bg-10-3507-2013.

Appendices

Key to sample identifiers: UL = Unlabeled sample, UL3 = UL from depth 3 (20-30 cm below surface), UL34 = UL3 replica 4. 13C34 = Labeled sample from depth 3, replica 4. Site identifiers A, B, and C are samples from unlabeled sites, D, E, and F are from labeled sites.

A I Soil properties

Table 17. Soil properties. Dry weight (weight of the total sample size) and bulk density are presented.

Identifier	Depth (m)	Dry weight (g)	Mean	SD	Bulk density (g cm^{-3})	Mean	SD
UL11	0-0.1	20.65	15.42	3.0	0.263	0.196	0.038
UL12		15			0.191		
UL13		11.81			0.150		
UL14		13.46			0.171		
UL15		16.18			0.206		
UL21	0.1-0.2	26.67	23.374	2.1	0.340	0.298	0.027
UL22		23.8			0.303		
UL23		21.76			0.277		
UL24		20.53			0.261		
UL25		24.11			0.307	0.000	0.000
UL31	0.2-0.3	16.77	26.166	6.5	0.214	0.333	0.083
UL32		23.4			0.298		
UL33		31.75			0.404		
UL34		23.9			0.304		
UL35		35.01			0.446		
UL41	0.3-0.4	40.21	43.78	4.7	0.512	0.557	0.060
UL42		40.69			0.518		
UL43		50.44			0.642		

Table 18. Soil properties. Particle size density, pore space (porosity), estimated water content per m^2 and C content are given in this table.

Identi-fier	Depth (m)	Particle Size density (g/cm^3)	Mean	SD	Pore Space (cm^3/cm^3)	Mean und SD	Water content (m^3/m^2)	C content Soil (%)	Mean	SD
UL11	0-0.1	2.08	2.09	0.01	0.874	0.907	0.091	17.44	15.30	1.40
UL12		2.07			0.908			16.11		
UL13		2.10			0.928			15.36		
UL14		2.09			0.918			14.03		
UL15		0.00			-			13.59		
UL21	0.1-0.2	2.49	2.52	0.03	0.864	0.882	0.088	5.60	6.85	1.06
UL22		2.52			0.880			5.72		
UL23		2.52			0.890			7.87		

UL24		2.52			0.896			6.87		
UL25		2.58			0.881			8.18		
UL31	0.2-0.3	1.68	2.19	0.52	0.873	0.856	0.086	8.78	7.31	1.70
UL32		3.03			0.902			8.13		
UL33		2.17			0.814			5.89		
UL34		1.87			0.837			9.03		
UL35		0.00			-			4.74		
UL41	0.3-0.4	2.33	2.48	0.18	0.780	0.776	0.093	5.93	5.91	0.11
UL42		2.37			0.782			5.77		
UL43		2.74			0.765			6.04		

Table 19. The dry weight and the percentage of total C for the sub-surface carbon pools

Depth (m)	C-pool	Dry weight (g Cm^2)	Percent of total C	sd
Vegetation	Vegetation (*Carex*)	15.27	0.2	0.07
0.0-0.1	Root (fine)	180.31	2.34	0.00
	Root (coarse)	15.63	0.2	0.00
	Root (old)	23.6	0.31	0.01
	old *Carex*	51.36	0.67	7.47
	Moss	1858.65	24.11	0.18
	residual soil	279.01	3.62	0.00
	diss. C	2.99	0.04	0.07
0.1-0.2	Root (fine)	149.05	1.93	0.04
	Root (coarse)	5.77	0.07	0.00
	Root (old)	22.76	0.3	0.00
	old *Carex*	7.62	0.1	0.00
	Moss	1582.26	20.53	4.31
	residual soil	372.6	4.83	0.24
	diss. C	6.37	0.08	0.00
0.2-0.3	Root (fine)	47.65	0.62	0.01
	Root (coarse)	5.25	0.07	0.00
	Root (old)	14.03	0.18	0.00
	old *Carex*	13.39	0.17	0.00
	Moss	836.51	10.85	1.30
	residual soil	22.49	0.29	0.00
	diss. C	10.02	0.13	0.00

0.3-0.4	Root (fine)	230.96	3	0.12
	Root (coarse)	5.41	0.07	0.00
	Root (old)	24.48	0.32	0.00
	old *Carex*	42.4	0.55	0.01
	Moss	1293.54	16.78	5.03
	residual soil	579.34	7.52	0.83
	diss. C	10.02	0.13	0
	Sum	7708.71		

A II Tables of carbon concentration and ^{13}C signature of dissolved sub-surface carbon pools

Table 20. Concentration of DIC in the depth of 6 cm below surface.

Date	**Concentration mg DIC L^{-1}**					
	Site A	Site B	Site C	Site D	Site E	Site F
15.08	-	-	10.15	6.81	13.89	5.49
18.08	-	7.42	8.56	8.21	12.86	3.99
19.08	16.12	7.86	6.95	12.95	19.41	7.69
20.08	14.31	5.7	6.35	13.18	18.45	8.82
21.08	18.6	5.25	7.58	12.28	18.42	5.66
22.08	18.86	5.62	8.52	-	19.15	7.23
23.08	15.21	5.93	7.9	13.16	19.47	5.02
24.08	5.71	17.62	6.86	11.55	17.45	-
25.08	-	-	7.23	10.43	17.43	1.71
26.08	14.62	6.36	8.45	11.82	11.65	1.91
27.08	17.62	8.28	6.78	9.84	18.61	2.48
29.08	16.86	7.22	7.81	8.86	17.09	3.16
mean	15.32	7.73	7.76	10.83	16.99	4.83
sd	3.7	3.4	1.0	2.1	2.6	2.3

Table 21. Concentration of DIC in the depth of 16 cm below surface.

Date	**Concentration mg DIC L^{-1}**

	Site A	Site B	Site C	Site D	Site E	Site F
15.08	-	19.46	20.55	20.96	24.8	27.84
18.08	-	23.9	22.51	24.68	26.05	26.63
19.08	30.22	25.88	21.66	29.89	30.41	28.21
20.08	25.97	22.04	23.95	32.76	28.18	33.31
21.08	27.08	22.14	24.57	33.62	33.63	34.6
22.08	30.23	24.21	26.34	27.08	30.78	31.39
23.08	28.82	23.05	23.53	33.48	25.4	32.64
24.08	25.79	30.15	24.94	33.83	-	-
25.08	-	-	28.91	38.44	31.89	35.45
26.08	27.92	25.44	24.94	19.94	29.57	29.94
27.08	30.54	24.61	25.77	33.69	34.87	36.91
29.08	30.33	25.52	23.77	33.28	32.08	34.28
mean	28.54	24.22	24.29	30.14	29.79	31.93
sd	1.8	2.6	2.1	5.5	3.2	3.2

Table 22. Concentration of DIC in the depth of 36 cm below surface.

Date	**Concentration mg DIC L^{-1}**					
	Site A	Site B	Site C	Site D	Site E	Site F
15.08	-	27.67	30.68	33.68	30.45	31.55
18.08	28.03	28.28	31.17	35.84	31.15	32.19
19.08	33.27	33.12	28.83	35.02	29.43	32.12
20.08	30.91	28.6	34.49	40.28	36.02	37.23
21.08	34.46	35.69	33.17	41.45	37.73	36.58
22.08	38.57	36.62	-	38.23	33.96	34.82
23.08	30.15	34.55	34.04	40.25	34.77	37.06
24.08	35.04	37.37	35.89	-	-	-
25.08	-	-	30.01	47.65	39.7	31.17
26.08	54.89	41.66	40.11	48.64	40.2	33.61
27.08	36.21	38.27	39.3	42.57	36	41.31
29.08	39.45	43.22	38.43	43.29	35.41	39.76
mean	36.10	35.00	34.19	40.63	34.98	35.22
sd	7.1	5.0	3.7	4.6	3.4	3.3

Table 23. Concentration of CH_4 in the depth of 6 cm below surface.

Date	**Concentration mg C-CH_4 L^{-1}**					
	Site A	Site B	Site C	Site D	Site E	Site F
15.08	-	-	0.62	0.5	1.38	0.24
18.08	-	0.26	0.44	0.43	1.03	0.23
19.08	0.97	0.45	0.43	0.88	1.92	0.49
20.08	0.75	0.56	0.48	0.96	0.95	0.75
21.08	0.95	0.33	0.61	0.65	0.96	0.15

22.08	1.09	0.51	0.82	-	1.26	0.32
23.08	0.74	0.43	0.63	0.74	1.19	0.12
24.08	0.47	1.01	0.64	0.65	1.04	-
25.08	-	-	0.67	0.73	1.34	0.11
26.08	0.98	0.65	0.69	1.47	1.18	0.12
27.08	1.1	0.78	0.54	0.63	1.24	0.11
29.08	1.06	0.45	0.94	0.65	1.04	0.18
mean	0.90	0.54	0.63	0.75	1.21	0.26
sd	0.2	0.2	0.1	0.3	0.3	0.2

Table 24. Concentration of CH_4 in the depth of 16 cm below surface.

Date	**Concentration mg C-CH_4 L^{-1}**					
	Site A	Site B	Site C	Site D	Site E	Site F
15.08	-	1.33	1.37	0.88	1.62	1.15
18.08	-	1.59	1.23	1.11	1.62	1.1
19.08	1.3	1.69	1.32	1.49	1.3	1.33
20.08	1.14	1.7	1.61	1.66	1.15	1.69
21.08	0.62	1.12	1.68	1.5	1.72	1.8
22.08	1.7	2.21	2.01	1.02	1.85	1.85
23.08	1.72	2.11	1.77	1.49	1.89	1.99
24.08	2.07	1.59	1.62	1.49	-	-
25.08	-	-	2.4	2.22	1.78	2.36
26.08	2.14	1.95	1.13	0.59	2.26	2.12
27.08	1.5	1.67	2.26	1.52	2.34	2.6
29.08	1.66	1.79	1.72	1.68	1.73	1.98
mean	1.54	1.70	1.68	1.39	1.75	1.82
sd	0.4	0.3	0.4	0.4	0.3	0.5

Table 25. Concentration of CH_4 in the depth of 36 cm below surface.

Date	**Concentration mg C-CH_4 L^{-1}**					
	Site A	Site B	Site C	Site D	Site E	Site F
15.08	-	1.33	2.4	2.29	3.6	3.27
18.08	0.17	1.38	1.97	1.81	4.86	2.88
19.08	1.95	1.34	1.45	1.8	2.77	3.13
20.08	1.64	1.83	2.45	2.82	3.64	3.65
21.08	2.23	2.37	1.84	2.73	4	3.3
22.08	2.88	2.65	-	2.37	3.56	3.72
23.08	1.51	2.22	2.62	2.18	3.85	3.51
24.08	1.86	2.26	2.77	-	-	-
25.08	-	-	2.27	3.44	4.59	1.94
26.08	4.49	2.63	3.04	3.35	4.66	3.52
27.08	1.4	1.9	2.94	2.26	3.19	3.48
29.08	2.66	2.68	2.93	2.3	2.16	3.57

mean	2.08	2.05	2.43	2.49	3.72	3.27
sd	1.1	0.5	0.5	0.5	0.8	0.5

Table 26. Concentration of DOC in the depth of 6 cm below surface.

Date	**Concentration mg DOC L^{-1}**					
	Site A	Site B	Site C	Site D	Site E	Site F
15.08	18.51	23.02	20.23	21.3	24.59	24.39
18.08	19.83	22.41	20.64	21.45	23.83	24.95
19.08	19.98	21.65	19.52	23.12	24.24	22.82
20.08	21.09	21.4	20.94	23.53	27.84	24.34
21.08	22.46	20.38	19.77	19.17	26.42	21.6
22.08	18.2	24.69	18.91	21.45	23.27	21.45
23.08	19.06	19.27	20.03	22.61	23.93	23.68
24.08	19.47	19.32	20.18	21.8	23.53	20.43
25.08	20.13	22.26	20.13	20.48	23.63	23.78
26.08	19.32	20.94	20.03	21.6	22.87	21.4
27.08	19.42	19.83	19.88	21.24	20.69	20.79
29.08	20.84	20.18	22.36	21.7	20.99	22.61
mean	19.86	21.28	20.22	21.62	23.82	22.69
sd	1.1	1.6	0.8	1.1	1.9	1.5

Table 27. Concentration of DOC in the depth of 16 cm below surface.

Date	**Concentration mg DOC L^{-1}**					
	Site A	Site B	Site C	Site D	Site E	Site F
15.08	28.75	28.04	24.49	23.63	34.32	34.43
18.08	24.29	29.1	27.18	27.53	32.55	32.55
19.08	23.07	27.63	24.44	25.76	41.47	50.6
20.08	29.81	31.38	29.36	35.24	47	47.86
21.08	22.97	28.7	27.84	27.33	36.91	51.36
22.08	-	19.01	25.66	28.29	33.36	47.71
23.08	28.14	26.77	27.84	34.93	44.46	43.55
24.08	28.7	24.54	26.72	32.9	39.34	45.38
25.08	23.68	26.77	26.77	33.51	36.05	42.59
26.08	22.87	28.85	26.87	32.19	34.37	39.55
27.08	24.08	26.06	25.3	31.89	37.77	50.29
29.08	31.13	29.15	28.9	35.44	42.64	51
mean	26.14	27.17	26.78	30.72	38.35	44.74
sd	3.0	3.0	1.5	3.9	4.5	6.2

Table 28. Concentration of DOC in the depth of 36 cm below surface.

Date	Concentration mg DOC L^{-1}					
	Site A	Site B	Site C	Site D	Site E	Site F
15.08	104.13	67.83	82.79	85.93	85.93	89.33
18.08	65.2	65.91	83.85	91.05	79.44	87.55
19.08	77.52	70.01	81.37	81.83	91.86	98.15
20.08	92.17	94.96	98.56	98.45	97.29	99.87
21.08	92.47	80.61	82.03	74.17	86.24	97.59
22.08	-	71.53	82.23	77.26	84.66	93.03
23.08	92.02	83.55	84.11	91.2	94.6	89.38
24.08	79.09	87.81	93.18	84.51	89.48	93.13
25.08	84.11	90.8	83.75	84.66	89.38	89.43
26.08	72.75	76.81	85.17	83.25	88.52	77.62
27.08	83.9	69.41	80.91	81.93	91.51	95.82
29.08	88.57	83.19	90.65	90.14	96.07	99.57
mean	26.14	27.17	26.78	30.72	38.35	44.74
sd	3.0	3.0	1.5	3.9	4.5	6.2

Table 29. Cox-and-Stuart trend test results for concentration development of DIC in three depths.

replica	z-value	p-value	hypothesis
06cm_A	0	1	monotonic trend
06cm_B	0.91	0.361	monotonic trend
06cm_C	0.5	0.617	monotonic trend
06cm_D	-0.35	0.728	monotonic trend
06cm_E	0.5	0.617	monotonic trend
06cm_F	1.74	0.082	monotonic trend
----	----	----	----
16cm_A	0	1	monotonic trend
16cm_B	0.7	0.486	monotonic trend
16cm_C	0.5	0.617	monotonic trend
16cm_D	0.5	0.617	monotonic trend
16cm_E	1.74	0.082	monotonic trend
16cm_F	1.74	0.082	monotonic trend
----	----	----	----
36cm_A	2.01	0.045	monotonic trend
36cm_B	1.74	0.082	monotonic trend
36cm_C	0.7	0.486	monotonic trend

36cm_D	1.74	0.082	monotonic trend
36cm_E	0.7	0.486	monotonic trend
36cm_F	0.7	0.486	monotonic trend

Table 30. Cox-and-Stuart trend test results for concentration of CH_4 in three depths.

replica	z-value	p-value	hypothesis
06cm_A	1.15	0.248	monotonic trend
06cm_B	2.01	0.045	monotonic trend
06cm_C	1.5	0.134	monotonic trend
06cm_D	-0.35	0.728	monotonic trend
06cm_E	-0.5	0.617	monotonic trend
06cm_F	1.74	0.082	monotonic trend
----	----	----	----
16cm_A	1.15	0.248	monotonic trend
16cm_B	0.7	0.486	monotonic trend
16cm_C	0.5	0.617	monotonic trend
16cm_D	0.5	0.617	monotonic trend
16cm_E	1.74	0.082	monotonic trend
16cm_F	1.74	0.082	monotonic trend
----	----	----	----
36cm_A	0.91	0.361	monotonic trend
36cm_B	1.74	0.082	monotonic trend
36cm_C	0.7	0.486	monotonic trend
36cm_D	0.7	0.486	monotonic trend
36cm_E	-0.35	0.728	monotonic trend
36cm_F	-0.35	0.728	monotonic trend

Table 31. Cox-and-Stuart trend test results for concentration of DOC in three depths.

replica	z-value	p-value	hypothesis
06cm_A	0.5	0.617	monotonic trend
06cm_B	1.5	0.134	monotonic trend
06cm_C	-0.5	0.617	monotonic trend

06cm_D	0.5	0.617	monotonic trend
06cm_E	1.5	0.134	monotonic trend
06cm_F	1.5	0.134	monotonic trend
----	----	----	----
16cm_A	-0.35	0.728	monotonic trend
16cm_B	1.5	0.134	monotonic trend
16cm_C	-0.5	0.617	monotonic trend
16cm_D	1.5	0.134	monotonic trend
16cm_E	-0.5	0.617	monotonic trend
16cm_F	0.5	0.617	monotonic trend
----	----	----	----
36cm_A	-0.35	0.728	monotonic trend
36cm_B	-0.5	0.617	monotonic trend
36cm_C	-0.5	0.617	monotonic trend
36cm_D	0.5	0.617	monotonic trend
36cm_E	-0.5	0.617	monotonic trend
36cm_F	0.5	0.617	monotonic trend

A III Carbon content and ^{13}C signature of major sub-surface carbon pools

Table 32. Carbon content.

	Total	**Fine roots in *Scorpidium* moss**	**old *Carex* roots**	***Scorpidium* moss**	**decayed *Carex***	**fresh *Carex* roots**	**Sand**	
Sample	Total [g]	A [g]	B [g]	C [g]	D [g]	E [g]	Sand [g]	Layer
13C 12	5.55	0.10425	0.01572	1.2085	0.0364	0.01898	3.54283	1
13C 11	4.48	0.08351	0.0096	1.67853	0.01816	0.00029	2.55649	1
13C 13	1.65	0.02931	0.00516	0.56372	0.01191	0.00136	0.94833	1
mean	3.89	0.0724	0.0102	1.1503	0.0222	0.0069	2.3492	
fraction	1.000	0.019	0.003	0.295	0.006	0.002	0.603	
sd	0.42	0.0081	0.0011	0.1174	0.0027	0.0022	0.2746	
N	3	3	3	3	3	3	3	

13C 22	9.14	0.04384	0.01253	1.29365	0.00961	0.0026	7.62724	2
13C 21	7.79	0.07454	0.00468	1.46168	0.00127	0.00065	6.19653	2
13C 23	6.75	0.10948	0.02261	1.21674	0.01302	0.0085	5.0211	2
mean	7.89	0.0760	0.0133	1.3240	0.0080	0.0039	6.2816	
fraction	1.000	0.010	0.002	0.168	0.001	0.000	0.796	
sd	0.12	0.0034	0.0009	0.0130	0.0006	0.0004	0.1350	
N	3	3	3	3	3	3	3	
13C 32	17.61	0.04173	0.01261	1.71611	0.01301	0.00335	15.6499	3
13C 34	19.34	0.04843	0.02159	2.02162	0.02134	0.01684	17.2905	3
13C 33	17.99	0.06497	0.01776	1.38889	0.06173	0.00262	16.3088	3
mean	18.31	0.0517	0.0173	1.7089	0.0320	0.0076	16.4164	
fraction	1.000	0.003	0.001	0.093	0.002	0.000	0.896	
sd	0.04	0.0005	0.0002	0.0141	0.0012	0.0004	0.0368	
N	3	3	3	3	3	3	3	
13C 41	12.65	0.26672	0.01695	0.16902	0.04348	0.00064	11.9567	4
13C 42	14.64	0.05325	0.01421	2.97497	0.02801	0.01049	5.19417	4
13C 43	27.07	0.14145	0.02179	3.0355	0.0716	0.00211	23.6007	4
mean	18.12	0.1538	0.0177	2.0598	0.0477	0.0044	13.5839	
fraction	1.000	0.008	0.001	0.114	0.003	0.000	0.750	
sd	0.35	0.0048	0.0002	0.0738	0.0010	0.0002	0.4195	
N	3	3	3	3	3	3	3	

Table 33. ^{13}C-excess % in the bulk soil and the Carex plants.

C-pool	^{13}C-excess %	sd	n
Vegetation (*Carex*)	0.034368	0.014029	6
Bulk C layer 0.0-0.1	0.004226	0.001588	5
Bulk C layer 0.1-0.2	0.001599	0.00079	5
Bulk C layer 0.2-0.3	0.001252	0.000807	5
Bulk C layer 0.3-0.4	0.000626	0.000673	3

Table 34. δ^{13}C signature in labeled major sub-surface carbon pools.

	Total	Fine roots in *Scorpidium* moss	old *Carex* roots	*Scorpidium* moss	decayed *Carex*	fresh *Carex* roots	Sand

Sample	Bulk [d13C]	A [d13C]	B [d13C]	C [d13C]	D [d13C]	E [d13C]	Sand [d13C]	Tiefe
13C 12	-22.79	-20.05	-24.52	-26.63	-28.16	37.53		1
13C 11	-25.07	-27.51	-24.03	-26.69	-28.09	41.50		1
13C 13	-26.20	-27.68	-23.43	-26.49	-27.48	-27.14		1
mean	-24.69	-25.08	-24.00	-26.59	-27.91	17.29		
sd	1.42	3.56	0.45	0.10	0.30	31.46		
n		3	3	2	3	3		
13C 22		-19.93	-27.89	-23.71	-28.61	-28.19		2
13C 21	-24.87	-11.23	-27.14	-25.68	-28.74	-5.30		2
13C 24	-25.49	-21.87	-28.25	-25.80	-25.80	-21.03		2
13C 25	-25.55	-27.24	-27.57		-29.00	-26.72		2
13C 23		-21.91	-28.22	-23.96	-29.51	-16.74		2
mean	-25.30	-20.56	-27.80	-23.83	-28.26	-17.45		
sd	0.30	5.20	0.42	0.96	1.30	8.24		
n		5	5	4	5	5		
13C 32	-26.48		-28.21	-26.55		-18.85		3
13C 31	-26.25	-25.81	-28.62	-25.20		-24.15		3
13C 35	-27.02	-26.93	-29.44	-24.93		-26.91		3
13C 34	-25.54	-25.29	-29.03	-25.03		-24.89		3
13C 33	-25.89	-17.72	-27.69	-26.85		-10.56		3
mean	-26.23	-23.94	-28.60	-25.71		-21.07		
sd	0.51	3.64	0.61	0.82		5.89		
n		5	5	5	0	5		
13C 41	-26.89	-25.71	-28.93	-26.70				4
13C 42	-26.52	-22.78	-29.10	-26.56		-26.53		4
13C 43	-26.80	-26.71	-28.82	-26.75	-27.74	-24.74		4
mean	-26.74	-25.06	-28.95	-26.67	-27.74	-25.63		
sd	0.16	1.67	0.11	0.08	0.00	0.90		
n		3	3	3	1	2		

Table 35. $\delta^{13}C$ signatur in non-labeled (control) major sub-surface carbon pools.

	Total	**Fine roots in *Scorpidium* moss**	**old *Carex* roots**	***Scorpidium* moss**	**decayed *Carex***	**fresh *Carex* roots**	**Sand**	
Sample	Bulk [d13C]	A [d13C]	B [d13C]	C [d13C]	D [d13C]	E [d13C]	Sand [d13C]	Tiefe
UL 12	-28.45	-28.45	-27.92	-27.75	-29.13	-28.72		1
UL 11	-28.52	-28.75	-27.88	-28.73	-30.52	-28.89		1
UL 13	-28.44	-28.49	-28.54	-28.21	-29.55	-29.28		1
mean	-28.47	-28.62	-28.11	-28.23	-29.73	-28.96	0	
sd	0.04	0.13	0.30	0.40	0.58	0.24	0	
n		3	2	3	3	3		
UL 22	-26.55	-27.25	-26.67	-25.42	-26.63	-28.00		2
UL 21	-27.20	-27.63	-27.92	-25.74	-28.39	-27.50		2
	-26.87	-27.63	-27.82	-25.65	-28.20	-29.10		2
UL 24	-25.69	-27.39	-27.53	-25.24	-28.05	-28.20		2

UL 23	-27.18	-27.64	-27.82	-25.24	-28.27	-28.09		2
mean	-26.73	-27.51	-27.45	-25.46	-27.91	-28.18	0	
sd	0.64	0.18	0.51	0.34	0.69	0.62	0	
n		5	5	3	5	5		
UL 32	-28.24							3
UL 31	-27.00							3
UL 35	-26.62							3
UL 34	-27.84							3
UL 33	-27.03							3
mean	-27.35	-27.35	-27.35	-27.35	-27.35	-27.35	0	
sd	0.51	0.51	0.51	0.51	0.51	0.51	0	
n		5	5	5	0	5		
UL 41	-26.74							4
UL 42	-28.10							4
UL 43	-27.05							4
mean	-27.30	-27.30	-27.30	-27.30	-27.30	-27.30	0	
sd	0.58	0.587	0.58	0.58	0.58	0.58	0	
n		3	3	3	1	2		

Table 36. T-test results for difference in means between control and labeled $\delta^{13}C$ in vascular plants (*Carex*, 0+) and bulk soil carbon.

Distance (cm)	p-value	significant	Hypothesis: label d13C greater than control d13C	t-test version
0+	0.001	significant	greater	Welch Two Sample t-test
00-10	0.032	significant	greater	Welch Two Sample t-test
10-20	0.01	significant	greater	Welch Two Sample t-test
20-30	0.011	significant	greater	Welch Two Sample t-test
30-40	0.153	not significant	greater	Welch Two Sample t-test

Table 37. T-test results for difference in means of control and labeled $\delta^{13}C$ in fine roots.

Depth (cm)	p-value	significant	Hypothesis: label d13C greater than control d13C	t-test version
00-10	0.15	not	greater	Welch Two Sample t-

		significant		test
10-20	0.027	significant	greater	Welch Two Sample t-test
20-30	0.102	not significant	greater	One Sample t-test
30-40	0.099	not significant	greater	One Sample t-test

Table 38. T-test results for difference in means between control and labeled $\delta^{13}C$ in "dead" roots

Depth (cm)	p-value	significant	Hypothesis: label d13C greater than control d13C	t-test version
00-10	0	significant	greater	Welch Two Sample t-test
10-20	0.792	not significant	greater	Welch Two Sample t-test
20-30	0.993	not significant	greater	One Sample t-test
30-40	0.999	not significant	greater	One Sample t-test

Table 39. T-test results for difference in mean $\delta^{13}C$ of control and labeled coarse roots

Depth (cm)	p-value	significant	Hypothesis: label d13C greater than control d13C	t-test version
00-10	0.087	not significant	greater	Welch Two Sample t-test
10-20	0.053	not significant	greater	Welch Two Sample t-test
20-30	0.05	not significant	greater	One Sample t-test
30-40	0.157	not significant	greater	One Sample t-test

Table 40. T-test results for difference in $\delta^{13}C$ means in *Scorpidium* moss.

Depth (cm)	p-value	significant	Hypothesis: label d13C greater than control d13C	t-test version
00-10	0.012	significant	greater	Welch Two Sample t-test
10-20	0.157	not significant	greater	Welch Two Sample t-test
20-30	0.008	significant	greater	One Sample t-test
30-40	0.004	significant	greater	One Sample t-test

Table 41. T-test results for difference in $\delta^{13}C$ means in "old" *Carex* - i.e. *Carex* remainder in the belowground with marks of decay.

Depth (cm)	p-value	significant	Hypothesis: label d13C greater than control d13C	t-test version
00-10	0.015	significant	greater	Welch Two Sample t-test
20-30	0.71	not significant	greater	Welch Two Sample t-test
nd	nd	nd	nd	nd
30-40	nd	nd	nd	nd

Table 42. $^{13}C/^{12}C$ ratio x 100 of DIC in labeled and control site (0 $\delta^{13}C \triangleq 0.0111802$ $^{13}C/^{12}C$).

Day	Depth.cm.	A.contr	B.contr	C.contr	D.lab	E.lab	F.lab
15.08	6			1.09607	1.09565	1.09545	1.09499
18.08	6		1.09567	1.09615	2.45372	1.6378	2.50155
19.08	6	1.09589	1.09515	1.09585	1.65201	1.3235	1.79743
20.08	6	1.09551	1.09437	1.09522	1.55761	1.28444	1.58095
21.08	6	1.09578	1.09454	1.09597	1.43557	1.29818	1.50485
22.08	6	1.09537	1.09512	1.09616	1.38713	1.30165	1.45619
23.08	6	1.09577	1.09555	1.0963	1.36031	1.30665	1.4187
24.08	6	1.09605	1.09598	1.097	1.33574	1.30592	1.36161
25.08	6	1.09597	1.09625	1.09696	1.31144	1.28297	1.32888

26.08	6	1.09545	1.09637	1.09742	1.29936	1.28932	1.3067
27.08	6	1.096	1.09642	1.09708	1.28699	1.27292	1.28591
29.08	6	1.09599	1.09593	1.09626	1.26876	1.26247	1.2652
-	-	-	-	-	-	-	-
15.08	16		1.09671	1.09638	1.09696	1.09613	1.09644
18.08	16		1.09707	1.09682	1.11085	1.10782	1.11256
19.08	16	1.09644	1.0967	1.09712	1.12377	1.11438	1.12338
20.08	16	1.09667	1.09643	1.09673	1.13326	1.11877	1.12735
21.08	16	1.09657	1.09679	1.09695	1.14119	1.12422	1.13127
22.08	16	1.09653	1.09639	1.09713	1.14806	1.13027	1.13508
23.08	16	1.09642	1.09623	1.09704	1.15239	1.13266	1.13806
24.08	16	1.09623	1.0965	1.0974	1.16019	1.13848	1.1431
25.08	16		1.09659	1.09719	1.16614	1.14325	1.14856
26.08	16	1.09583	1.0966	1.0974	1.16989	1.14624	1.15153
27.08	16	1.0969	1.09666	1.09731	1.1768	1.15061	1.1554
29.08	16	1.09674	1.09646	1.09757	1.1822	1.15767	1.15989
-	-	-	-	-	-	-	-
15.08	36		1.10043	1.10077	1.10057	1.10134	1.10108
18.08	36	1.10094	1.10021	1.10067	1.10123	1.10166	1.10232
19.08	36	1.10126	1.09977	1.10068	1.10241	1.10195	1.10366
20.08	36	1.10114	1.09951	1.1003	1.10411	1.10262	1.10474
21.08	36	1.10098	1.09965	1.10062	1.10601	1.10318	1.10641
22.08	36	1.10093	1.09968	1.10017	1.10745	1.10371	1.10716
23.08	36	1.10082	1.09954	1.10039	1.10899	1.10406	1.10744
24.08	36	1.09969	1.10095	1.10024	1.11112	1.10444	1.10858
25.08	36	1.10077	1.09998	1.10079	1.11176	1.10486	1.1093
26.08	36	1.10135	1.10022	1.10062	1.11254	1.10524	1.10827
27.08	36	1.10099	1.10005	1.10079	1.11413	1.10571	1.11023
29.08	36	1.1008	1.09958	1.10085	1.11462	1.1059	1.11086

Table 43. $^{13}C/^{12}C$ ratio x 100 of CH_4 in labeled and control site (0 $\delta^{13}C \triangleq 0.0111802$ $^{13}C/^{12}C$).

Day	Depth.cm.	A.contr	B.contr	C.contr	D.lab	E.lab	F.lab
15.08	6			1.05831	1.05667	1.05732	1.05738

18.08	6		1.05862	1.05835	1.18009	1.12061	1.26185
19.08	6	1.05744	1.0568	1.05842	1.15309	1.09175	1.20967
20.08	6	1.05783	1.05843	1.05931	1.15712	1.09335	1.2014
21.08	6	1.05856	1.0584	1.05932	1.13436	1.10207	1.18518
22.08	6	1.05812	1.05819	1.05942	1.12543	1.1102	1.17093
23.08	6	1.05818	1.05881	1.05882	1.1204	1.11377	1.1659
24.08	6	1.05862	1.05913	1.05878	1.12024	1.12073	1.14824
25.08	6	1.05861	1.05865	1.05721	1.12047	1.12182	1.14555
26.08	6	1.05835	1.05813	1.05773	1.11932	1.12528	1.1366
27.08	6	1.05719	1.05788	1.05816	1.11867	1.12206	1.13365
29.08	6	1.05723	1.05824	1.057	1.1221	1.12363	1.13159
-	-	-	-	-	-	-	-
15.08	16		1.05774	1.05727	1.05722	1.05711	1.05838
18.08	16		1.05695	1.05671	1.05842	1.05762	1.06013
19.08	16	1.05731	1.05635	1.05666	1.06174	1.0605	1.06268
20.08	16	1.05829	1.05732	1.05824	1.06564	1.06145	1.06425
21.08	16	1.05842	1.05799	1.0574	1.06751	1.06333	1.06462
22.08	16	1.0589	1.05782	1.057	1.06896	1.06505	1.06592
23.08	16	1.05876	1.05772	1.05707	1.07057	1.06577	1.06658
24.08	16	1.05779	1.05885	1.05718	1.07323	1.0671	1.06798
25.08	16	1.05842	1.05821	1.05754	1.07423	1.06802	1.06882
26.08	16	1.0576	1.05732	1.05676	1.07672	1.06905	1.06979
27.08	16	1.05759	1.05727	1.05637	1.08085	1.07089	1.07076
29.08	16	1.05768	1.0569	1.05668	1.08276	1.07415	1.07299
-	-	-	-	-	-	-	-
15.08	36		1.05604	1.05343	1.05498	1.05283	1.05373
18.08	36	1.05488	1.05577	1.05321	1.05535	1.05267	1.0539
19.08	36	1.05387	1.05581	1.05317	1.05619	1.05314	1.05424
20.08	36	1.05455	1.05653	1.05417	1.05805	1.05353	1.05614
21.08	36	1.05495	1.05623	1.05394	1.05902	1.05393	1.05667
22.08	36	1.05479	1.05639	1.05387	1.05975	1.05386	1.05747
23.08	36	1.05481	1.05648	1.05411	1.0601	1.05449	1.05744
24.08	36	1.05618	1.05527	1.05403	1.06079	1.05427	1.05812

25.08	36	1.05545	1.05694	1.05295	1.06103	1.05409	1.05811
26.08	36	1.05511	1.05626	1.05383	1.06163	1.05419	1.05866
27.08	36	1.05487	1.05609	1.05368	1.06202	1.05485	1.0585
29.08	36	1.05541	1.0561	1.05358	1.06252	1.055	1.05938

Table 44. $^{13}C/^{12}C$ ratio x 100 of DOC in labeled and control site (0 $\delta^{13}C \triangleq$ 0.0111802 $^{13}C/^{12}C$).

Day	Depth.cm.	A.contr	B.contr	C.contr	D.lab	E.lab	F.lab
15.08	6	1.09089	1.09094	1.09047	1.09109	1.09066	1.09056
18.08	6	1.09085	1.09134	1.09091	1.09478	1.09255	1.09783
19.08	6	1.09116	1.08994	1.09055	1.09521	1.09377	1.09733
20.08	6	1.09113	1.09282	1.09046	1.09544	1.09298	1.09698
21.08	6	1.09137	1.08988	1.09055	1.09515	1.09333	1.09787
22.08	6	1.09031	1.09084	1.0906	1.09518	1.09348	1.1003
23.08	6	1.09083	1.09022	1.09143	1.09596	1.09426	1.09634
24.08	6	1.09101	1.09149	1.0908	1.09666	1.09368	1.09818
25.08	6	1.09063	1.09032	1.09021	1.096	1.0944	1.10085
26.08	6	1.09096	1.09022	1.09026	1.09718	1.09474	1.10174
27.08	6		1.09009	1.09012	1.09783	1.09402	1.10054
29.08	6		1.09022		1.09761	1.09448	1.10188
-	-	-	-	-	-	-	-
15.08	16	1.09203	1.09281	1.09174	1.09178	1.09218	1.09236
18.08	16	1.09135	1.09149	1.0909	1.0917	1.09272	1.09271
19.08	16	1.09139	1.09135	1.09151	1.0922	1.09235	1.09261
20.08	16	1.09283	1.09185	1.09133	1.09314	1.09231	1.09295
21.08	16	1.09219	1.09165	1.09137	1.09246	1.09237	1.09233
22.08	16	1.09158	1.09161	1.09198	1.09487	1.09242	1.09292
23.08	16	1.09167	1.09167	1.09143	1.093	1.09295	1.09266
24.08	16	1.09201	1.09141	1.09148	1.09259	1.09268	1.09252
25.08	16	1.0917	1.0914	1.09141	1.09217	1.09245	1.09249
26.08	16	1.09199		1.09126	1.09235	1.09278	1.09233
27.08	16				1.09239	1.0925	1.09248
29.08	16				1.0923	1.09247	
-	-	-	-	-	-	-	-

15.08	36	1.09251	1.09104	1.09109	1.09236	1.09253	1.09219
18.08	36	1.09237	1.09254	1.09183	1.09309	1.09256	1.09246
19.08	36	1.09243	1.09289	1.09262	1.09247	1.09288	1.09244
20.08	36	1.09288	1.09242	1.09233	1.09105	1.09296	1.09298
21.08	36	1.09184	1.09242	1.09271	1.09286	1.09279	1.09295
22.08	36	1.09289	1.09296	1.09257	1.09258	1.09314	1.09289
23.08	36	1.09246	1.0925	1.09265	1.09325	1.09285	1.09314
24.08	36	1.09261	1.09244	1.09271	1.09351	1.09279	1.09316
25.08	36	1.09252	1.09257	1.09291	1.09307	1.09291	1.093
26.08	36	1.09254	1.09263	1.09289	1.09369	1.09344	1.09276
27.08	36	1.09278	1.09262	1.09269	1.09363	1.09277	1.09325
29.08	36				1.09326		

A IV Fluxes obtained by the best-fitted model parametrizations

Flux identifiers (e.g. "a21") are explained in Table 7.

Flux-Data (already multiplied by 4 to get the hourly values)

	a21	a31	a41	a51	a61	a12	a32	a42	a52	a62	a43	a53	a63	a17	a27	Cin	CO2/Cin	CH4/Cin	CO2 :	CH4-ratio	X6_in	X6_in/Cin
	0.005	0.000	0.182	0.209	0.109	0.148	0.001	0.002	0.002	0.058	0.000	0.001	0.000	0.357	0.206	0.563	0.634	0.366	1.000	0.577	0.168	0.297
	0.086	0.000	0.199	0.174	0.099	0.254	0.002	0.052	0.012	0.040	0.000	0.001	0.002	0.303	0.275	0.578	0.525	0.475	1.000	0.905	0.141	0.243
	0.003	0.001	0.133	0.137	0.200	0.169	0.002	0.009	0.002	0.005	0.000	0.001	0.002	0.304	0.185	0.489	0.621	0.379	1.000	0.609	0.207	0.423
	0.194	0.001	0.226	0.176	0.318	0.196	0.002	0.053	0.064	0.058	0.000	0.000	0.002	0.720	0.179	0.899	0.801	0.199	1.000	0.249	0.379	0.421
	0.122	0.003	0.090	0.129	0.045	0.151	0.004	0.047	0.040	0.125	0.000	0.001	0.005	0.237	0.246	0.483	0.491	0.509	1.000	1.037	0.175	0.363
	0.184	0.001	0.050	0.078	0.058	0.189	0.002	0.084	0.042	0.059	0.000	0.001	0.002	0.183	0.191	0.373	0.489	0.511	1.000	1.044	0.119	0.318
	0.017	0.000	0.095	0.116	0.192	0.262	0.002	0.039	0.008	0.010	0.000	0.001	0.001	0.159	0.304	0.463	0.343	0.657	1.000	1.915	0.203	0.439
	0.025	0.000	0.137	0.156	0.094	0.226	0.005	0.057	0.004	0.035	0.000	0.001	0.004	0.186	0.301	0.487	0.382	0.618	1.000	1.620	0.133	0.272
	0.141	0.000	0.176	0.172	0.128	0.136	0.002	0.077	0.082	0.073	0.000	0.001	0.001	0.481	0.229	0.711	0.677	0.323	1.000	0.477	0.202	0.285
	0.015	0.002	0.069	0.111	0.292	0.251	0.002	0.005	0.004	0.029	0.001	0.001	0.002	0.239	0.275	0.514	0.465	0.535	1.000	1.152	0.323	0.629
	0.013	0.001	0.197	0.211	0.153	0.293	0.001	0.006	0.014	0.021	0.000	0.001	0.001	0.282	0.322	0.604	0.467	0.533	1.000	1.140	0.176	0.291
	0.139	0.001	0.079	0.099	0.055	0.163	0.002	0.046	0.076	0.088	0.000	0.001	0.002	0.209	0.236	0.445	0.470	0.530	1.000	1.127	0.145	0.325
	0.020	0.000	0.175	0.181	0.115	0.181	0.004	0.063	0.016	0.077	0.000	0.001	0.003	0.309	0.322	0.631	0.490	0.510	1.000	1.040	0.195	0.309
	0.066	0.000	0.238	0.246	0.154	0.239	0.003	0.049	0.020	0.045	0.000	0.001	0.002	0.465	0.289	0.754	0.617	0.383	1.000	0.622	0.200	0.266
	0.017	0.001	0.131	0.200	0.105	0.236	0.001	0.031	0.010	0.035	0.000	0.001	0.001	0.216	0.296	0.513	0.422	0.578	1.000	1.369	0.140	0.274
	0.026	0.001	0.127	0.111	0.127	0.226	0.002	0.066	0.006	0.020	0.000	0.001	0.001	0.165	0.295	0.460	0.359	0.641	1.000	1.785	0.148	0.321
	0.094	0.000	0.062	0.101	0.145	0.297	0.002	0.024	0.015	0.023	0.000	0.001	0.002	0.105	0.268	0.372	0.281	0.719	1.000	2.561	0.170	0.456
	0.061	0.000	0.103	0.106	0.151	0.258	0.003	0.043	0.007	0.043	0.000	0.000	0.002	0.163	0.293	0.456	0.358	0.642	1.000	1.792	0.196	0.430
	0.005	0.000	0.077	0.103	0.188	0.172	0.001	0.005	0.001	0.028	0.000	0.000	0.001	0.201	0.201	0.402	0.500	0.500	1.000	0.999	0.217	0.539
	0.005	0.001	0.142	0.163	0.076	0.188	0.003	0.037	0.004	0.019	0.000	0.001	0.003	0.199	0.247	0.445	0.446	0.554	1.000	1.243	0.098	0.220
Mean	0.062	0.001	0.134	0.149	0.140	0.212	0.002	0.040	0.021	0.045	0.000	0.001	0.002	0.274	0.258	0.532	0.492	0.508	1.000	1.163	0.187	0.356
SD	0.062	0.001	0.055	0.045	0.070	0.048	0.001	0.024	0.025	0.029	0.000	0.000	0.001	0.140	0.045	0.130	0.124	0.124	0.000	0.545	0.064	0.103

A V Additional study: mosses as system barrier in a stable carbon isotope labeling experiment (Semi in-vitro labeling experiment)

Introduction:

In the course of the model´s conceptual development, it became important to understand whether moss layers act as a barrier that prevent $^{13}CO_2$ enriched CO_2 from diffusing into the active root layer or whether they take actively part in the photosynthesis-related carbon transport into the sub-surface soil. This knowledge poses an important precondition for stable carbon isotope labeling experiment designs that assume that the label, detected in the rhizosphere, is plant-transported and therefore represents the plant-transported atmospheric C pool fraction of the sub-surface carbon dioxide C pool. As for the conceptual model, it becomes necessary to know whether mosses and plants can be treated as a single compartment in a compartmental model or whether they have to be modelled as two different pools. For this experiment the working hypothesis is formulated as:

Figure 46. Label experiment conducted on the rooftop of the Institute of Soil Science, Hamburg. The mesocosms, representing a *Sphagnum* spec. - *Eriophorum* spec. plant association, are partly sealed with a layer of acrylic glas and silicon glue. This seal separates the mosses from the atmosphere in the chamber and hence hampered uptake of ^{13}C-enriched CO_2.

H1: The photosynthesis rate of *Sphagnum* spec significantly effects the total photosynthesis-related carbon allocation into the plant-soil system.

Method and experiment

The labeling set-up was similar to the setup used for in-situ experiments on Samoylov island.

Six mesocosm-cores were carefully cut out from the Himmelmoor peatland on May 7, 2015. The mesocosms represented an *Eriophorum-Sphagnum* plant association. The six mesocosms were placed on the rooftop of the Institute of Soil Science and were given to adjust to the new conditions for more than 2.5 months (84 days).

The labeling was conducted on July 30, 2015. The label photosynthesis period was about 2.5 hours (13:55-16:22, 2:27 hours). Every 10 to 20 minutes the total CO_2 concentration in the label chamber was measured. A sample was taken through the septum with a syringe and detected within a few minutes on the GC. In comparison to in-situ experiments this is a great advantage, because the problem of detecting high $^{13}CO_2$ concentrations with a common infrared gas analyser (e.g. Li-840) is still not satisfactorily solved. In this experiment, detecting the accurate total CO_2 concentration with the GC allows the insertion of $^{13}CO_2$ whenever the total CO_2 concentration drops beneath a certain value (in this experiment the range of $^{13}CO_2$ was set from 350 to 450 ppm).

Results

Subsequently, the concentration and $\delta^{13}C$ of dissolved CO_2 have been measured on a non-regular basis Figure 47. This data is then used to evaluate the tracer concentration in the dissolved CO_2. The $\delta^{13}C$ difference in both replicas is interpreted as the difference between a system in which only vascular plants photosynthesize and a system in which both vascular plants and mosses photosynthesize.

Interpretation

In Figure 47 is shown that those replicas, in which mosses and vascular plants (*Sphagnum* and *Eriophorum*) are exposed to enriched ^{13}C-CO_2, the tracer concentration is significantly higher. Interestingly, in both replica series, the total tracer concentration keeps rising - after the label-pulse had stopped - until the experiment was terminated. The dC/dt function of the control mesocosms (both plants exposed to ^{13}C-enriched CO_2) is steeper than in those mesocosms where the moss is constrained from the atmosphere.

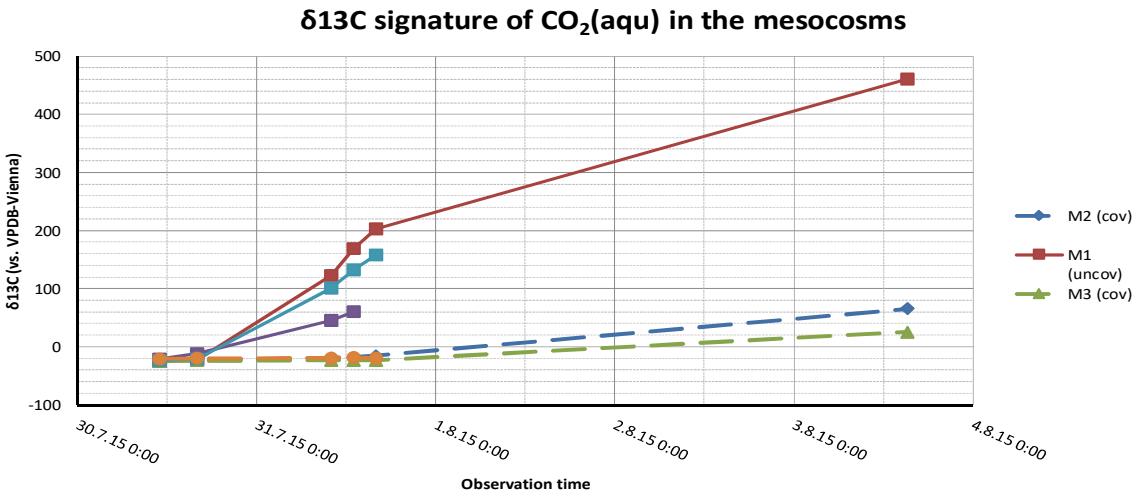

Figure 47. $\delta^{13}C$ value of CO_2(diss) in six mesocosms. The data series with the attribute M*X*(cov) and a dashed line are the replicas, in which carbon dioxide uptake by the mosses was hampered (during the labeling period of 2.5 hours). The solid lines represent mesocosms, in which vascular plants and mosses form a unit, i.e. they both photosynthesized the ^{13}C-enriched carbon dioxide.

This demonstrates not only the difficulties in determining the "system's" turnover rates, it also shows that even when a small label-pulse is delivered, the system can store huge amounts of tracer and is hence label-affected for a long time.

Conclusion

The data shows clearly that it has an effect, whether the total plant community is exposed to the tracer-CO_2 or only the vascular plants.

This experiment shows that the mosses might act as a temporal storage of atmospheric-derived carbon, which can be released consecutively over days (and maybe weeks). Moreover, it shows that the tracer concentration in the produced CO_2 is strongly influenced by the mosses atmospheric-C storing response. Finally, it demonstrates that the moss is no natural border between soil-dissolved CO_2 and atmospheric CO_2, but acts more like a "sponge" on it: It takes it up quickly and releases it with some delay into the system.

Again, this shows the necessity to improve our understanding of small-scale carbon allocation processes that occur in the sub-surface environment of tundra wetland (and not only) soils, in order to properly predict their response to changing climatic conditions. If we compare the data from this

additional experiment with the data obtained from Samoylov, one gets the impression that the mosses on Samoylov display a stronger "sponge"-like behavior. The steep decline of tracer in the carbon dioxide pool is only after weeks somewhat compensated by the increase of tracer addition by other, slower pools in the system. Hence, it does not seem too far-fetched to relate the steep decline of tracer in the Samoylov carbon dioxide pool with an outwash from vascular plants (turnover of recently acquired LMW organic compounds in the plant tissue) and the general higher tracer concentration in the same system after two weeks with a slowly but relentlessly contributing source – the *Scorpidium* mosses.

A VI Determination of pH, porosity, and sample plume radius

With respect to the small amounts of available soil material, the following method of pH measurement was applied:

5 g of soil material are dissolved in 12.5 ml of H_2O bidest. Each 15 minutes the solution is shaken for 1 minute (4 times in total). Dried soil samples have been directly added to 12.5 ml of water, samples with natural water content (frozen until the analysis started) have been weighted and only that much water have been added that the total amount of water is 12.5 ml.

The samples were shaken for about a minute each 15 minutes for about an hour and afterwards measured within two hours. Before the measurement started, each sample was stirred up in order to create an equally mixed solution. The pH value was measured and the actual pH of a soil sample was calculated in accordance with the following procedure:

Calculations:

Transformation of the pH to mol/L (H^+/mol):	the pH value was taken to the power of ten.
Calculation of the total amount of H^+ in the sample:	H^+ /mol value was multiplied with the amount of water in the solution (and divided by 1000, because the operational unit is milliliters and not liters)
mol H^+/g Soil:	total amount of H^+ was divided by the amount of soil in the solution
mol H^+/ cm^3:	mol H^+/g soil was multiplied with the bulk density (g/cm^3) of the soil sample. The bulk

	densities are taken from a previous experiment.
concentration of H^+ in the nature:	the mol/H^+ value was divided by the pore space (cm^3/cm^3). So the H^+ concentration per gram soil was related to the amount of water that surrounds each gram of solid soil matter in the nature.
calculated pH:	the negative decadal logarithm of the concentration of H^+ in the nature was taken.

The electrical conductivity was calculated with a similar procedure. The measured conductivity was taken as mol per ml. Then the relation to solution factor and gram soil was done according to the procedure for pH. The results are displayed in Table 45.

Table 45. Analysis of pH. The measured and the re-calculated pH values are shown.

SampleNo	Depth (cm)	Weigh vessel (g)	Weigh Soil+Vessel (g)	Weigh Water+Vessel+Soil (g)	pH-value (pH)	Electrical Conductivity (microsiemens/ cm)	theoretical pH (pH)
13C11	0-10	12.92	15.66	49.27	5.04	234	4.73
13C12	0-10	12.91	15.36	47.3	4.89	208	4.56
13C13	0-10	12.92	14.27	41.6	5.11	174	4.59
13C21	10-20	12.9	16.43	55.23	5.04	189.7	4.59
13C22	10-20	12.87	17.38	59.11	5.13	182.3	4.76
13C23	10-20	12.93	15.88	50.1	5.14	363	4.67
13C31	20-30	12.93	20.23	52.75	5.36	168.5	5.26
13C32	20-30	12.94	18.47	55.58	5.31	253	5.03
13C33	20-30	12.89	20.78	55.86	5.37	211	5.27
13C41	30-40	12.65	18.42	47.5	6.26	189.1	5.92
13C42	30-40	12.9	17.79	41.65	5.43	318	5.11
13C43	30-40	12.95	20.41	57.07	6.06	269	5.73

Protocol of measuring the particle size density

For the bulk density, a core of soil was cut out from the fresh soil profile with a drill head (5 cm diameter, 4 cm deep, total volume of 78.54 cm^3). This core sample was dried (105 °C) and the bulk density was calculated by the equation

$$bulk\ density\ (gcm^{-3}) = \frac{dry\ weight\ (g)}{sample\ volume\ (cm^3)}$$

Measuring particle size density:

The particle size density was measured as follows: a 400 ml cylindric beaker was outweighted and filled with so much water that the soil sample, which is dried (at 105 °C), will be completely covered by water. The net weight of the water has to be determined and the water level had to be marked at the beaker (with a fine liner). Now the beaker is emptied and thoroughly dried, without removing the fine liner markings. Afterwards, the soil sample is placed into the beaker. The weight of the soil sample and the total weight of the beaker + soil sample is to be noted. Deionized water is filled into the beaker (not until the fine liner marking) and the soil-water suspension is heated to 100 °C (to remove small air bubbles in the soil sampler material). Finally, after cooling to room temperature, deionized water is added until the water level reaches the fine liner markings. The total weight of beaker + water + soil is noted. The weight beaker + soil is subtracted from the weight beaker + water + soil. The difference between this value and the previously reported net weight of the water in the beaker corresponds to the amount of water volume which is displaced by the soil sample.

Effective sample plume radius

The effective sample plume radius is a term to describe the 3-dimensional area inside the soil pore water space for the sample is representing. With other words, the sample is an integral over the soil properties and pore water concentrations inside a plume (sphere) of about 3 cm radius. Respective values are given in Table 46.

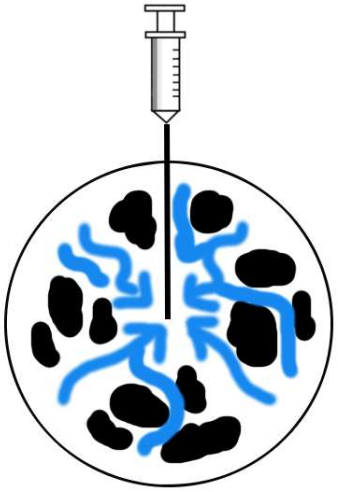

Figure 48. Conceptual model of the sample plume concept. The extracted pore water sample volume corresponds to a sample sphere (plume) around the extraction point, which size depends on the extraction volume and the porosity.

The conceptual model of the sample plume is shown in Figure 48.

Table 46. Effective sample plume radius and soil porosity

Soil layer (cm below surface)	Extraction volume (ml)	Porosity (%)	Effective sample plume radius (cm)	SD[7]
00-10	100	0.91	2.97	0.02
10-20	100	0.88	3.00	0.02
20-30	100	0.86	3.03	0.07
30-40	100	0.78	3.13	0.05

The sample plume is obtained by the following equation:

$$16) \qquad r_{sample-plum} = ((V_{sample\_volume} \frac{1}{Porosity})/(\frac{4}{3} \pi))^{1/3}$$

where $r_{sample\text{-}plume}$ is the radius of the sample plume, V_{sample_volume} is the total volume of pore water extracted from the volume, and *Porosity* is the soil porosity.

A VII Correction factors for $\delta^{13}C$ and concentration values of CO_2

After being sampled, the soil pore water sample was inserted into a lab vessel, sealed by a chlorobutyl rubber stopper and filled with saturated NaCl-solution (~6.12 m NaCl). This was

[7] The standard deviation is obtained by calculating the radius of the sample plume for the Porosity + SD and Porosity - SD, taking their difference and multiplying this difference by 0.5.

achieved by guessing the amount of sample being inserted prior to sampling and adding the respective amount of NaCl in the vessel that is necessary to oversaturate this sample amount. While the recovery of methane and methane- $\delta^{13}C$ did not pose a problem (due to the low solubility of methane in the pore water, the methane was assumed to be totally salted-out into the headspace), the CO_2 was readily soluble in the NaCl-solution. For the planned analysis, it was important to transform all the DIC in the soil pore water to CO_2. This would lead to a new CO_2 concentration equilibrium between headspace and solution. The carbon dioxide in the headspace would then be interpretable as the total amount of carbon dioxide stored in the amount of pore water injected into the lab vessel. Moreover, due to isotopic fractionation processes, the $\delta^{13}C$ signature of that fraction of carbon dioxide in the headspace would also be different from that fraction still dissolved in the solution.

To compensate for this, a correction factor for the headspace concentration and the $\delta^{13}C$ signature of the carbon dioxide in the headspace was developed.

In this section, the development of this constant is to be described and explained.

A sub-set of all CO_2 samples (CO_2 in headspace over saturated NaCl- solution) had been chosen. Now HCl was added (0.09 ml 0.5 m HCl) to reduce the pH value of the NaCl solution to pH 2. This had an effect of degassing more of the CO_2 into the headspace, which was previously in the solution, because the DIC is entirely transformed into CO_2 and this causes a re-equilibrium with the headspace CO_2 concentration. The $\delta^{13}C$ and CO_2 concentration of the sample set was plotted vs. the same parameters measured before the HCl addition. The relationship was linear and could be modelled by a linear model (see Figures 49 and 50).

With this function, the already measured headspace concentrations of the entire set of samples were recalculated and the total amount of CO_2 in the sample was calculated based on this newly obtained values.

Additionally, the $\delta^{13}C$ in the headspace CO_2 is measured again (after lowering of pH) and a linear model is fitted to the $\delta^{13}C$ before and after the HCl addition to the samples. A linear model is used to recalculate the $\delta^{13}C$ of the headspace in the sample vessels (Figure 50).

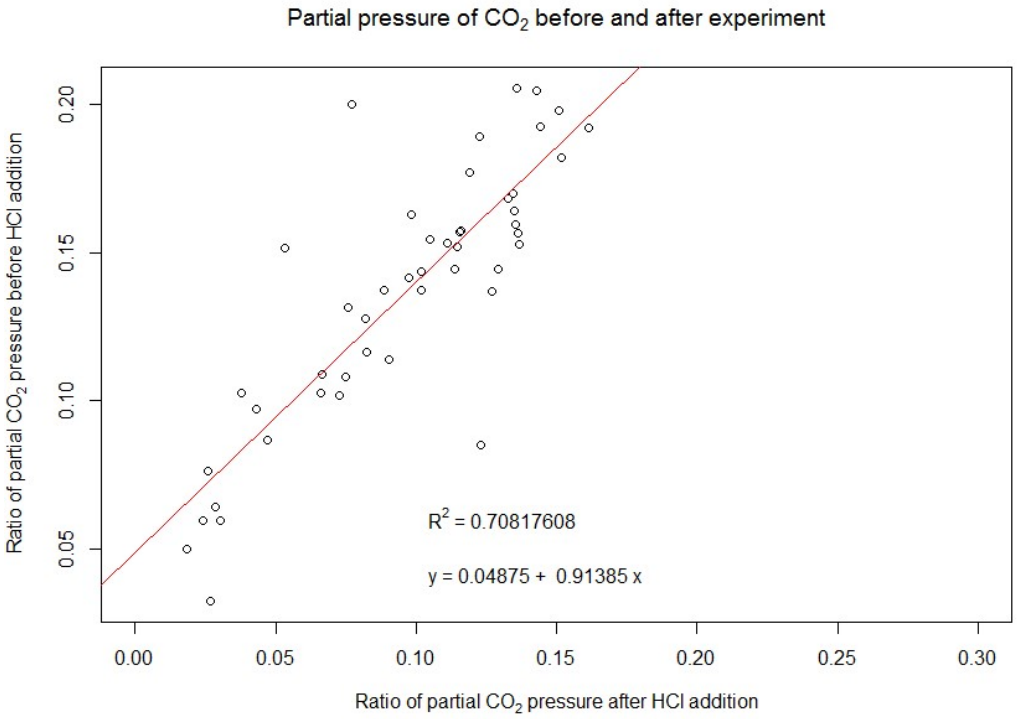

Figure 49. CO_2 partial pressure before and after pH dropped to pH 2. The linear model allows calculating the CO_2 concentration for the other samples.

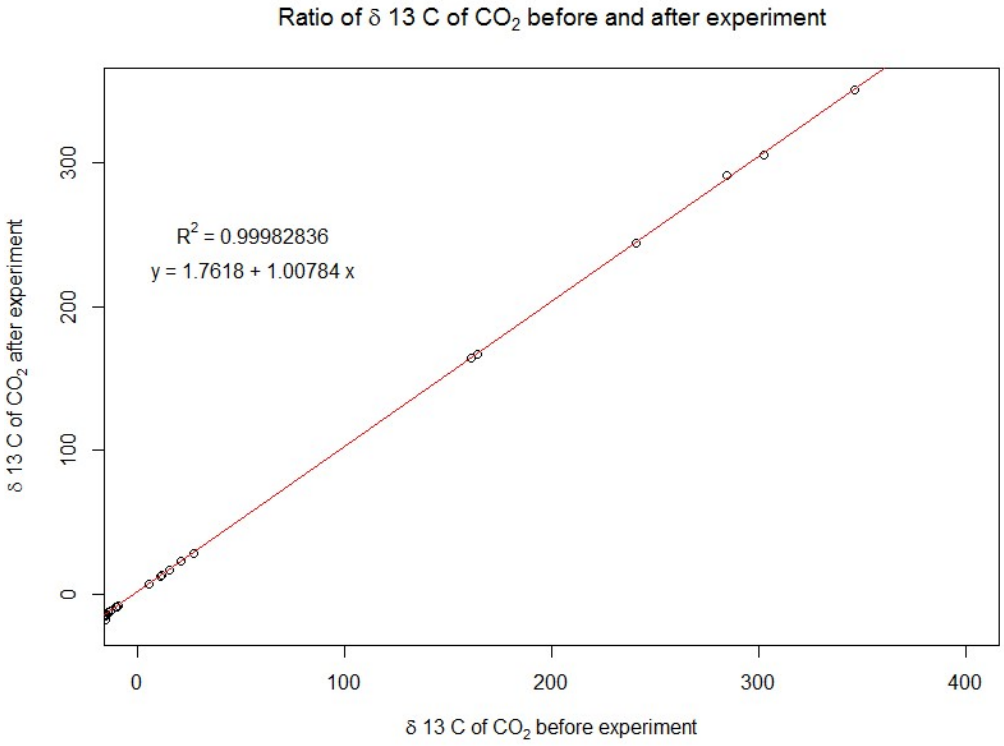

Figure 50. $\delta^{13}C$ in CO_2 before and after HCl addition. This model is then used to recalculate the $\delta^{13}C$ of CO_2 in the headspace.

Finally, after the correction factors for CO_2 concentration and $\delta^{13}C$ are obtained, the total amount of carbon dioxide is to be calculated. The total carbon dioxide concentration in the sample volume is calculated by applying the Henry's law on the head space concentration in the sample vessel. Thus, the concentration in the solution in the sample vessel is obtained. Now, with the additional information of the headspace volume and the amount of solution in the lab vessel, the total CO_2 amount in the sample can be calculated.

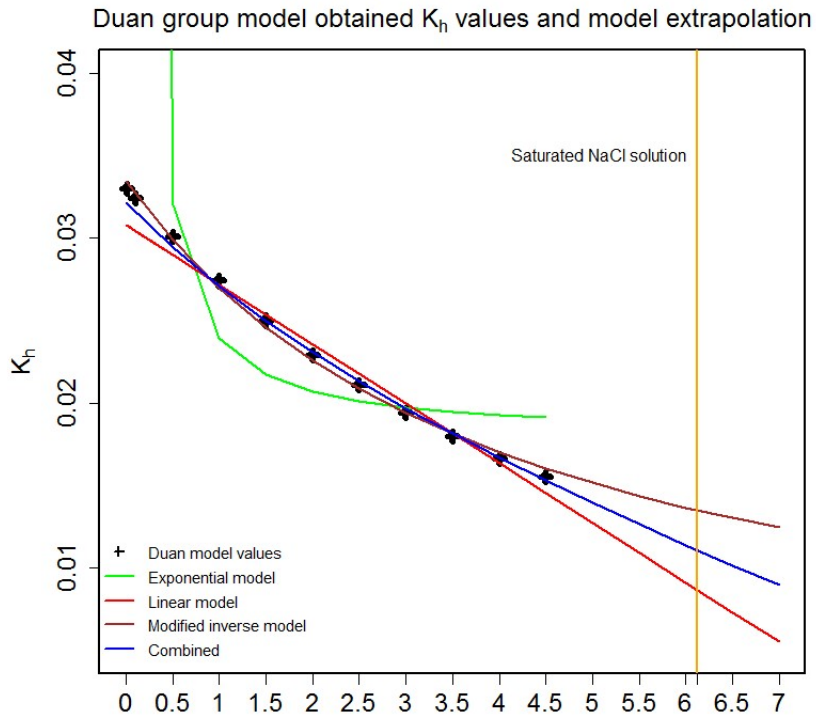

Figure 51. Different extrapolations of the solubility constant k_h of CO_2 in sat. NaCl solution. The black dots are values calculated with the Duan's working group model ('The Duan Group - Models - H2O-CO2-NaCl' 2015). This model was only defined to work up to 4.5 m NaCl. In order to have a "guestimate" for the k_h value at 6.12 m NaCl solution, several models have been fit to the Duan model values and their function have then been further used to extrapolate k_h down to a NaCl concentration of 6.12 m.

A problem is the choice of the Henry's constant applied for these calculations. A thorough literature research did not deliver this constant (as used for example by Hope et al. (1995) and Butler (1982) , because the Henry constant depends on the NaCl concentration and empirical data series are usually only available for lower salt concentrations.

Fortunately, the working group of Zhenhao Duan ('The Duan Group - Models - H2O-CO2-NaCl', 2015) presents chemical equilibrium models, among those a model to determine the solubility of CO_2 in the NaCl-H_2O system. Unfortunately, this model was operable to up to 4.5 NaCl concentrations. This model was used on-line to produce a data series of the Henry constant for several NaCl

concentrations. This data series was then fit to a model (exponential model), which was used to extrapolate the Duan Group data to a 6.12 molar NaCl-solution k_h.

A VIII Determination of DOC concentration with the Shimadzu TOC-L and Genesys UV10 Photospectrometer

During the analysis of DOC concentration with the Aurora device, a methodological mistake[8] was discovered and the concentration analysis had to be repeated, because they were biased. Unfortunately, due to the relatively high amount of solution consumed by the Aurora device, there was no original sample material left. However, some milliliters of the pore water sample originally envisaged and used for the dissolved DOC and CH_4 concentration determination, was still available. Here, the sample material was stored in concentrated NaCl solution. Some of the samples, of which more material was still available, were separated into two sub-samples: one prepared to be measured at the TOC-L Shimadzu, the other prepared to be measured at the Genesys Photospectrometer.

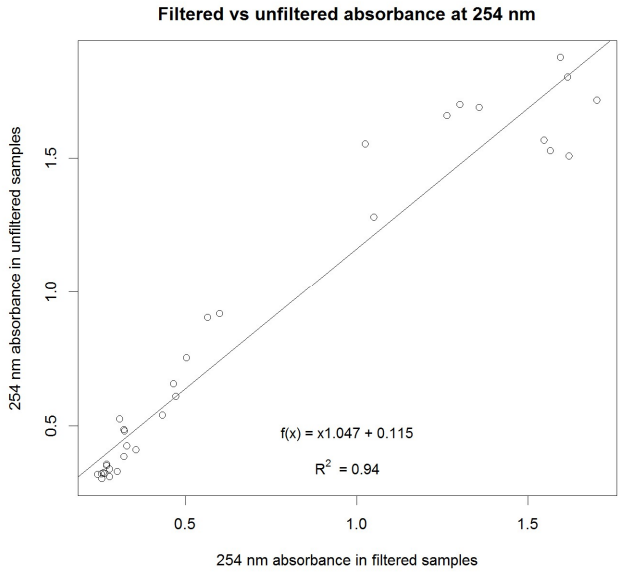

Figure 52. Linear model depicting the relation between 254 nm-absorbance of filtered and unfiltered DOC-concentration samples.

The idea was to obtain a data base of concentrations from DOC sample in the solution and to correlate this concentration with the extinction characteristics of certain wavelengths. This

[8] The DOC concentration was determined based on a dissolved solution. The factor, which would have allowed compensating for this dissolution factor, was, due to communication problems, not noted and hence the concentration was that of the original solution, which was dissolved by an unknown factor – unsolvable.

strategy was chosen, because the technical equipment of the TOC-L device does not allow measuring huge numbers of high-salt concentration samples, and because the total sample volume still available was small. The Spectrophotometer, however, needs only about a milliliter of solution and delivers reproducible extinction values with great efficiency.

The sub-sample series, from which both the concentration and the characteristic extinction pattern have been determined, were used to produce a function (wavelength x = a concentration). With this function at hand, the concentration of all other samples was determinable. The DOC concentrations, produced by this method, were the DOC concentrations which were finally used for this project.

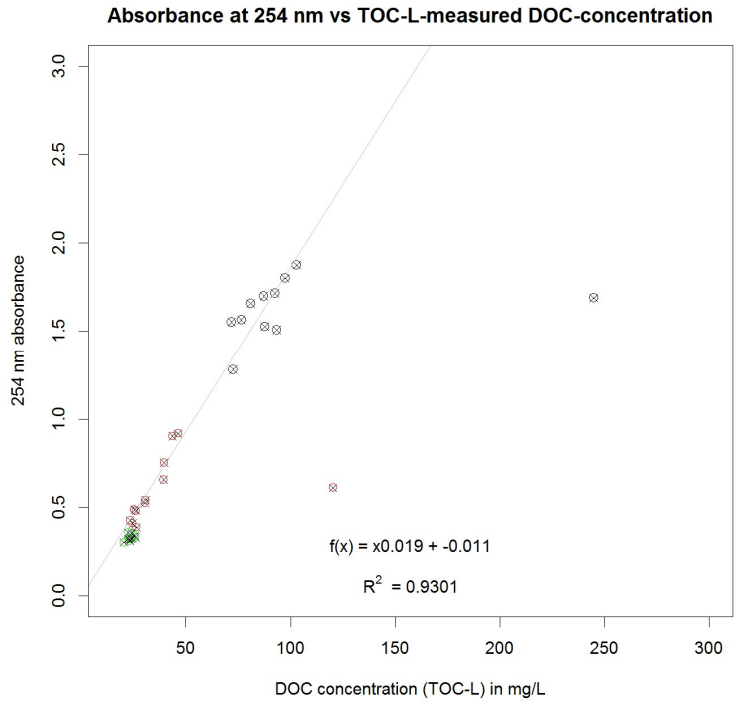

Figure 53. Linear model explaining the DOC concentration (measured by TOC-L analyzer) and the absorbance at 254 nm (measured by photospectrometer). This model is applied to calculate the DOC-concentration with absorbance values obtained by UV-VIS photo spectrometry.

Eidesstaatliche Erklärung

Hiermit versichere ich an Eides statt, dass ich die vorliegende Dissertationsschrift selbstständig verfasst und keine anderen als die angegebenen Hilfsmittel – insbesondere keine im Quellenverzeichnis nicht benannten Internet-Quellen – benutzt habe. Alle Stellen, die wörtlich oder sinngemäß aus Veröffentlichungen entnommen wurden, sind als solche kenntlich gemacht. Ich versichere weiterhin, dass ich die Arbeit vorher nicht in einem anderen Prüfungsverfahren eingereicht habe und die eingereichte schriftliche Fassung der auf dem elektronischen Speichermedium entspricht.

Ich versichere an Eides statt, dass ich bisher weder an der Universität Hamburg noch an einer anderen Universität einen Versuch zur Promotion unternommen habe.

Hamburg, den 29.3. 2017 Norman Rüggen